Republic of Iraq
Ministry of Higher Education and Scientific Research
University of Maysan/College of Engineering
Civil Engineering Department

BEHAVIOR OF SLURRY INFILTRATED FIBROUS CONCRETE (SIFCON) DEEP BEAMS

A THESIS

SUBMITTED TO THE COLLEGE OF ENGINEERING OF MAYSAN UNIVERSITY IN PARTIAL FULFILLMENT OF THE REQUIREMENTS FOR THE DEGREE OF MASTER OF SCIENCE IN CIVIL ENGINEERING

(STRUCTURES)

BY

AMMAR ABBAS ABD

B.Sc. in Civil Engineering, 2018

Supervised by

Assist.Prof.Dr. Mohammed Salih Abd-Ali

October 2018 **Shaban 1440**

To the Memory of my Father

To my Mother, my Wife and my daughter Jana

To my Sisters and my Brother

To my Kinsfolk and my Friends with Respect.

To The Heroes (Iraqi Army, ICTS and Popular Mobilization Forces)

Eng. Ammar Abbas Abd

2018/10/23

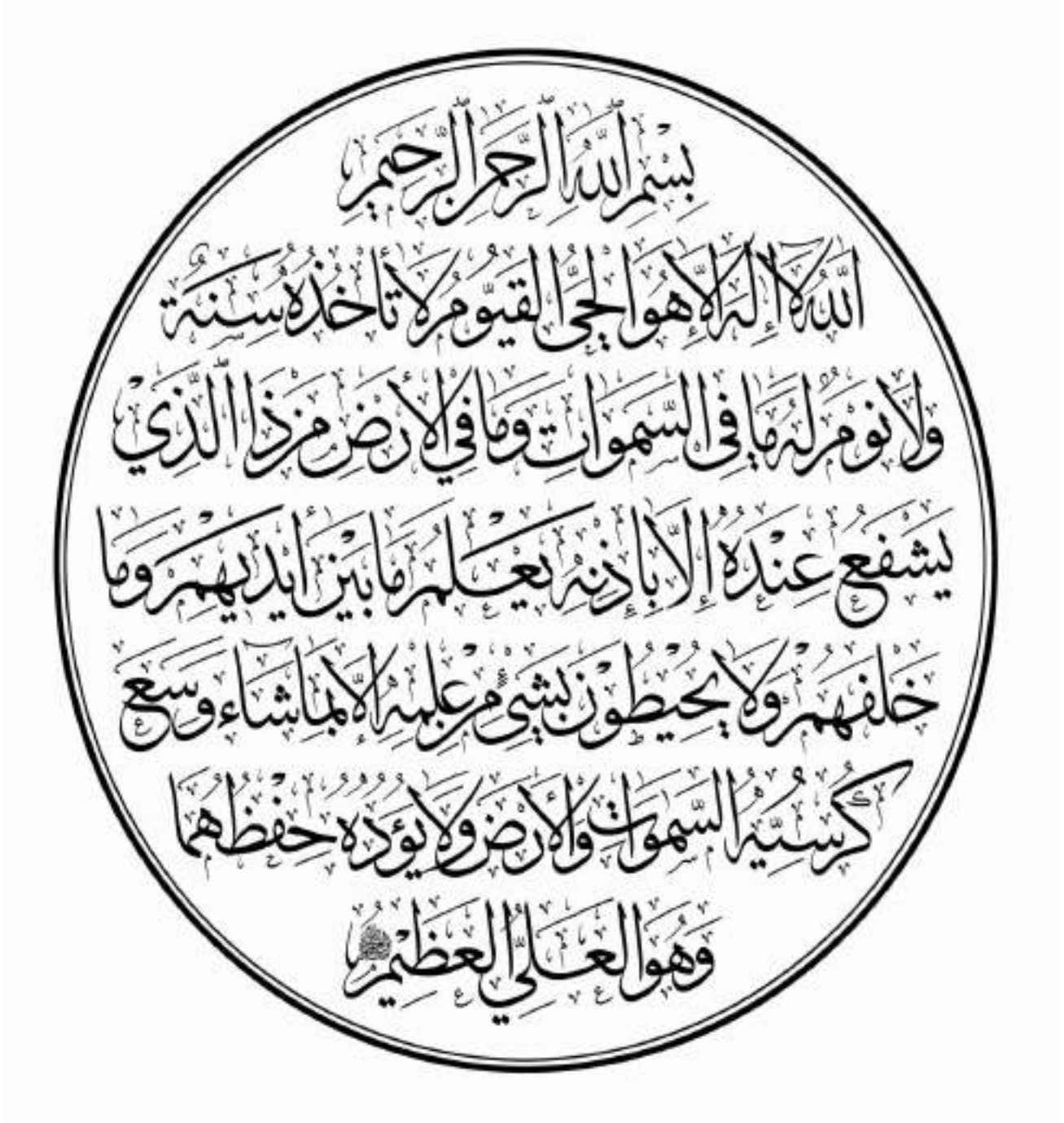

سورة البقرة (255)

ABSTRACT

Due to absence of study or research deals with the effect of SIFCON on deep beams, this study was conducted

The experimental work had been implemented for the purpose of studying two aspects. The first aspect was the study of mechanical properties of SIFCON. In this study, three trail mixes of sifcon were proposed and another fourth of conventional concrete was designed for comparison purposes. The mechanical properties of these mixes were tested which include compressive strength, tensile strength, flexural strength and shear strength. It was found that the concrete mix which contains a percentage of steel fiber by 9% gave the best results, so it was adopted as a reference mix in the deep concrete beams. The second aspect was the study of behavior of SIFCON deep beams with and without openings. The study was divided into two groups: the first group was solid deep beams and second group was deep beams with openings. The experimental program consists of casting and testing of sixteen SIFCON deep beams under two symmetrical points for both groups. The first group was prepared to cover the following cases: the variation in steel fiber ratio, the effect of shear span to depth ratio, removing of vertical web reinforcement and removing of main and web reinforcement. While, the second group was prepared to study the following cases: the variation in steel fiber ratio, the openings reinforcement effect and the effect of opening shape.

The increase of steel fiber ratio by (6% to 9%) gave increasing in the cracking and ultimate load about of (275% to 362.5%) and (196% to 239.4%) respectively for solid deep beams and about of (60% to 236%) and (223.8% to 309.5) respectively for deep beams with openings in comparison with conventional concrete.

Although it was removed either vertical web reinforcement or main and web reinforcement, it showed an increase in ultimate load for solid deep beams with steel fiber ratio of (9%), about of 215.6% and 226.9% respectively than the conventional concrete.

The results showed that the ultimate load was increased with deceasing the effective shear span to depth ratio.

The SIFCON deep beam with inclined reinforcement around the openings gave increasing in the ultimate load about of 234.5% compared to conventional concrete deep beam with inclined reinforcement.

Also, the SIFCON deep beam with circular opening gave high cracking and ultimate loads than square and triangular openings.

The toughness and ductility were increased for all sifcon deep beams.

The three dimensional Nonlinear finite element analysis using Ansys package showed that, the predicted values for all SIFCON deep beams were in acceptable agreement with the experimental results for the load – deflection relationships, toughness and ductility.

The ratios of numerical failure loads to experimental failure loads were ranging from 86.67% to 96.72% for solid deep beam and 73.66% to 97.6% for deep beams with openings.

Acknowledgements

First of all, praise and thanks be to **Allah** who led me during my way to complete this work.

I would like to express my cordial thanks and deepest gratitude to my supervisor **Assist. Prof. Dr. Mohammed Salih Abd-Ali,** whom I had the honor of being under his supervision, for his help, continuous encouragement, and invaluable guidance during this study.

I would like to extend my thanks to **Prof. Dr. Ahmed Kadhim AL-Sharaa,** Dean of the Engineering College, and **Assist. Prof. Dr. Abbas Oda Dawood**, Head of the Civil Engineering Department.

Special thanks goes to **Assist. Prof. Dr. Abdulkhaliq Abdulyimah Jaafer** and **Assist. Prof. Dr. Saad Fahad Resan** for help me and supported.

Also, I would like to express my thanks and gratitude to my parents for their encouragement, patience, and assistance which gave me a great support.

Finally, I extend my sincere gratitude to my brother, my sisters, and my friend's master students (**Wathiq Jasim, Ali Wathiq and Mustafa Raad**) for their help and kindness during the time of hardship.

AMMAR ABBAS ABD

2018

CONTENTS

NOTATION

The major symbols used in the text are listed below; others are defined as they first appear:

a	Shear span measured from center of load to center of support, mm
b	Width or thickness of beam, mm
d	Effective depth of beam, distance from extreme compression fiber to centroid of longitudinal tension reinforcement, mm
E_c	Modulus of elasticity of concrete, MPa
f'c	Cylinder compressive strength of concrete, MPa
f_{cu}	Cube compressive strength of concrete, MPa
f_r	Flexural strength of concrete, MPa
f_t	Splitting tensile strength of concrete, MPa
f_y	Yield stress of reinforcing steel bar and wire, MPa
h	Total depth of deep beam, mm
L	Overall length of deep beam, mm

L_n Clear span measured face to face of supports, mm

T_{50} The time recorded in 500 mm diameter circle of self-compacted mix

Tn Tolerance [varied between (0.0005-0.01) in this study].

Vs Shear stress of double L – shape

S_v Spacing of vertical shear reinforcement in direction of longitudinal reinforcement, mm

S_h Spacing of horizontal shear reinforcement, mm

$W_{int.}$ Internal work (strain energy)

$W_{ext.}$ External work (work done by the applied force)

P_{cr} Load causing first initiation of crack ,kN

P_u Ultimate load , kN

Ø Steel bar diameter, mm

(υ) Poisson's ratio

δ Max mid span deflection

{Ɛ} Elements of virtual strain vector.

{σ} Elements of real stress vector.

[C] Constitutive matrix

[N] Shape function matrix

{a} Unknown nodal displacements vector (local displacements)

{U} Body displacements vector (global displacements).

[B] Strain-nodal displacement relation matrix, based on the element shape functions.

{F} Nodal forces applied to the element

[Ke] Element stiffness matrix

{r} Out of balance force vector.

{ΔDi} Incremental displacement vector at (i) iteration.

Abbreviations

ACI	American Concrete Institute
ASTM	American Society for Testing and Materials
BS	British Standards
CSA	Canadian standard associated
ECP	Egyptian code
FRC	Fiber Reinforcement Concrete
IQS	Iraqi Standard
PCC	Plain cement concrete
RCC	Reinforced cement concrete
SF	Steel Fiber
SCC	Self-Compacting Concrete
STM	Strut and Tie Method
V_F	Volume Fraction

LIST OF FIGURES

LIST OF PLATES

LIST OF TABLES

CHAPTER ONE

INTRODUCTION

Chapter One

INTRODUCTION

1.1 General

Reinforced concrete deep beams are exceedingly used in civil engineering for parking or storage facility, bridge, transfer girders, wall footings, foundation pile caps, floor, diaphragms and shear walls [1]. Plate (1.1) show some applications of deep beam. In some multistory buildings, it is often desirable to have the lower floors free of columns, therefore; these beams may be designed as beams spanning across the column free space.

Plate (1.1) Herman B. Fultz Bridge [2]

The ACI 318M-14 code [3] defines deep beams as members that are loaded on one face and supported on the opposite face such as strut-like compression elements can develop between the loads and the supports. Deep beam considers the structural

members in which most of the applied load transferred directly to the supports by tied arch after formation of the inclined cracks. Deep beam should satisfy a or b [3]:

a) Clear span does not exceed four times the overall depth (h).

b) Concentrated load exist within a distance (2h) from the face of the support.

According to Eurocode 2 (EC2) [4] beams can be classified as deep beams when the ratio of span to depth is smaller or equal to three ($L/h \leq 3$).

Canadian standard association (CSA) A23.3-04 [5] states that a flexural member with clear span to overall depth ratio less than 2 must be designated as a deep flexural member by strut and tie method and take into a count nonlinear distribution of strain.

In many cases, openings are required in deep beams to provide accessibility or to facilitate essential services such as drainage pipes, water supply and air conditioning ducts as shown in Plate (1.2) below:

Plate (1.2) Prestressed concrete beams with opening [2].

1.2 Behavior of Deep Beams

The strength of deep beams is usually controlled by shear rather than flexure [6]. Deep beam should be design taking into account nonlinear distribution of longitudinal strain over the depth of beam [3]. The strut-and-tie model, was pioneered

by Ritter [7] and Morsch [8], is a rational method for analyzing and designing reinforced concrete beams especially deep beams. The Strut and Tie Method (STM) is a lower bound solution approach for capacity that is recognized as an important tool for the design of non-slender beams, since it considers the member capacity as a function of a/d [9,10].

The major differences of deep beam element compared with ordinary beam based on the design assumption [11], as follows:

- **Two-Dimensional Action**: because of the dimension of deep beam they behave as two-dimensional action rather than one-dimensional action.
- **Plane Section:** do not remain plane, the assumption of plane section remain plane cannot be used in the deep beam design. The strain distribution is no longer linear.
- **Shear Deformation**: the shear deformation cannot be neglected as in ordinary beam. The stress distribution is nonlinear even in the elastic stage. At the ultimate limit state, the shape of concrete compressive stress block is not parabolic shape.

1.3 Failure Modes of Deep Beams without Web Openings

The behavior of reinforced concrete deep beams is affected by many factors like shear span to the effective depth ratio (a/d), clear span to overall depth ratio (L_n/h), position and type of the load, percentage of main longitudinal reinforcement, type and amount of web reinforcement, width of the support zone anchorage of the main reinforcement, concrete strength, and the addition of other materials like fibers [12, 13]. Failure of reinforced concrete deep beams without web openings may be one of the following modes that are summarized [14-15]:

1.3.1 Flexural failure:

This mode of failure happens when the (a/d) ratio is high and the beam has a little percentage of main longitudinal reinforcement, therefore it fails by yielding of tension reinforcement at the section of maximum moment as shown in Fig. (1.1).

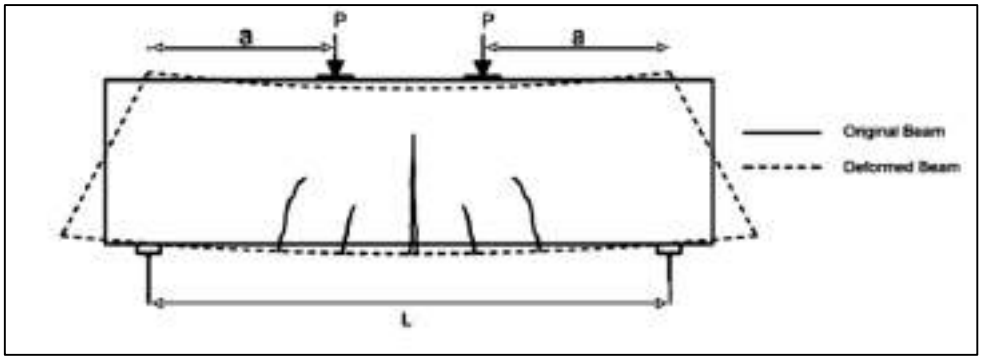

Fig. (1.1) Flexural failure of deep beam.

1.3.2 Flexural-shear failure:

This mode of failure happens in beams with moderate tension reinforcement and the development of the inclined shear cracks is normally preceded by flexural cracks at section of maximum moment. The main cracks are developed upwards starting from the support toward load point as shown in Fig. (1.2).

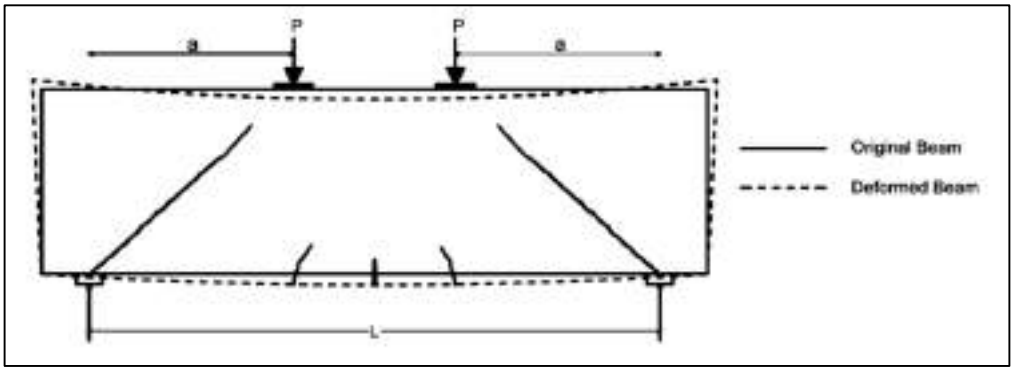

Fig. (1.2) Flexural-shear failure of deep beam.

1.3.3 Diagonal splitting failure:

This mode of failure happens when the final shear crack is initiated in the middle of the shear span and extends toward the load and support points. This mode of failure is like the splitting of a cylinder under diametrical compressive forces, as shown in Fig. (1.3).

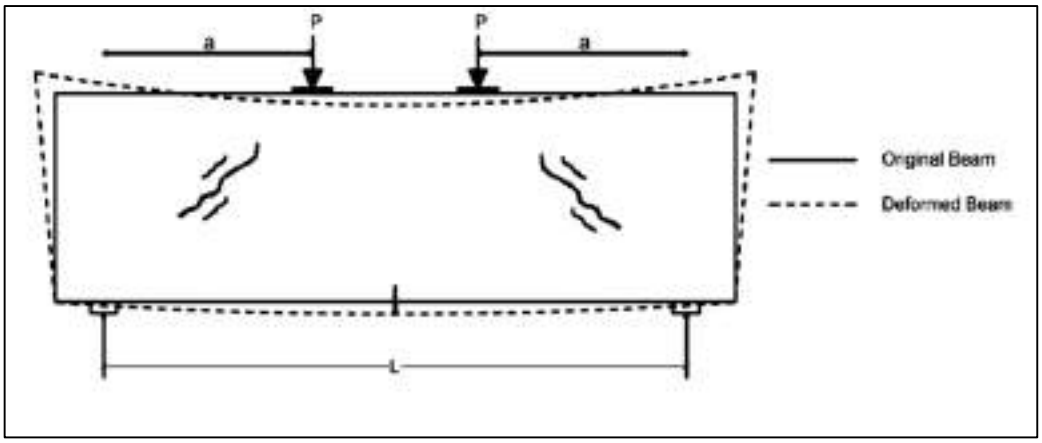

Fig. (1.3) Diagonal splitting failure of deep beam.

1.3.4 Diagonal compression failure:

This mode of failure happens when diagonal crack is initiated near the load path. After a small further increase in the load, another one is formed closer to the support than the first one and extends upwards as the load increases. The final failure occurs by the destruction of the portion of concrete between these two cracks, Fig. (1.4).

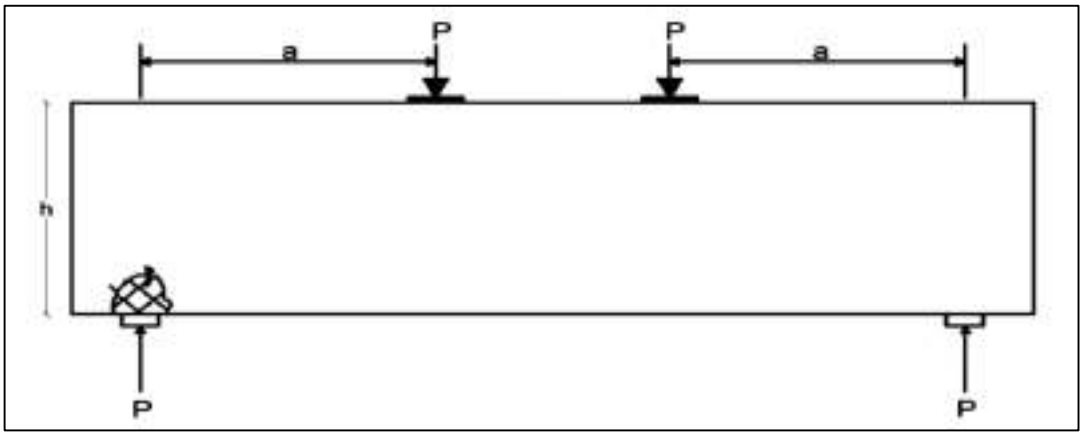

Fig. (1.4) Diagonal compression failure of deep beam.

1.3.5 Bearing failure:

This mode of failure happens either under the load regions or above the supports as a result of the development of high stresses in these regions. This mode of failure occurs in very deep beams, Fig. (1.5).

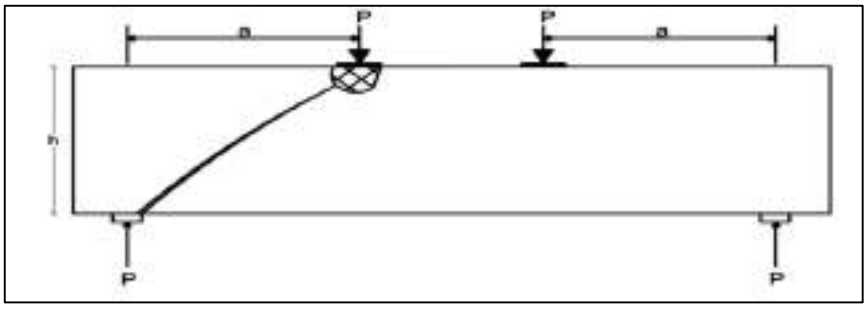

Fig. (1.5) Bearing failure of deep beam.

1.3.6 Anchorage failure:

This mode of failure happens when the strains and stresses in the steel bar near the supports increase rapidly during the formation of inclined cracks, until they are of the same order of magnitude as those occurring at mid-span. After inclined cracking, the steel strains and stresses closer to the support increase at a little greater rate than those at mid-span and become approximately constant along the span. So, if the tension steel is not properly anchored near the support, anchorage failure may happen, as shown in Fig. (1.6).

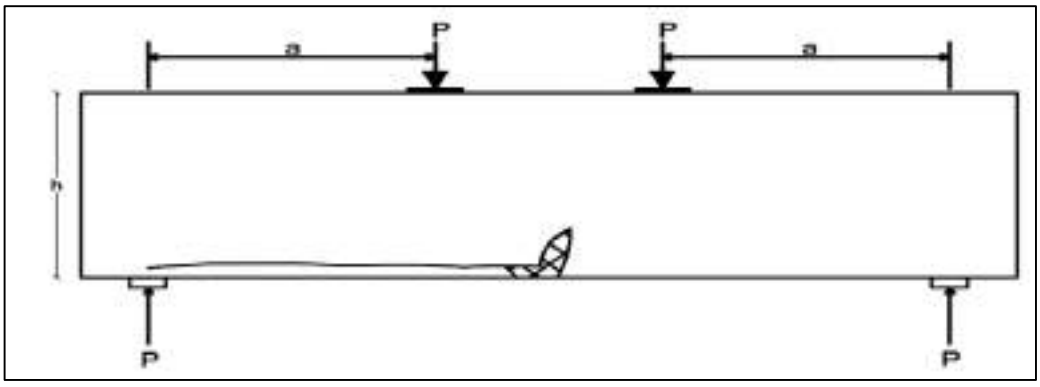

Fig. (1.6) Anchorage failure of deep beam.

1.4 Failure Modes of Deep Beams with Web Openings

The main factors affecting the behavior and performance of deep beams with web openings is similar to factors in solid deep beams in addition to Size, shape and location of web opening. [11]:

Failure modes which have been observed in the previous tests for the case of the rectangular opening are schematically presented in Fig. (1.7) below. These modes are categorized as modes A, B and C [15]:

Mode A: is the typical shear failure of a solid deep beam by diagonal cracking along the load path (the line joining the load and support bearing edges) when the opening did not intersect the load path as shown in Fig. (1.7 a). When the opening intersects the load path, failure occurs in either mode B or mode C.

Mode B: is identified by sudden collapse as a result of diagonal cracking along the two critical paths joining the loading as well as reaction points with the furthest corners of the openings as illustrated in Fig. (1.7 b)

Mode C: is the failure which occurs in a gradual manner. It is caused by deformation mainly in the shear span, with a relative rotation of three distinct segments of the beam as shown in Fig. (1.7 c).

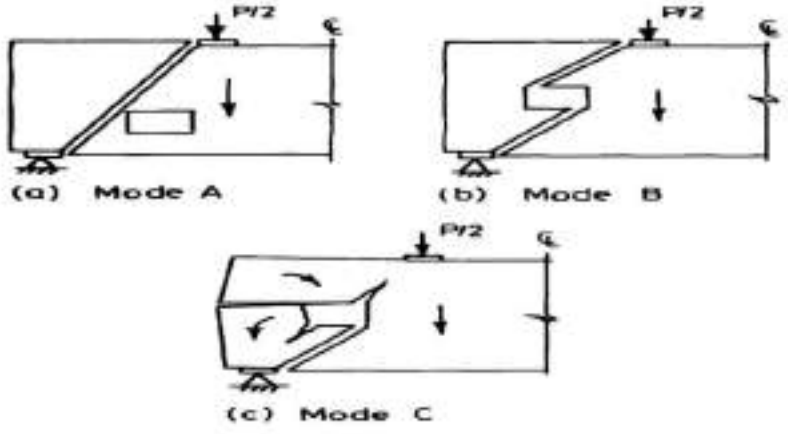

Fig. (1.7) Failure modes for deep beams with rectangular opening [15].

In deep beams with a circular opening, two failure modes are found [12]:

- The first one is marked by crack joining the bottom-most diametrical edge of the opening with support and loading point. Fig. (1.8 a) shows .
- The second one occurred along the crack joining the support and loading points and openings tangents opposite to them, Fig. (1.8 b).

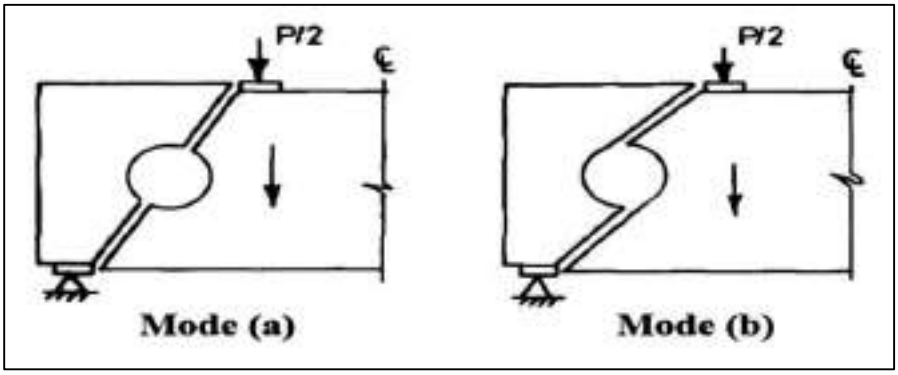

Fig. (1.8) Failure modes for deep beams with circular opening [12].

1.5 Slurry Infiltrated Fibrous Concrete (SIFCON)

SIFCON was explored by David Lankard (1984) [16]. David limited of steel fiber ratio between (5-18) % and possible to casting slurry into substrate bed of fiber.

The ACI code defined SIFCON as advanced type of fiber reinforced concrete in which formwork molds are filled to capacity with randomly-oriented steel fibers, usually in the loose condition, and the resulting fiber network is infiltrated by a cement-based slurry. Infiltration is usually accomplished by gravity flow aided by light vibration, or by pressure grouting. SIFCON composites differ from conventional steel fiber reinforcement concrete (SFRC) in at least two respects: they contain a much larger volume fraction of fibers (usually 8 to 20 volume percent), and they use a matrix consisting of very fine particles (absence of coarse aggregates in SIFCON). As such, they can be made to simultaneously exhibit outstanding strength and ductility [17].

Furthermore, SIFCON contains relatively high cement and water contents when compared to conventional concrete [16].

Table (1.1) listed difference between Lankard and ACI code in sifcon description:

Table (1.1) Listed to deference between Lankard and ACI

Items	ACI [17]	Lankard [16]
Compressive strength f´c (MPa)	21- over 140	103 - 207
Modulus od rupture f_r (MPa)	Up to 90	27 - 69
Tensile Strength f_t (MPa)	Up to 41	------
Percentage of volume fiber %	Usually (8-20)	(5-18)

All steel fiber types namely straight, hooked and crimped can be used in SIFCON. SIFCON possess [19]:

1- Excellent durability, energy absorption capacity, impact, abrasion resistance and toughness.
2- Modulus of elasticity (Ec) values for SIFCON specimens is more compared with plain concrete.
3- SIFCON exhibits high ductility.

1.6 Applications of SIFCON

Because the properties such as ductility, crack resistance and impact resistance are found to be very high in SIFCON when compared to other materials, it is the best suited material for the application in the following areas [20]:

1. Pavement rehabilitation.
2. Overlays, bridge decks and protective revetments.
3. Seismic and explosive resistant structures.

4. Primary nuclear containment shielding.
5. Repair, rehabilitation and strengthening of concrete structures and
6. Refractory applications.
7. Security concrete applications (safety vaults, storing rooms, etc.).
8. Precast impact resistance panels.
9. Heavily loaded precast slabs.
10. Missile silo structural concepts.
11. Fragment resistant walls.
12. Protective works in marine environment.

1.7 Research Objectives

Slurry infiltrated fibrous concrete (SIFCON) proves to be an innovative high performance fibrous concrete material and can be used in RC deep beams. The main objectives of the thesis are:

1- Studying the mechanical properties of SIFCON trail mixes (compressive strength, tensile strength, flexural strength, shear strength and modulus of elasticity) and determine the best mix.
2- Studying the effect of steel fiber ratio on solid deep beams.
3- Studying the effect of removing vertical reinforcement in the solid deep beams.
4- Studying the effect of (a/d) ratio on solid deep beam.
5- Studying the effect of removing mesh reinforcement in the solid deep beams.
6- Studying the effect of steel fiber ratio on deep beams with openings.
7- Studying the effect of openings reinforcement.
8- Studying the effect of openings shape.
9- Development a finite element model for conventional and sifcon deep beams and prediction the general load-deflection behavior using ANSYS 15 software.

9- To study crack pattern and failure modes of deep beams using ANSYS 15 software.

1.8 Layout of the Thesis

Chapter 1: this chapter deals with the general background to the problem, motivation for the present work, objectives of the present study and organization of the thesis.

Chapter 2: presents a detailed literature review. The literature review focuses on four different topics such as deep beam, SIFCON, and finite element modelling and analysis.

Chapter 3: deals with the materials, mix proportions and the preliminary studies on the mechanical properties of SIFCON and conventional concrete like compressive strength, flexural strength, split tensile strength and shear strength. Also it provides details of cast specimens, test setup and the testing procedure.

Chapter 4: presents the experimental of the specimens of tested deep beams and their discussions. Then, the overall behavior and the load-deflection response of the model that obtained from experimental investigation are listed with their discussions.

Chapter 5: shows cases the finite element model and the analysis RC deep beams with SIFCON using ANSYS 15 and compared with experimental work.

Chapter 6: gives the conclusions that listed from this study and the recommendations for further studies.

CHAPTER TWO

LITERATURE REVIEW

Chapter Two

LITERATURE REVIEW

2.1 General

SIFCON is a result of developing process in concrete technology. It is a new type of composite material satisfying the increasing demands for high strength, high durability, offering superior ductility and workability.

A detailed literature survey has been made on the previous works that are directly related to the present thesis.

The summary of the review is presented under the following topics:

1- Experimental and numerical investigation on solid deep beam.
2- Experimental and numerical investigation on deep beam with openings.
3- Slurry infiltrated fibrous concrete (SIFCON).
4- Strengthening Techniques with SIFCON.

2.2 Experimental and numerical investigation on solid deep beam

Kong et al. (1970) [20] carried out tests on 35 simply supported deep beams with varied clear shear span to depth ratio (a/d) from 0.23 to 0.70. The effects of seven different web reinforcement configurations on the behavior of the beams were studied. It was concluded that the suitable arrangement of web reinforcement depends on the shear span to depth ratio. For low (a/d) ratios only horizontal web reinforcement placed near the bottom was effective. Where (a/d) ratio equals 0.7 vertical stirrups were preferable.

R. Narayanan, and I.Y.S. Darwish (1988) [21] reported the results of tests on twelve reinforced concrete deep beams including eleven steel fibers contents, provided to act as web reinforcement. Three parameters were varied in the study, namely, the volume fraction of fibers, shear span-to-depth ratio and the concrete

compressive strength. Based on the test results the authors drew the following conclusions:

1- The inclusion of steel fibers in concrete deep beams resulted in enhanced stiffness and increased spall resistance at all stages of loading up to failure and reduced crack widths.
2- Deep beams of fiber concrete under shear loading develop zones of approximately zero stress in many cases over a height of 0.15 to 0.3h.
3- In general, the primary cause of failure was diagonal cracking, which led to the splitting of the beam along the diagonal cracks.
4- Both shear cracking load V_{fo} and ultimate shear load V_{uo} were influenced by the fiber factor F.

Tan and Lu (1999) [22] investigated the effect of size on reinforced concrete deep beams. The test program consisted of twelve reinforced concrete deep beams with simple clear span ℓ ranging from 1500 to 4520 mm and height h ranging from 500 to 1750 mm. They were tested under two equal symmetrically placed point loads. The (a/h) values were 0.5, 0.75 and 1. The compressive strength, f'c, of about of 40 MPa and main steel ratio (ρ_t) was 2.60 percent. Test results indicated that the ultimate shear stress of deep beams was size-dependent. Meanwhile, the diagonal cracking load was strongly size-dependent. Also, it was shown that the size effect has a great influence on the failure mode in addition to a/h ratio. While, the failure in large deep beams was more brittle than smaller ones.

Brown and Bayrak (2007) [23] investigated the influence of the load distribution and web reinforcement on deep beam behavior. The test program consisted of testing ten reinforced concrete deep beams with a simple span of 3048 mm, effective depth of 686 mm and width of 150 mm under various types of loading (uniformly distributed loads, two point loads, and concentrated load). The results

indicated that the concentrated loads type was most severe condition than uniformly distributed loads. On the other hand, a little amount of vertical web reinforcement changed the mode of failure from diagonal tension to strut crushing.

Ahmed M. Yousef et al. (2018) [24] investigated the effected of minimum shear reinforcement for ultra-high performance fiber reinforced concrete deep beams. The experimental results showed that increasing the provided vertical web reinforcement ratio has slight effect on the diagonal cracking strength and the ultimate shear strength. The maximum spacing between the vertical web reinforcement required by ACI 318-14 for reinforced concrete beams (d/5) is not suitable for ultra-high performance fiber reinforced concrete deep beams, while for the EC-2 (2b) and that required by the Egyptian code ECP-203-2017 (200 mm) was applicable.

2.3 Experimental and Numerical Investigation on Deep Beam with Openings

Kong and Sharp (1973) [25] carried out an experimental and analytical study to examine the effect of web opening on strength and cracking of a total of 24 reinforced lightweight concrete simply supported deep beams had 1500 mm span, 750 mm depth and 100 mm width. The x/h ratios were 0.25 and 0.4 where x is the distance from center of the opening to the edge of beam whereas ℓ/h was kept constant at 2. Thirteen rectangular opening with different sizes and locations established to confirmed this study. The test results indicated that the crack patterns and mode of failure depend basically on the range to which the opening intercepted the load path (line joining the load and support bearing edges) and the position at which the interception occurs regardless of the type and amount of web reinforcement. On the other hand, when the opening was located far away from the load path, the mode of failure was the same as in solid deep beam case. In addition,

the results displayed that trimming the openings with reinforcement loops did not influence the ultimate strength.

Swaddiwudhipong and Shanmugam (1985) [26] tested fifteen simply supported steel fiber reinforced concrete deep beams with rectangular web openings and compared it with established analytical solution using finite element method. The variables were the ratio of steel fiber, positions of openings, and types of loading. It was concluded that openings in deep beams should not be placed across the natural load path or too close to the side edge of the beam or in the tension zone near the support. Steel fibers was effective in providing extra shear strength to deep reinforced concrete beams. Also, the first crack loads of beams with openings could predicted with reasonable accuracy by finite elements method adopting the splitting strength of concrete as the criterion for first crack.

A. Akhtaruzzaman and A. Hasnat (1989) [27] showed the results of the tests of twenty-six concrete deep beams with and without a transverse opening tested to failure under torsion with varying span-depth ratio, concrete strength and size and location of the opening. The presence of an opening significantly reduced torsional strength. For span-depth ratios greater than 3.0, the torsional strength of beams remained practically constant. It significantly increased, however, as the span-depth ratio decreased. The crack inclinations on the beam surfaces followed a similar trend and were also influenced by concrete strength and web opening size.

Mansur et al. (1991) [28] experimentally investigated eight reinforced concrete continuous deep beams containing a large transverse opening. The beams were rectangular in cross-section and all contain the same amount and arrangement of longitudinal reinforcement. The number of spans, the size of opening and its location along the span were considered as major variables. Final failure of the beam occurred by the formation of a mechanism i.e. the formation of hinge and the two

opening ends represent the most vulnerable locations for the development of plastic hinges. Besides early cracking, the strength and stiffness of the beam decreased with an increase either in the length or depth of opening. Similarly, openings located in the high moment region produce larger deflections and result in early collapse of the beam. The authors observed that the location of opening had very little influence on cracking load but affects the load deflection response. Similarly, the opening location had no influence on the mode of failure.

Campione and Minafo (2012) [29] tested 23 simply supported deep beams to provide additional experimental results regarding the effect of circular web openings on the concrete deep beams. All deep beams had 480 mm in depth, 200 mm in width and in 820 mm length with 0.27 a/h ratio and various reinforcement arrangements with two opening locations. The results indicated that the effect of openings depends on their locations. Though, if the openings were situated in the mid-span section, they do not affect on the behavior of the deep beam. It was also shown that the ultimate strength decreased by 18-30 % when the openings were placed at the center of the shear span, and vertical stirrups increased the ultimate strength by about 15% in solid beams or beams with web opening located in the mid-span section. When the opening was located in the center of the shear span, the vertical web reinforcement had a slight effect on the strength, meanwhile, the horizontal web reinforcement increased the ultimate strength by about 20%.

Nair and Kavitha (2015) [12] investigated the effect of openings in deep beams using strut and tie model approach. Seven deep beams had a width of 200 mm, length of 800 mm and an overall height of 400 mm were tested under a point load at mid span with various position of opening as per strut and tie formation, and were analyzed in ANSYS 14 software. The results showed that, the ultimate load gained from the finite element software has only (5%) variation compared to

experimental work results. Meanwhile, deep beams with opening showed a decrease in the ultimate load carrying capacity compared to solid deep beams, whereas, deep beams containing rectangular openings showed a decrease in ultimate load carrying capacity compared with deep beams containing circular openings.

Hasan (2016) [30] constructed eleven self-compacted concrete (SCC) deep beams and tested them under symmetrically two point top loading to investigate the influence of the transverse circular opening on their behavior. The beams had 1400 mm in total length, 400 mm in depth, and 150 mm in width. The flexural reinforcement consisted of three bars with a nominal size of 16 mm while the web reinforcement was made with steel wires of 4 mm diameter spaced at 60 mm in both horizontal and vertical directions. All beams had the same concrete compressive strength of 65.57 MPa. The beams were classified into four groups in addition to the solid one according to the parameters investigated. The first group was used to examine the influence of shear span to the effective depth ratio (a/d =0.8, 1 and 1.2). The second group was used to study the varying of openings diameter d (D=75, 110 and 160 mm). While, the third group was used to study the influence of opening location (center of the load path, the upper left, and the lower right panels of the shear span). The last group was assigned to study the effectiveness of the inclined reinforcement around openings. Three amounts of inclined reinforcement were used 2, 4 and 6 steel wires of 8 mm diameter positioned above and below the openings to make 45 degrees with the longitudinal axis of the beams. The test results indicated that, when a/d was increased the ultimate load capacity decreases linearly while the deflection was increased. Furthermore, increasing the opening diameter decreases the shear cracking load and the ultimate shear strength of the beams. While mid span deflection was not considerably influenced. Also, the positioning of the opening in the lower right panel of the shear span (E-W direction) panel increases the ultimate load capacity by 6.9 % rather than when positioned in the upper left panel. While,

the shear cracking load and mid span deflection was not affected. Meanwhile, the incorporation of the inclined reinforcement around openings was found very effective in improving the shear strength and the deflection of the tested beams.

2.4 Slurry Infiltrated Fibrous Concrete (SIFCON)

David Lankard (1984) [16], described SIFCON with regard to Properties, applications, also, given some information about SIFCON and gave method of preparation of SIFCON. Lankard identified SIFCON as a highly strength and highly ductility material, also SIFCON contain volume ratio of fibers between (5-20) %. SIFCON can be used in pavement overlay, precast slabs, precast refractory shapes and impact resistant structures. Lankard described method to cast SIFCON by pre-packed steel fiber in mold then cast slurry above network of steel fiber or by Spread a steel fiber as stratum in the mold height.

Balaguru and kendzulack (1987) [31] was assessed the behavior of SIFCON in compression, tension, flexure and shear under monotonic and high amplitude cyclic loading. Dog bone specimens were used to determine the direct tensile strength and double L specimens were used to determine the shear strength of SIFCON. The author has concluded that the length of fibers does not have significant effect on strength and the addition of silica fume has increased the compressive and flexural strength and cement-sand ratio up to 1:1.5 can be used for cement slurry without affecting the strength of SIFCON.

Josifek and Lankard (1987) [32] had investigated the various properties of SIFCON like density, compressive strength, modulus of elasticity, flexural strength and freeze/thaw resistance and found that SIFCON has improved strength characteristics compared to conventional SFRC with 2% volume of fibers.

Naaman et al. (1991) [33] conducted experimental investigation on the elastic modulus of SIFCON in tension and compression. Two different types of fibers (deformed and hooked steel fibers), two different aspect ratios (60 and 100), seven different levels of

volume fractions and four different matrix compositions were used in the study. Fly ash, fine aggregate and superplasticizer were added to the cement slurry. Dog-bone shaped tension specimens and cylindrical compression specimens were used to determine the elastic modulus, the stress- strain response and the peak strength of composite. The study reveals that the value of modulus of elasticity was found to be not only dependent upon the ultimate compressive strength, but also factors such as fiber volume fraction, fiber aspect ratio, fiber orientation, alignment and testing procedure. For the range of variable tested, the ultimate strength and elastic modulus of SIFCON in tension do not seem to be very sensitive to the water-cement ratio. At a constant fiber length, the elastic modulus of SIFCON in tension was directly proportional to the volume fraction of fibers. Everything else being equal, the higher the length of the fiber, the higher was the elastic modulus of SIFCON.

Wang and Maji (1992) [34] this researcher found the shear properties from the deep beams of the sifcon and compared it with the results of the torsion cylinder. The authors have studied the anisotropy of sifcon by cutting a core from the specimen and by visual inspection of the orientation of fibers. The cylindrical core specimens were tested under pure torsion to obtain the shear strength. The orientation of fibers had a significant impact on the shear stress. The authors have correlated the shear strength with fiber content and compressive strength which provides easy means of determining shear strength from compressive strength results for certain mix designs. In deep beams, tests were conducted to obtain information on deep beams of SIFCON in shear to compare with the torsion test results. In this study, deep beams were tested to ensure that the failure was in shear rather than in flexure. Three beams were tested; however, the first beam failed at the support due to improper placement and was rejected. The second beam had an ultimate load of (680 KN) with a corresponding deflection of (6.4 mm). A visible crack originated at the loading point, at approximately 94% of the peak load and travelled down towards the support. Only one diagonal crack appeared along the line joining the support and loading points. The second diagonal crack did not appear until well after the ultimate load had been reached. It

is proposed that the torsion test provides a reliable lower-bound shear strength that may be used for design purposes.

Naaman and Baccouche (1995) [35] had analyzed the shear response of SIFCON with and without dowel reinforcement. The specimens were subjected to monotonically increasing shear loading. It was found that the addition of steel fibers greatly enhanced the shear strength and energy absorbing capacity of cement matrices. The addition of dowel bars to SIFCON has increased the maximum shear strength up to 15 percent. The shear strength of dowel reinforced SIFCON was found to be 2.7 to 3.5 times more than that of dowel reinforced concrete. The energy absorption capacity at the failure of SIFCON specimens was found to be 5.6 to 12.2 times more than that of dowel reinforced concrete specimens. Reinforcement concrete (RC) specimens experienced multiple cracking and spalling of concrete well before the ultimate loading whereas the SIFCON specimens did not suffer any spalling even though they were subjected to much higher stresses and shear displacements.

Balasubramanian et al. (1997) [36] concluded that SIFCON possesses high torsional strength when compared with FRC specimens. 'Z' shaped SIFCON and FRC specimens were used to find the torsional strength. Three different types of fibers were used in the study. For SIFCON specimens, fiber content by volume was varied from 6% to 8% for straight fibers and was maintained at 6 % for both crimped and trough shaped fibers. For FRC specimens, 1% fiber volume fraction was used. The test was designed in such a way that the specimen could freely rotate due to the applied torque. The study revealed that the torsional strength was maximum at a fiber content of 6 % and decreased with the increase in fiber content thereafter. For specimens with straight fibers, the torsional strength increased with an increase in aspect ratio.

Thirugnanam et al. (2002) [37] had studied the flexural behavior of conventional RC, FRC and SIFCON beams. The study reveals the advantages of using SIFCON in structural members with respect to ductility and energy absorption characteristics. The author had also investigated the use of SIFCON only in the hinges zones of the flexural members. The results proved that the use of SIFCON may be restricted only in the selected fuse locations of flexural members.

Sashidhar et al. (2005) [38] have investigated the properties of SIFCON such as compressive and tensile strength at elevated temperatures. Three different volume fraction of fibers were used (8, 10 and 12%). The properties were studied at three different temperatures (100C^o, 200C^o and 300C^o) and at three different exposure timings (4, 6 and 8 hours). The compressive strength and tensile strength of SIFCON were found to be increased when the specimens were exposed to 100C^o for 4 hours. At a temperature of 200C^o and more the compressive and tensile strength of SIFCON decreased. Further, the strength of SIFCON decreased as the exposure duration increased.

H. Sudarsana Rao, N. V. Ramana (2005) [39], in their paper entitled 'Behavior of slurry infiltrated fibrous concrete (SIFCON) simply supported two-way slabs in flexure' have reported the information on behavior of two-way slabs in flexure. Slurry infiltrated fiber concrete (SIFCON) is one of the recently developed construction material. SIFCON could be considered as a special type of fiber concrete with high fiber content. The matrix consists of cement slurry or flowing cement mortar. This composite material has already been used for structures subjected to blast loading, repair of pre-stressed concrete beams and safe vaults'. Flexure and cyclic load tests have been conducted and compared with fiber reinforced concrete (FRC) and plain concrete slabs. Both strength and deflection characteristics have been studied.

Rao et al. (2008) [40] had proposed a regression model analysis for estimating the punching shear strength of reinforced SIFCON slabs by conducting a detailed study on the behavior of SIFCON two-way slabs in the punching shear. The results are compared with FRC and conventional RC slabs. SIFCON slabs were cast with 8, 10 and 12% fiber volume fraction and for FRC slabs the fiber volume fraction was 2%. Square slabs of size 600 x 600 x 50 mm were used as test specimens. It was concluded that the ultimate punching shear load of SIFCON with 12% fiber volume fraction was nearly 12 times more than that of conventional RC specimens and 10 times more than that of FRC specimens.

Farnam et al. (2010) [41] had compared the triaxial compressive behavior of high strength concrete, high performance fiber reinforced concrete and SIFCON and found that SIFCON has unique triaxial compression characteristics such as high ductility, high triaxial compressive strength and hardening behavior. The test was conducted on 75 mm x 150 mm cylindrical specimens with different fiber volume fractions (0, 2, 5 and 10%). The test was conducted under four confining pressure levels (0, 5, 15 and 21.5 N/mm2) according to triaxial conditions. The results indicated that the increase in fiber volumes increased the peak stress, energy absorption, toughness and Poisson's ratio while increasing confining pressures increased the peak stress, energy absorption and toughness.

SudarsanaRao H. et al. (2010) [42] have investigated the behavior of slurry-infiltrated fibrous concrete (SIFCON) slabs under impact loading. Fiber-reinforced concrete (FRC), reinforced cement concrete (RCC) and plain cement concrete (PCC) slabs were also cast and tested for comparison purposes. The impact force was delivered with a steel ball drop weight. The test results revealed that SIFCON slabs with 12% fiber volume fraction exhibit excellent performance in strength and energy-absorption characteristics when compared with other slab specimens.

Regression models have been developed to estimate the energy absorption for SIFCON slab specimens.

Murat Tuyan and Halit Yazıcı (2012) [43] had studied "Pull-out behavior of single steel fiber from SIFCON matrix", In this experimental study, the effect of mix proportions of SIFCON matrix (slurry), curing conditions, aspect ratio of steel fiber, embedded length and fiber type on the single fiber pull-out behavior from SIFCON matrix was investigated. Test results indicated that fiber type, embedded length of fiber, curing conditions, fiber end condition, and matrix strength has a considerable effect on fiber–matrix bond. Increasing the diameter of the fiber and improving the curing conditions increased matrix–fiber bond. In addition, increasing bond strength was observed with increasing strength of SIFCON matrix. The pull-out toughness increased by increasing embedded length of fiber. It has been observed that hooked end fibers have shown better interface bond compared to the smooth fibers.

Ahsanollah Beglarigale et al. (2016) [44] Carried out a study the investigation of the flexural performance of SIFCON composites subjected to high temperature. Due to synergistic interaction of different mechanisms, mechanical performance can be lowered especially for the multi-component composite materials exposed to high temperature. Standard or steam cured slurry infiltrated fiber concrete (SIFCON) and slurry specimens were subjected to 300, 600, 750 and 900 C^o in the scope of present study. Exposing the specimens to 300 C^o enhanced the mechanical performance, while higher temperatures have detrimental effects on the SIFCON composites such as the loss in the cross section of steel fibers and the destruction of C–S–H structure.

2.5 Strengthening Technics with SIFCON

Shannag et al. (2001) [45] had studied the structural behavior of shear deficient RC beams repaired with SIFCON and presented a simple analytical procedure for predicting the shear capacity of the repaired beams. Shear deficient

RC rectangular beams were strengthened by externally applied SIFCON jackets. The specimens were tested under third-point (monotonic) loading. The parameters such as shear span to effective depth ratio, amount of longitudinal reinforcement and the thickness of SIFCON jacket were investigated. The study revealed that the use of SIFCON jackets as external shear reinforcement eliminated the brittle shear failure and increased the ultimate shear strength of the repaired beams from 25 -55 % and that SIFCON might be used as an effective material for the repair and rehabilitate programmer of concrete structures.

Rajai Z.Al-Rousan and Mohammad J.Shannag (2018) [46] had studied "shear repairing and strengthening of reinforced concrete beams using SIFCON" The experimental part of the study was divided into three stages. The first stage involved testing of thirteen shear deficient beams under four-point loading as control beams taking into account the effect of shear span-to-effective depth ratio (a/d = 1.2, 2.2, and 3.0) and amount of longitudinal reinforcement (ρ = 1.29%, 1.76%, and 2.28%). The second stage involved four shear deficient beams strengthened with SIFCON. For purpose of comparison, two of the tested control beams with a/d of 2.2 and ρ of 1.76% and 2.28% were repaired with SIFCON jacket. The test results indicate that all the beams strengthened with SIFCON jackets displayed an excellent shear capacity. The use of SIFCON jackets as external shear reinforcement eliminated the brittle shear failure and increased the ultimate shear strength of strengthened beams from 37 to 53%. Therefore, SIFCON jacket can be considered as a promising material for strengthening and repairing of RC structures. Finally, an analytical model was proposed for predicting the shear behavior of the strengthened RC beams with SIFCON Jackets with an acceptable error of less than 30%.

2.6 Concluding Remarks

The following concluding remarks are made from the existing literature in the area of RC deep beams: with and without openings and the area of sifcon:

1- While a few studies on fiber-reinforce solid deep beams are available in the refereed previous literature, no such information available on SIFCON in solid deep beam just (Wang 1992), so there is a little information available.
2- There is no research dealing with the behavior of reinforced SIFCON deep beams with opening.

CHAPTER THREE

EXPERIMENTAL WORK

Chapter Three

Experimental Work

3.1 Introduction

This chapter describes the properties of materials, mix proportions, casting and curing, fresh and hardened properties of SIFCON, deep beams with SIFCON and testing procedure.

3.2 Material Properties

3.2.1 Cement

Ordinary Portland cement (type I) is used during this work, named Karasta. It is stored in dry place to avoid exposure to undesirable atmospheric conditions. The chemical and physical properties of the cement are illustrated in Tables (3.1) and (3.2), respectively. The obtained results indicate that the adopted cement complies with the requirements of the Iraqi Standard Specifications IQS NO.5/1984 [47].

Table (3.1) Chemical composition of cement with IQS 5/1984 limitations.

Compound Composition	Chemical Composition	% By Weight	Limits of Iraqi Specification No. 5/1984[48]
Lime	CaO	63.96	-
Silica	SiO2	21.32	-
Alumina	Al2O3	4.58	-
Iron Oxide	Fe2O3	3.25	-
Magnesia	MgO	2.44	≤ 5
Sulfate	SO3	2.32	≤ 2.8
Loss on ignition	L.O.I	3.61	≤ 4
Insoluble residue	I.R	1.17	≤ 1.5
Lime saturation factor	L.S.F	0.75	(0.66-1.02)%
Tricalcium Silicate	C3S	50.69	-
Dicalcium Silicate	C2S	18.28	-
Tricalcium Aluminate	C3A	8.14	-
Tetracalcium Alumminoferrite	C4AF	9.89	-

Note: All tests were conducted by laboratory of Amara technical institute.

Table (3.2) Physical properties of cement compared with IQS 5/1984 limitations.

Physical Properties	Test Results	Limits of Iraqi Specification No. 5/1984[47]
Fineness Using Blaine Air Permeability Apparatus (m^2/kg)	382	≥230
Setting Time Using Vicat's Method **Initial (hrs: min)** **Final (hrs: min)**	 2: 00 3: 45	 ≥ 45 min ≤ 10 hrs
Soundness Using Autoclave Method	0.22	<0.8
Compressive Strength of Mortar **3 Days (MPa)** **7 Days (MPa)** **28 Days (MPa)**	 21.2 27.8 34.7	 ≥ 15 ≥ 23 -

Note: All tests were conducted by Technical Institute Laboratories in Amara.

3.2.2 Fine Aggregate

Natural sand from Gabal Sanam region in Basrah- Iraq was used in concrete mixes in this work. Table (3.3) and Figure (3.1) show the sieve analysis results, whereas Table (3.4) illustrates the physical and chemical properties of the fine aggregate used. The gained results show that the fine aggregate grading and the sulfate content are within the limits of Iraqi Specification No. 45/1984 [48].

Table (3.3) Sieve Analysis of fine aggregate.

Size (mm)	Passing %	Passing min and max according IQS 45/1984 for Zone (3)[48]
10	100	100
4.75	95.6	90-100
2.36	87.73	85-100
1.18	78.04	75-100
0.6	65.6	60-79
0.3	18.4	12-40
0.15	2.4	0-10

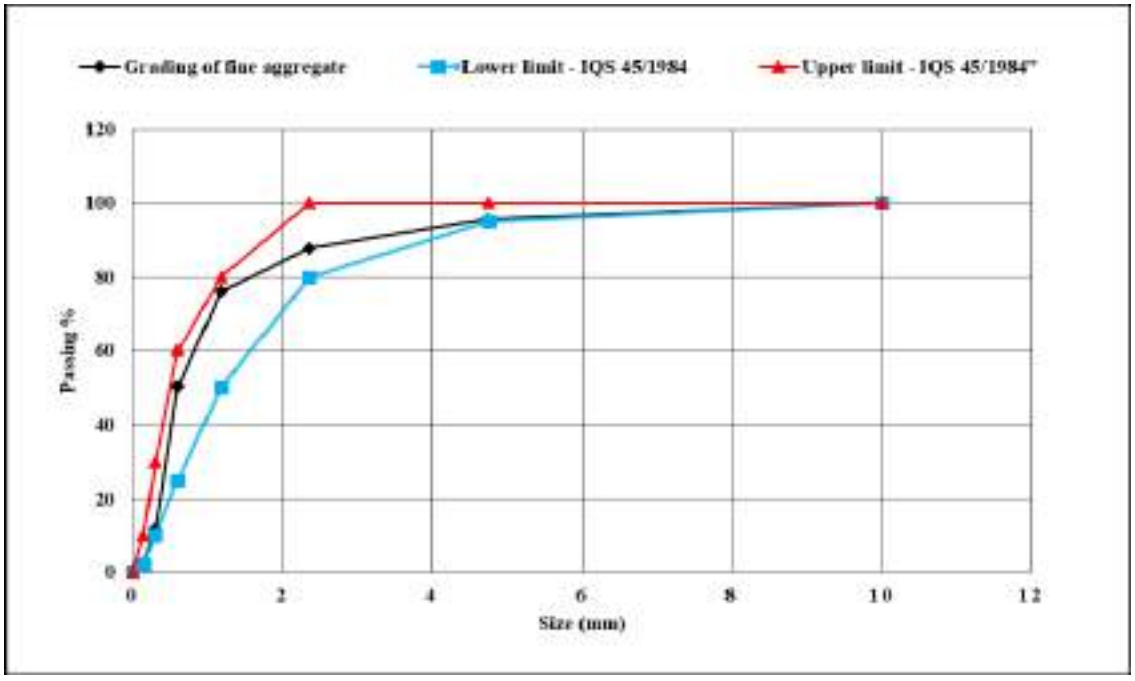

Figure (3.1) Grading of fine aggregate.

Table (3.4) Physical and chemical properties of fine aggregate.

Physical Properties	Test Results	Limits of Iraqi Specification No. 45/1984 [48]
Specific Gravity	2.56	-
Sulfate Content %	0.13	≤ 0.5 %
Absorption %	0.75	-

3.2.3 Coarse Aggregate

Crushed gravel (passing sieve 12mm) from Chlat region was used. Grading of this aggregate is shown in Table (3.5) and figure (3.2). Physical and chemical test results are presented in Table (3.6). The results show that the coarse aggregate grading is within the requirements of Iraqi Standard IQS No.45/1984 [48].

Table (3.5) Grading of coarse aggregate.

Physical Properties	Test Results	Limits of Iraqi Specification No. 45/1984 [48]
Specific Gravity	2.55	-
Sulfate Content %	0.045	0.1 max
Absorption %	0.73	-

Table (3.6) Physical and chemical properties of coarse aggregate.

Size (mm)	Passing (%)	Passing min and max according to IQS No.45/1984
14	100	90-100
10	78	50-85
5	6.5	0-10

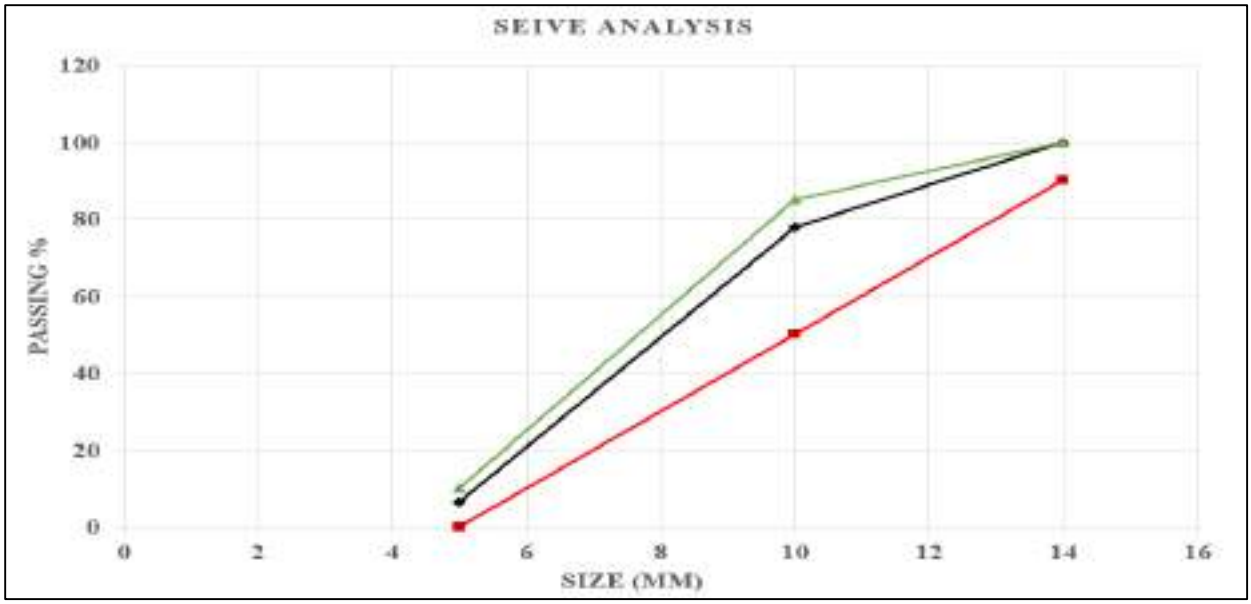

Figure (3.2) Grading of coarse aggregate.

3.2.4 Water

Reverse Osmosis (R.O.) water was used for mixing and curing all the concrete specimens used in this research.

3.2.5 High Range Water Reducing Admixture

A superplasticizer commercially named Flocrete PC 260 which confirms to ASTM C494-99[49] type A and G was used in the mixes. It has been primarily developed for producing high performance concrete, self-compacting concrete and mortar, and for concrete production in hot and windy weather with extended workability time. It is almost free from chlorides. Flocrete PC 260 is a high performance superplasticizer admixture based on polycarboxylic ether polymer with long chain specially designed to enable the water content of concrete to perform more effectively. This effect can be used in high strength concrete and flowable concrete mixes, to achieve highest concrete durability and performance. Table (3.7) shows the technical description of Flocrete PC260.

Table (3.7) Technical description of Flocrete PC 260

Chemical Base	Modified polycarboxylates based polymer
Appearance / Colors	light yellow liquid
freezing point	-7◦c approximately
Specific gravity@ 25◦c	1.1± 0.02
air entrainment	Typically, less than 2% additional air is entrained above control mix at normal dosages
Dosage	0.5 to 4.0 liter per 100 kg of cement
Storage Condition / Shelf Life	12 months if stored at temperatures between 2◦c and 50◦c

* Supplied by the manufacturer.

3.2.6 Silica Fume

A grey densified grade 920 D silica fume (which is a product from the manufacture of silicon or ferro-silicon metal) was used, which imported from the Elkem company in UAE. Silica fume are an extremely fine powder, as shown in plate (3.1), its particles hundreds of times smaller than cement particles, always used in 15 to 25% by of cement [50], as partial replacement of cement or as an additive (as used in the present work) to enhance concrete properties. Chemical composition of silica fume used in this investigation is shown in Table (3.8). The used silica fume conforms to the chemical and physical requirements of ASTM C1240-04[51] as shown in Tables (3.9).

Plate (3.1) Sample of silica fume used in present investigation.

Table (3.8) Chemical Analysis of Silica Fume

Oxide composition	Oxide content %
SiO_2	86.46
Al2O3	1.6
Fe2O3	1.11
Na2O	0.3
K2O	1.9
CaO	1.8
MgO	1.9
SO3	0.25
L.O.I.	4.02

Table (3.9) Chemical and Physical Requirements of Silica Fume ASTM C 1240-04.

Requirement	Analysis %	Limit of specification requirement ASTM C 1240
Moisture content	0.72**	<3.0
L.O.I	4.02*	<6.0
Percent Retained on 45µm (No.325) Sieve, Max.	8	<10
Accelerated Pozzolanic Strength Activity Index with Portland Cement at 7 days, Min. Percent of Control	129.1	>105
Specific Surface, Min, cm^2/g	210000	>15

*Tests were carried out at the General Company of Geological Surveying and Mining.

**According to its certificate of conformity.

3.2.7 Hooked-End Steel Fiber (HESF)

Throughout this work, two type of hooked-end steel wire fibers was used as in plates (3.2 and 3.3). This type of steel fiber is manufactured by Dramix® Company,imported from Turkey. According to ASTM-A820 [52], this type of steel

fiber is classified as (Type II). The properties of the steel fibers are presented in Table (3.10).

Plate (3.2) Steel fiber with Aspect ratio (Lf/Df) = 60

Plate (3.3) Steel fiber with Aspect ratio (Lf/Df) = 55

Table (3.10): Properties of steel fiber with aspect ratio = 60 and 55

Aspect Ratio = 60	
Property	**Specifications**
Density	7860 kg/m^3
Ultimate strength	1150 MPa
Modulus of Elasticity	200x10^3 MPa
Poisson's ratio	0.28
Average length	60 mm
Nominal diameter	1.0 mm
Aspect ratio (L_f/D_f)	60
Aspect Ratio = 55	
Property	**Specifications**
Density	7860 kg/m^3
Tolerances average (+ or -)	7.5%
Ultimate strength	1345 MPa
Modulus of Elasticity	200x10^3 MPa
Poisson's ratio	0.28
Average length	30 mm
Nominal diameter	0.55 mm
Aspect ratio (L_f/D_f)	55

*Data sheet of hooked-steel fiber for two type.

3.2.8 Steel Reinforcement

Deformed longitudinal steel bars was used in this study with nominal diameter of 16 mm and 10 mm while, deformed steel wires of diameter 4 mm were utilized for both vertical and horizontal shear reinforcement. Deformed steel wire of 10 mm in diameter was used as inclined reinforcement around openings. Table (3.11) illustrates the properties of steel bars utilized. Tensile tests of the steel bars and wires were carried out according to ASTM A370-14 [53] using three specimens for each diameter. The test was performed at the University of Misan Laboratories, plate (3.4) shows testing machine for tensile strength test of steel bars. Test results indicated that the adopted steel reinforcement complies with the requirements of ASTM A615/615M-14 [54] for grade 60 bars of minimum yield strength fy = 420 MPa, tensile strength fu = 620 MPa and elongation = 9%. Also the deformed wire reinforcement conforms to the requirements of ASTM A1064/A1064M-14[55] which recommended minimum values for fy and tensile strength fu of 515 and 585 MPa, respectively.

Table (3.11) Tensile test results of steel reinforcement.

Bar diameter mm	Actual diameter mm	Area mm^2	Yield strength MPa	Tensile strength MPa	Elongation %	Maximum Gap (Chord of 12.5 % of Nominal Perimeter)
16	15.95	199.7	595	680	18	6.1
10	9.95	78.5	576	655	12.5	3.6
4	4.5	15.9	548	629	9.5	-

Plate (3.4) Testing machine available at the laboratory civil engineering department, university of Maysan.

3.3 SIFCON Mix Design

Three mixes of SIFCON were made, according to components of these mixes. Six cubes (100 x 100 x 100) mm were cast for testing of compressive strength, three cylinders (100 x 200) mm for testing of tensile strength, three prisms (500 x 100 x100) mm for testing flexural strength and three double L shape for testing shear strength at 28 days for all, plate (3.5). Normal mix also was cast for comparison purposes. Table (3.12) showed the mix proportions.

Plate (3.5) Casting and testing of sifcon specimens

Table (3.12) Mix proportions.

items	Mix 1	Mix 2	Mix 3	Mix 4
Cement kg/m³	1000	1000	1000	1000
Fine Sand kg/m³	1000	1000	1000	1000
Silica fume from cement kg/m³	100	150	200	-
Water kg/m³	350	350	350	400
superplasticizer pc260 % from cement kg/m³	50	50	50	-
Steel fiber kg/m³	471	588	706	-
Gravel kg/m³	-	-	-	1100

3.4 Preferable Fiber Aspect Ratio

Program of work consist of casting (3 cubes, 3 cylinders, 3 prisms and 3 double L Shapes) for each aspect ratio with one trail of mix (mix 3). Table (3.13) below listed result average of tests:

Table (3.13) The difference between aspect ratio 55 and 66.

Items	Aspect ratio = 55	Aspect ratio = 60
Compressive strength (MPa)	82	78.4
Tensile strength (MPa)	14.5	18.7
Flexural Strength (MPa)	35.1	54.5
Shear Strength (MPa)	45	62.3

It is clear from the table of test results that steel fiber with (aspect ratio = 60) show high results and easy in cast of sifcon specimens. Deficiency in workability of mix and steel fiber with aspect ratio equal to 55 is the main factors that influence in infiltration of the slurry to the fiber network. High-range water-reducing admixtures (superplasticizers) are used in order to improve the workability of the slurry to ensure complete infiltration without increasing the water-cement ratio (W/C). The dosage of superplasticizers has the greatest effect on fluidity, cohesiveness and penetrability of cement slurries. In the case of fine steel fiber, if fiber is distributed to full depth of mold this may be lead to prevent infiltrate slurry to the fiber network because it reduces pores between fibers. Plate (3.6) shown some failed samples.

Plate (3.6) Failed samples due to the lack of fluidity of slurry.

3.5 Mechanical Properties of SIFCON

3.5.1 Fresh concrete

3.5.1.1 Slump flow test

Sifcon mix consider self-compacted concrete (SCC) because high fluidity to ensure complete infiltration through fiber network, so one of the tests of SCC is slump flow. It done by a slump cone put in square plate with thickness at least 2 mm. Slump tests were carried out to determine the fluidity of all mixes as shown in Figure (3.3). The test is done by measure time to 500mm flow, drawing a circle 500mm in diameter is recommended [57], as shown in Table (3.14):

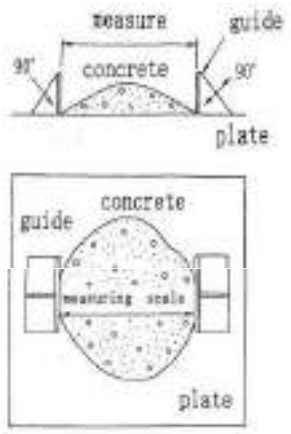

Figure (3.3) Slump flow measurement.

Table (3.14) Test result of slump flow test.

Test method	Result	EFNARC Limits [56]	ACI237R-07 Limits [57]
Slump flow (mm)	670	650-800	450-760
T_{50} (sec)	3	2-5	2-5

3.5.1.2 L- Box flow test method

The standard L-Box flow tester shall be a device made of steel having shapes and dimensions as shown in **Figure (3.4)**.

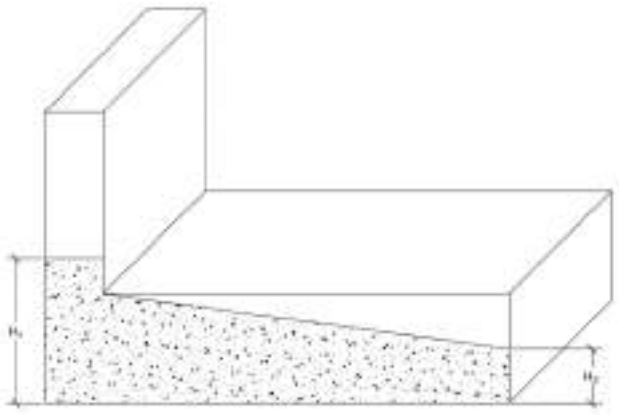

Figure (3.4) Shapes and dimension of L-type flow tester

L-Box flow tester shall have a sliding gate to prevent the flow of concrete at the time of charging. The sliding gate shall be made of a material that is not deformed or damaged during concrete charging or when raised. The test is done by measure the maximum L-flow and subsidence to the nearest 1 mm and round off to the nearest 5 mm as shown in **Table (3.15).**

Table (3.15) Test result of L-type flow test.

Test method	Result	EFNARC Limits [56]	ACI237R-07 Limits [57]
L-Box (H_1/H_2)	0.9	0.8-1	0.8-1

3.5.2 Hardened Concrete Testing

3.5.2.1 Compressive Strength (f_{cu})

The compressive strength was obtained by testing six cubes for all trails according to BS 1881 - 116: 1983, as given in **Table (3.16) and Plate (3.7)**.

Table (3.16) Test results of compressive tests.

Trail 1	**7 days (MPa)**			**average**
	52.9	51.9	55.0	53.3
	28 days (MPa)			
	58.1	62.0	63.0	61.0
Trail 2	**7 days (MPa)**			
	56.7	60.1	57.2	58.0
	28 days (MPa)			
	60.3	65.6	67.2	64.4
Trail 3	**7 days (MPa)**			
	74.2	75.2	73.5	74.3
	28 days (MPa)			
	81.8	81.1	80.4	81.1
Trail 4	**7 days (MPa)**			
	28.7	28.1	29.9	28.9
	28 days (MPa)			
	42.4	44.0	43.4	43.4

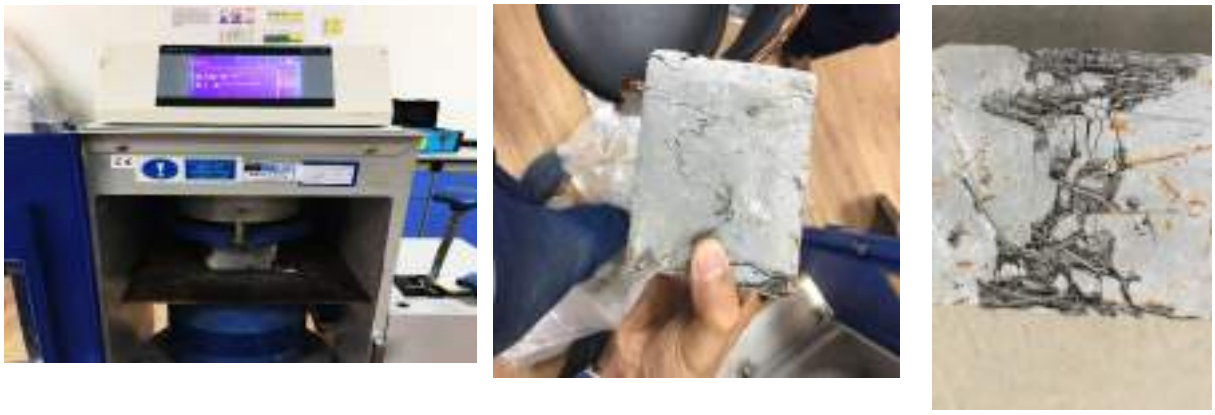

Plate (3.7) Compression Testing Machine.

3.5.2.1.1 Modulus of Elasticity

Measurements of static modulus of elasticity of concrete (E_c) were carried out according to ASTM C469-02 [58] using three concrete cylinders of 150 × 300 mm for trail3. This test was performed with the same type of machine used for compression

test, as shown in Plate (3.8). The modulus of elasticity, is the slope of the straight line drawn from the origin through the point of 0.4 fc′. The value of modulus of elasticity is 43531 MPa for mix 3. Figure (3.5) shown stress – strain curve:

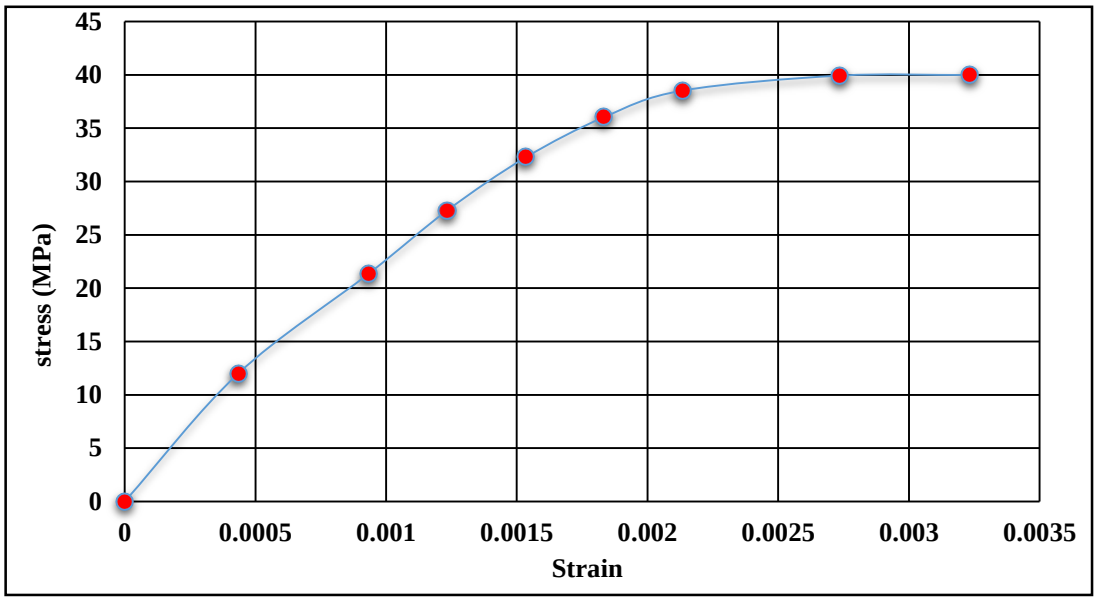

Figure (3.5) Compressive stress – strain curve for normal mix concrete

Plate (3.8) Concrete modulus of elasticity test.

3.5.2.2 Splitting Tensile Strength (f_t)

Splitting tensile strength test was conducted on 200x100 mm concrete cylinders according to ASTM C496/C496M -11 [59]. The test was carried out with the same type of machine used for compressive test at the laboratories of civil Engineering Department, University of Missan as shown in plate (3.9). Testing was performed at 28 days and average result respectively. The average value of three specimens for each mix and age was determined and recorded. Table (3.17) list the results for all trails.

(a) **(b)** **(c)**

Plates (3.9a, b and c) Digital compression machine used for concrete splitting tensile strength test with failure samples.

Table (3.17) Test results of splitting tests.

Trail 1	**28 days (MPa)**			**average**
	13.1	13.8	13	13.3
Trail 2	**28 days (MPa)**			15.6
	14.9	16.6	15.2	
Trail 3	**28 days (MPa)**			18.5
	19.4	18	18.2	
Trail 4	**28 days (MPa)**			2.8
	3.8	2.2	2.4	

3.5.2.3 Flexural Strength (f_r)

A prism specimen with dimensions of 100×100×500 mm was used throughout this test. Prisms are tested using the one-point loading with simple span between support of 450 mm according to the ASTM C293 – 02 [60] using MIE type testing machine from MARUI company as shown in Plate (3.10). Testing was conducted at ages of 28 days, see Table (3.18).

Plate (3.10) Testing machine and some samples tests.

Table (3.18) Test results of flexural tests.

Trail 1	**28 days**			**average**
	30.72	28.39	32	30.4
Trail 2	**28 days**			
	38.42	36.26	39.29	38
Trail 3	**28 days**			
	56.8	54.62	55.2	55.5
Trail 4	**28 days**			
	5.57	6.48	5.6	5.5

3.5.2.4 Shear Strength (V_s)

Double L shear specimens proposed by Balaguru (1987) [31] were used to define the shear strength. The schematic representation of the specimen and fabrication are shown in Plate (3.11). The test is done by compressive machine by apply concentrated load on upper plate in the direction of shear plane. Shear strength is obtain by divided applied load on area of shear plane.

$$Vs = \frac{P}{A} \qquad \ldots\ldots\ldots\ldots \quad 3.1$$

P = Applied load.

A = Area of Shear plane.

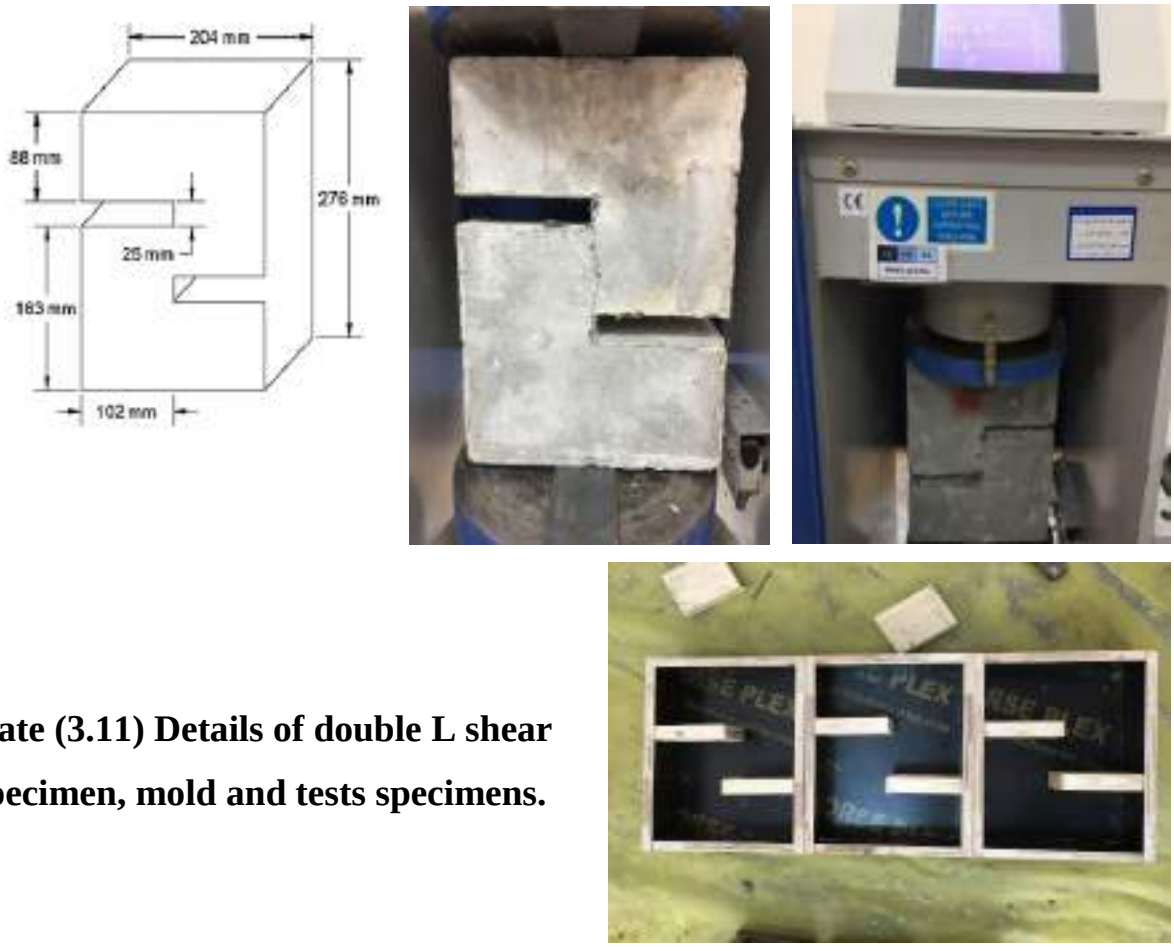

Plate (3.11) Details of double L shear specimen, mold and tests specimens.

Table (3.19) shown below result of test:

Table (3.19) Result of double L shear test.

Trail 1	**28 days**			**average**
	38.48	35.92	37.48	37.3
Trail 2	**28 days**			45.1
	43.76	44.96	46.72	
Trail 3	**28 days**			61.8
	59	62.16	64.12	
Trail 4	**28 days**			6.9
	7.32	5.24	8	

3.6 SIFCON Deep Beams

An experimental work was carried out to examine the behavior of slurry infiltrated fibrous reinforced concrete deep beams with and without openings. The study consists of constructing and testing two groups:

1- **First group:** testing of eight solid deep beams.

2- **Second group:** testing of eight deep beams with openings.

All deep beams are with an overall height (h = 320 mm), width (b = 110 mm), total length (L = 1000 mm) and clear span (L_n = 770 mm) which gives L_n/h ratio equal to 2.406, which is less than 4 that recommended by the provision of ACI 318M-14 code [3]. According to ACI code, deep beam can be design by strut and tie method. The main longitudinal tension reinforcement consisted of two deformed steel bars having a nominal diameter of 16 mm and one deformed steel bar having nominal diameter

of 10 mm. Web shear reinforcement made with 4 mm diameter deformed steel wires distributed at a spacing of 50 mm c/c in both vertical (Sv) and horizontal (Sh) directions to control cracking [3]. The diameter of openings was chosen 75 mm. To prevent local crushing of concrete at load and bearing points, steel plates of 110 mm length, 50 mm width and 20 mm thickness were used. Details about the tested deep beams are listed in Tables (3.20) and (3.21). Deep beams notation consisted of three parts; the first part indicates the number of the group; the second part represents the type of the mix; and the third part represents the number of deep beam. Thus, the number of the group is (G1), the type of the mix is (N) for Normal, (S) for SIFCON, and the number of deep beam is (A1).

Table (3.20) Details of Solid deep beams.

	Deep beam No.	Steel fiber ratio %	a/d ratio	Reinforcement
Group 1	**NA1**	0	0.9	As shown in fig. 3.6
	SB1	6%	0.9	As shown in fig. 3.7
	SB2	7.5%	0.9	As shown in fig.3.7
	SB3	9%	0.9	As shown in fig. 3.7
	SC1	9%	0.9	without vertical web reinforcement as fig.3.8
	SD1	9%	1.08	As shown in fig. 3.9
	SD2	9%	0.727	As shown in fig. 3.10
	SE1	9%	0.9	Without main and web reinforcement fig.3.11

Table (3.21) Details of deep beams with openings.

	Deep beam no.	Steel fiber ratio %	a/d ratio	Inclined reinforcement	Shape of opening	Distance from edge side to opening center (mm)	Reinforcement of deep beam
Group 2	**NA1**	0	0.9	------	Circular opening 75 mm	220	As shown in fig.3.12
	SB1	6%	0.9	------	Circular opening 75 mm	220	As shown in fig.3.13
	SB2	7.5%	0.9	------	Circular opening 75 mm	220	As shown in fig.3.13
	SB3	9%	0.9	------	Circular opening 75 mm	220	As shown in fig.3.13
	NC1	0	0.9	2ϕ10mm	Circular opening 75 mm	220	As shown in fig. 3.14
	SC2	9%	0.9	2ϕ10mm	Circular opening 75 mm	220	As shown in fig. 3.14
	SE1	9%	0.9	------	Square opening 70 * 70 mm	220	As shown in fig. 3.15
	SE2	9%	0.9	------	Triangular opening	220	As shown in fig. 3.16

3.6.1 First group (Solid deep beams)

All the dimension of beams in mm, reinforcement size in mm and all unit of forces in kn

Group A (Normal concrete): This group consists of one solid deep beam (G1NA1), is cast of normal concrete with main and web reinforcement as shown in **figure (3.6)**:

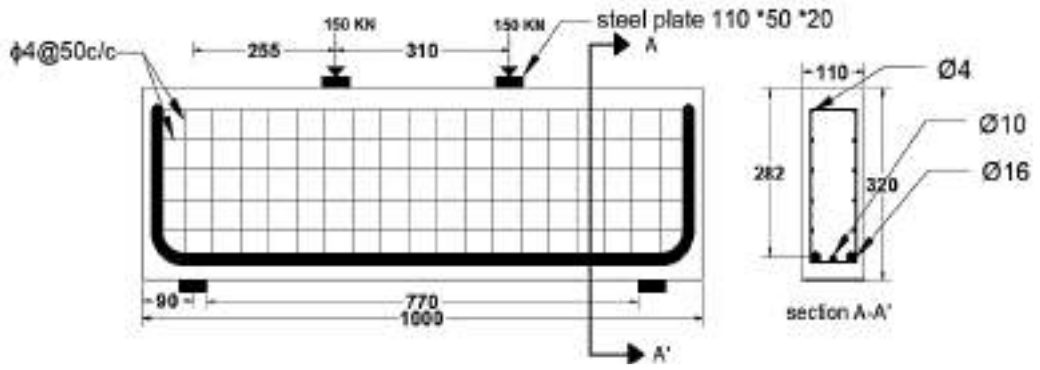

Figure (3.6) Details of (G1NA1).

Group B – Variation of steel fiber ratio:

To study the effects of the fiber volumetric ratios. Three deep beams (G1SB1, G1SB2 and G1SB3), with steel fiber percent of (6%, 7.5%, and 9%) were constructed, **figure (3.7).**

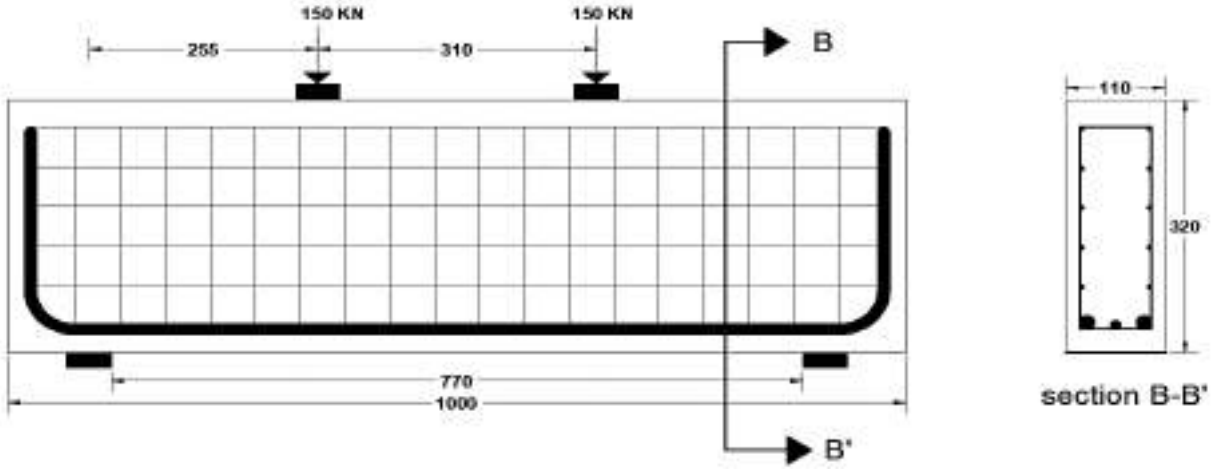

Figure (3.7) Details of (G1SB1, G1SB2 and G1SB3)

Group C - Removal of vertical web reinforcement:

The third group has one deep beams (G1SC1) with removal of vertical web reinforcement and compared it with (G1SB3) as shown in figure (3.8):

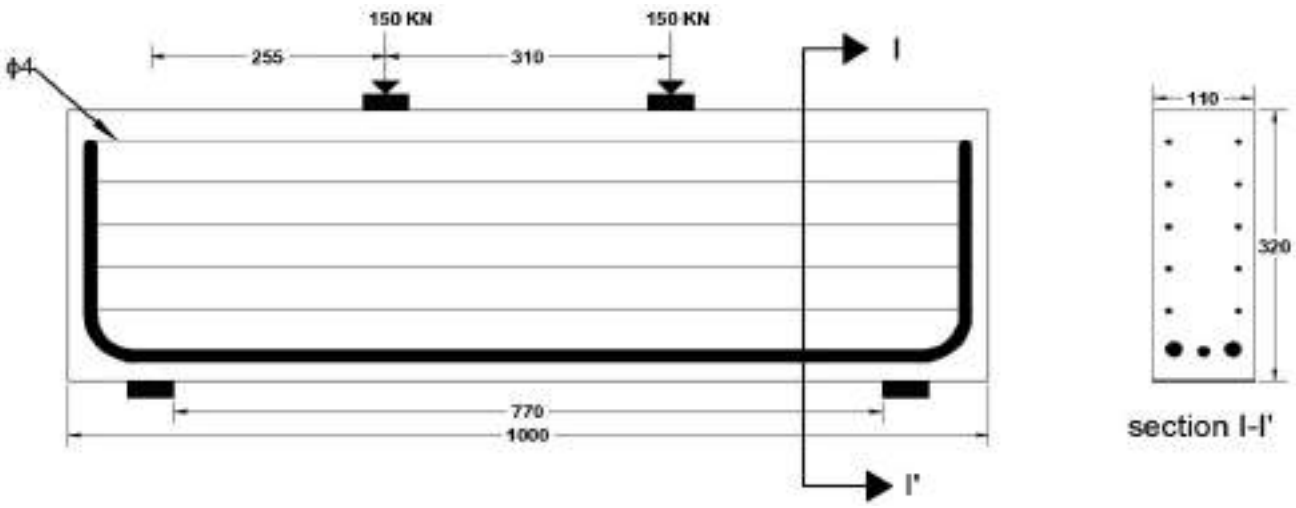

Figure (3.8) Details of (G1SC3).

Group D – Variation of Shear span to depth ratio (a/d) :

The type of shear failure depends mainly on a/d ratio, so thus two deep beams (G1SD1and G1SD2) with 1.08 and 0.727 of a/d ratios were used to study this behavior, as in **figure (3.9) and (3.10):**

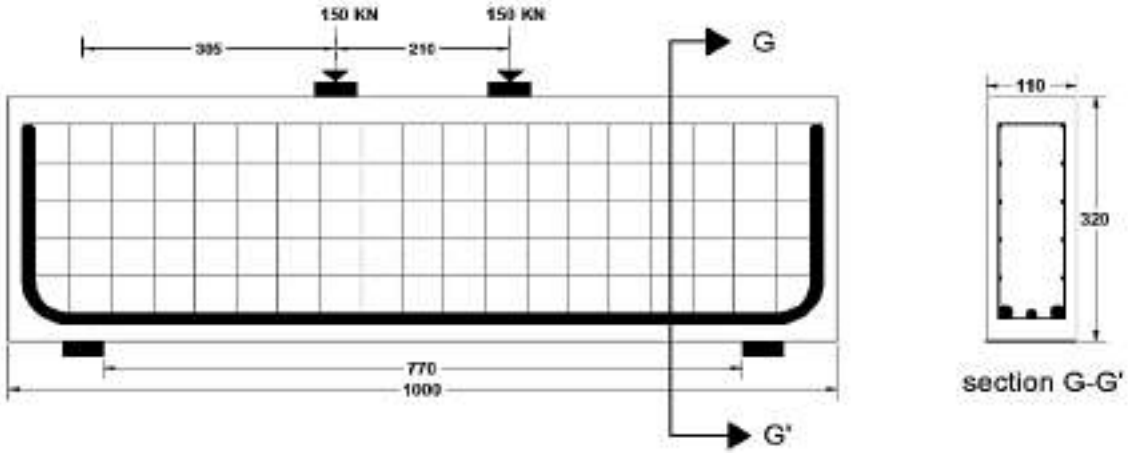

Figure (3.9) Details of deep beam (G1SD1) with (a/d) = 1.08

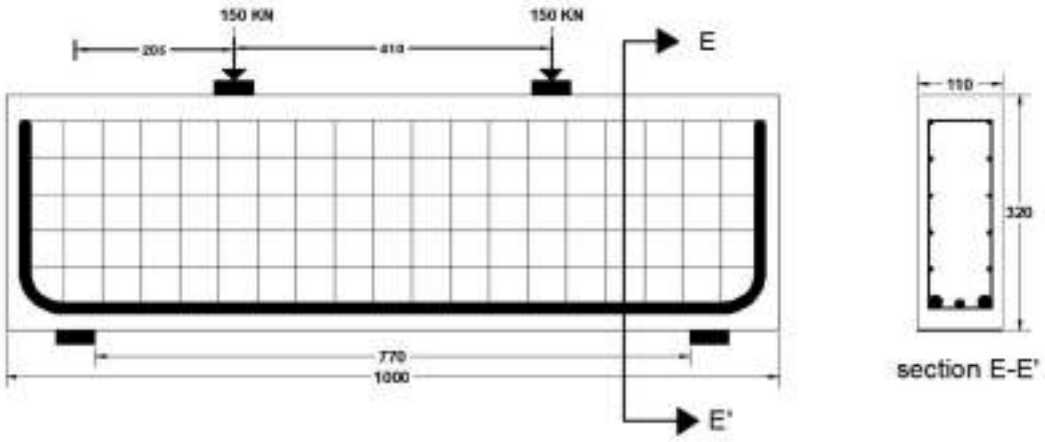

Figure (3.10) Details of deep beam (G1SD2) with (a/d) = 0.727

Group E – Plain sifcon deep beams:

This group consisted of one deep beam (G1SE1) without main and web reinforcement, this beam containing only SIFCON with volume ratio steel fiber of 9% and it is compared with G1SB3, as in **figure (3.11):**

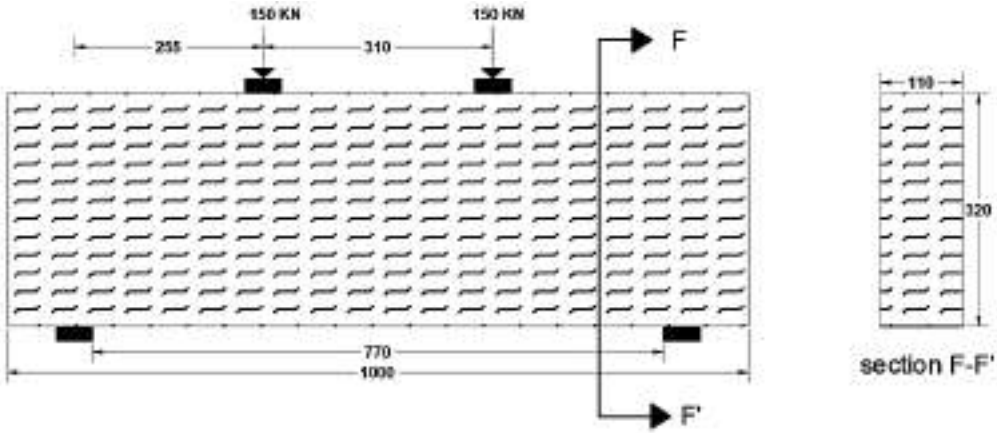

Figure (3.11) Details of deep beam (G1SE1).

3.6.2 Second group (deeps beams with opening)

All the dimension of beams in mm, reinforcement size in mm and all unit of forces in kn. Not that the diameter of circular opening is 75 mm for all deep beams.

Group A (normal concrete):

This group consists of one deep beam with circular opening (G2NA1), is cast of normal concrete with main and web reinforcement as in figure (3.12):

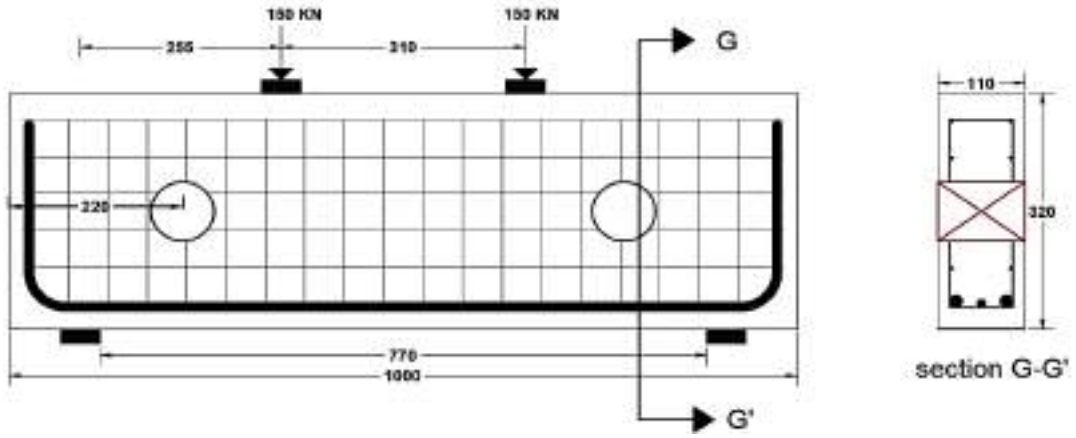

Figure (3.12) Details of deep beam (G2NA1).

Group B variation of steel fiber ratio:

To study the effect of steel fiber ratio, three deep beams (G2SB1, G2SB2, and G2SB3), with steel fiber percent of (6%, 7.5%, and 9%) were constructed in same **figure (3.13):**

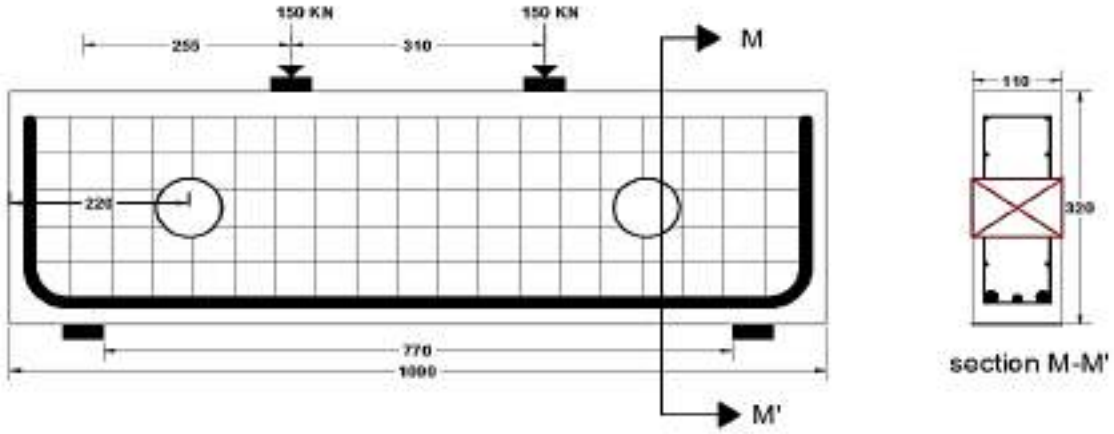

Figure (3.13) Explain details of deep beam (G2SB1, G2SB2 and G2SB3).

Group C – Inclined reinforcement around openings:

This group has two deep beams (G2NC1 and G2SC2). Each beam has eight inclined reinforcements around the openings as shown in figure (3.14). Where, the beam

(G2NC1) was cast with normal concrete, while the beam (G2SC2) was cast with (SIFCON).

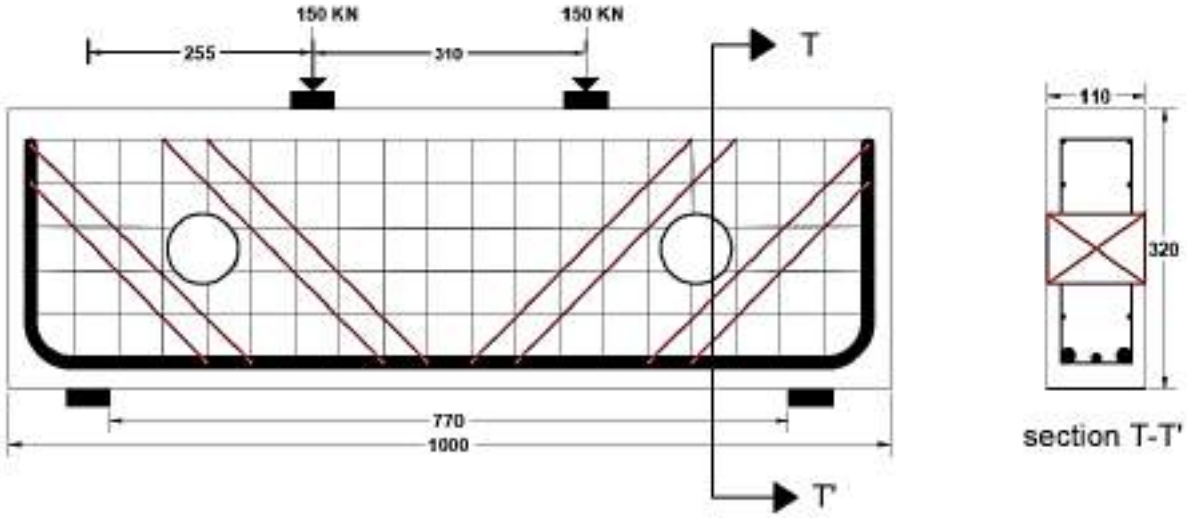

Figure (3.14) Details of deep beam (G2NC1 and G2SC2).

Group E – Shape of opening:

This group has two deep beams (G2SE1and G2SE2). The two beams were designed with the shape of openings differ from the shape of openings of control beam. Where, the beam (G2SE1) had triangular openings. While, the beam (G2SE2) had square openings. Note that the area of triangular and square openings equals the area of circular openings with diameter 75 mm. Figures (3.15) and (3.16):

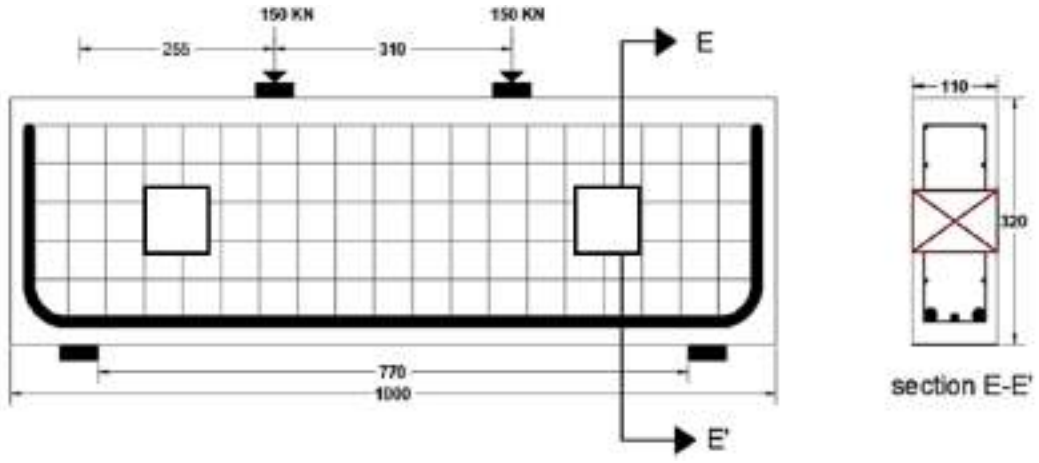

Figure (3.15) Details of deep beam (G2SE1).

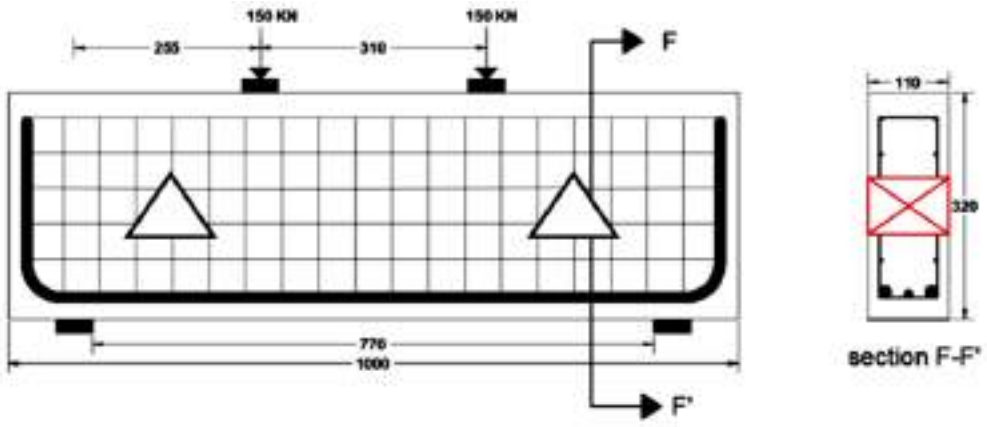

Figure (3.16) Details of deep beam (G2SE2).

3.7 Steel Reinforcement Mesh

All deep beams had the same flexural reinforcement at the bottom of 2Ø16 and 1Ø10 mm. Each bar was hooked at both ends using 90° standard hooks with 190 mm extended lengths for Ø16 and 120 mm for Ø10 in order to prevent bond failure [2]. Deformed steel wires having a nominal diameter of 4mm were used as vertical and horizontal web shear reinforcement. The vertical and the horizontal web reinforcement were in the form of closed stirrups. For deep beams having inclined reinforcement, deformed steel wires of Ø 10 mm were placed to make an angle of 45° with the longitudinal direction of the concrete deep beam. All reinforcement mesh was supplied with two lifting hooks made of Ø4 mm steel wire to handle and place the deep beams. All steel bars and steel wires were arranged and connected together by using 1 mm steel wire to make up the required reinforcement mesh as shown in Plate (3.12). To gain a bottom cover of 30 mm for tension bars and side cover of 15 mm for the web shear reinforcement, two types of plastic spacers were used, as shown in Plate (3.13)

Plate (3.12) Steel reinforcement mesh.

Plate (3.13) Plastic spacers.

3.8 Casting Procedure of SIFCON Deep Beams

All molds, which made from steel plate, were cleaned and their internal surfaces were oiled to prevent adhesion of concrete after hardening. Specimen preparation and mixing procedure are described below:

a) Before mixing, all quantities were weighted and packed in a clean container, and the molds were oiled one day before casting as shown in Plate (3.14).

b) Steel reinforcement mesh were placed in their correct positions and the specified protection cover is checked by placing concrete spacers between the opposite sides and bottom of mold.

c) For all Mixing, the silica fume and cement were mixed in dry state for about 5 minutes to disperse the silica fume particles throughout the cement particles, then the sand was added and the mixing continued for another 10 minutes as shown in Plate (3.15). Then, the superplasticizer was dissolved in water and the solution of water and superplasticizer was added to the rotary mixer and the whole mix ingredients were mixed for a sufficient time.

The mixer was stopped and mixing was continued manually especially for the portions not reached by the blades of the mixer. The mixer then was operated for 5 minutes to attain reasonable fluidity until become slurry.

Then, to obtain a homogenous mixture, pour the mixing in to the mold in three layers. Firstly, the fibers is placed as random distribution in the mold about one third of the depth. Then, the concrete slurry is pour over bed layer of steel fiber to infiltrate inside of network fiber. This process is then repeated to the other layers until the required depth is achieved, as shown in Plate (3.16).

Plate (3.14) Material of all deep beams at container.

(**a**) (**b**)

(Plate 3.15) a: Silica fume mix with cement b: Silica fume and cement mix with sand

Plate (3.16) Shown cast of SIFCON layer and specimens after cast.

3.9 Molds

Two steel mold forms were used in the casting for all deep beams as shown in **Plate (3.17).**

Plate (3.17) Steel molds used for fabrication of deep beams.

The inside dimensions of each mold were 1000mm x320mm x110mm (length x depth x width). The forms were made of steel plate of 3 mm thickness, the mold consists of two pieces connected by four steel bolts at the both. The openings were made by using PVC pipes, triangular and square thin plate (3mm) as shown in **Plate (3.18a,b)**. The molds were cleaned and oiled before being used.

(a) **(b)**

Plate (3.18) a: Circular openings formed from plastic pipe.

b:Triangular and Square openings formed from thin plate (3mm).

3.10 Curing of Specimens

All specimens were demolded after 24 hours, and then they were cured at a water bath and left until the end of water curing at 28 days as shown in **Plate (3.19).**

Plate (3.19) Curing of specimens

3.11 Tests and Measurement Devices of Deep Beams

3.11.1 Load Measurements

Torsee Universal Testing Machine in Basrah university with a capacity of (2000) (KN) was used to apply the load, **Plate (3.20):**

Plate (3.20) Torsee Universal Testing Machine

3.11.2 Deflection Measurements

Vertical deflection was measured at the mid-span of the deep beams by using mechanical dial gauge with an accuracy of 0.01mm fitted to magnetic stands attached to the independent steel frame that carried the displacement transducers as shown in **Plate (3.21)**. The dial gauge was placed under the bottom face of the tested deep beam at mid-span.

Plate (3.21) Dial gauge used for deflection measurements.

3.11.3 Electrical Strain Gauges

3.11.3.1 Type of Strain Gauges

Tokyo Measuring Instruments (TML) strain gauges (Tokyo Sokki Kenkyujo Co., Ltd.) were used to measure the strains in the present study. Strain gauges are easy to use and offer a high degree of accuracy and stability. The type of strain gauge used in this study was PFL-10-11 as in **Plate (3.22)** it was used in all tests. All gauges had a nominal resistance of 120 ± 0.3 ohms and a nominal gauge factor of 2.12 ± 1%. The Gauge Factor is an expression for the change in resistance given and it is dependent on Poisson's ratio of the material on which the gauge was tested. When a material was subjected to external force, physical deformation was generated and that caused change in electrical resistance of material. Strain gauges measure proportional strain to the changes of resistance by electrical resistance of the material of which it consists. When strain is generated in a test material and strain gauge has been bonded, consist of electrical resistance material and measure proportional strain to the resistance changes. Due to this variation in electrical resistance, the strain is generated proportional to variation [61] as shown in **Figure (3.17)**.

Plate (3.22) Strain Gauges Type.

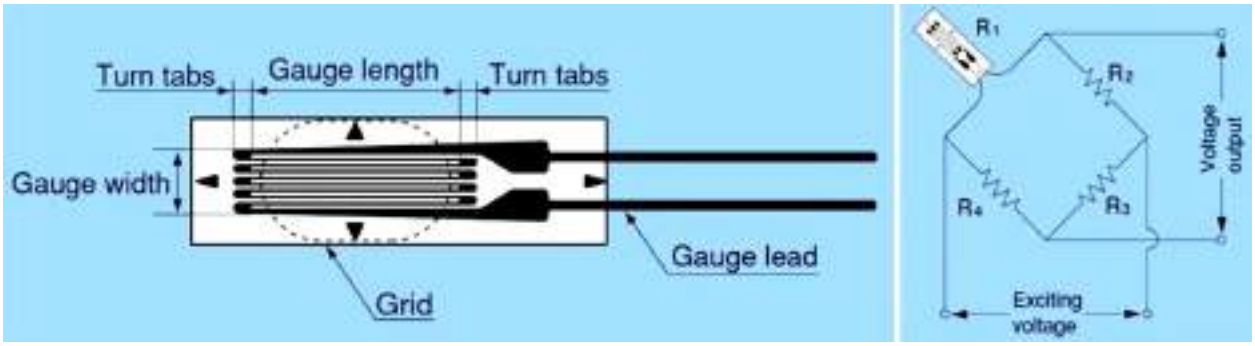

Figure (3.17) Strain Gauge Configurations

$$\varepsilon = \frac{\Delta L}{L} = \frac{\Delta R}{R} * \frac{1}{K} \qquad \text{…….. (3.2)}$$

Ɛ: is the strain measured.

R: is the resistance of gauge.

ΔR: is the resistance change due to strain.

K: is the gauge factor existing on package.

3.11.3.2 Strain Gauge Coding System

For the selected TML strain gauge PFL-10-11, PF is gauge series (polyester foil gauge), L is pattern configuration (single), 10 is gauge length in mm,

11 is compensation material ppm/C^{o} and lead wires length is 3m. The installation of strain was cleared in appendix (A).

3.11.4 Geo Data Logger series 6000

A **data logger** by wykeham farrance **(**GEODATALOGGER series 6000) (also named as **data recorder**) is an electronic device that records data over time or in relation to location either with a built in instrument or sensor or via external instruments and sensors. Increasingly, but not entirely, they are based on a digital processor (or computer). They generally are small, battery powered, portable, and equipped with a microprocessor, internal memory for data storage, and sensors. Strain of data loggers interface with a personal computer, and use software to activate the data logger and view and analyze the collected data, **see Plate (3.23)**. Strain gages is connected to data logger by 16 channel to read the resistance in ohm.

Plate (3.23) Data Logger and Computer connection.

3.11.5 Strains Distribution

Figures (3.18a and b) show strains distribution for group one and two**, also Table (3.22 and 3.23)** show detailing of distribution of strains in front face of solid deep beams and deep beams with openings.

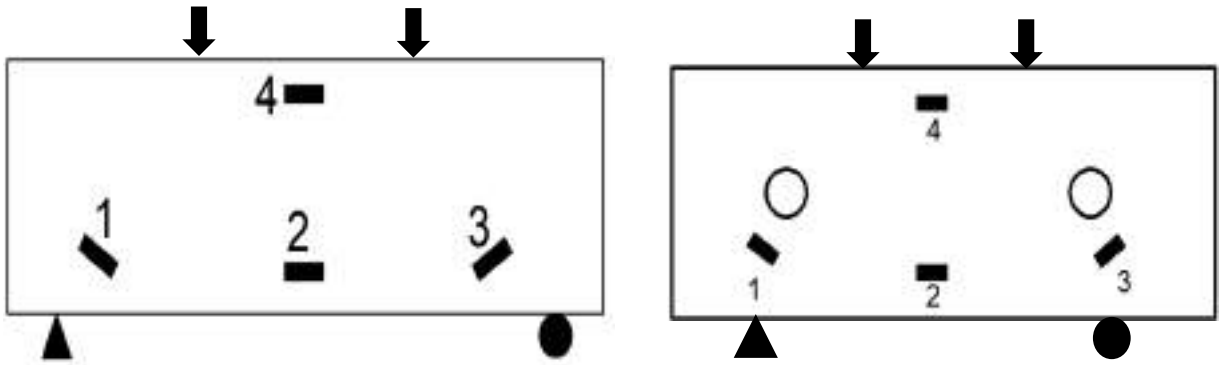

(a) **(b)**

Figure (5.18) a: Strain distribution of solid deep beams.

b: Strain distribution of deep beams with openings.

Table (3.22) Strains positions of solid deep beams.

Specimens	Position of strains			
	Zone 1	Zone 2	Zone 3	Zone 4
G1NA1	✓		✓	
G1SB1	✓		✓	
G1SB2	✓		✓	✓
G1SB3	✓		✓	✓
G1SC1	✓	✓	✓	
G1SD1	✓	✓	✓	
G1SD2	✓	✓		✓
G1SE1	✓	✓	✓	✓

Table (3.23) Strains positions of deep beams with openings.

Specimens	Position of strains			
	Zone 1	Zone 2	Zone 3	Zone 4
G1NA1	✓		✓	
G1SB1	✓		✓	
G1SB2	✓	✓	✓	✓
G1SB3	✓		✓	
G1NC1	✓		✓	
G1SC2	✓		✓	
G1SD1	✓		✓	
G1SD2	✓		✓	

CHAPTER FOUR

RESULTS AND DISCUSSIONS

Chapter Four

Results and Discussions

4.1 General

The results of the experimental work that were carried out to investigate the behavior of slurry infiltrate fibrous reinforced concrete deep beams with and without openings. The results of finite element investigation to SIFCON deep beams are presented in this chapter.

Two groups of deep beams with and without openings are tested with many variables. The experimental variables are steel fiber ratio, shear span to depth ratio (a\d), presence of the vertical web shear reinforcement, shape of opening and removing of steel reinforcement mesh (with SIFCON only).

4.2 Experimental Results of SIFCON Mixes

The results of compressive strength, tensile strength, flexural strength and shear strength for all four mixes are summarized in Table (4.1)

Table (4.1) Properties results of mixes

Items	Compressive strength (MPa)	Tensile strength (MPa)	Flexural strength (MPa)	Shear strength (MPa)
Mix 1	61	13.3	30.4	37.3
Mix 2	64.4	15.6	38	45.1
Mix 3	81.1	18.5	55.5	61.8
Mix 4	43.4	2.8	5.9	6.9

It can be seen from Table (4.1) the best results are for the mix 3, so this mix is later used in construction of deep beams.

4.3 Experimental Results of SIFCON Deep Beams

The sixteen SIFCON deep beams tested in this study are divided into two groups according to experimental work. The deep beams were tested up to failure

under symmetrical two point loads. When load is applied, the load of first crack, ultimate load, mid span deflection, toughness and ductility recorded.

Tables (4.2) and (4.3) illustrate the experimental and numerical load of the first crack and ultimate load; as well as the experimental and numerical maximum deflection for both solid deep beams and deep beams with openings. Deep beams (G1NA1, G2NA1 and G2NC1) were established for comparison purposes as reference specimens to observe the differences among the deep beams.

Table (4.2) Loads at first crack and ultimate loads for (experimental and numerical) solid deep beams.

Group no.	Deep beam no.	First Crack load (Pcr.) (kN)			Ultimate load (kN)			Max mid deflection (mm)		
		P (Exp.)	P (Num.)	$\frac{P(Num.)}{P(Exp.)}$	P_u (Exp.)	P_u (Num.)	$\frac{Pu(Num.)}{Pu(Exp.)}$	δ Exp.	δ Num.	$\frac{\delta \text{ Num.}}{\delta \text{ Exp.}}$
Group 1	NA1	160	144	0.9	330	316.63	0.95	2.8	1.35	0.49
	SB1	600	530	0.88	977	945	0.96	8.4	8.1	0.96
	SB2	690	600	0.87	1010	944	0.93	11.7	9.9	0.84
	SB3	740	670	0.95	1120	1060	0.94	14.4	13.4	0.93
	SC1	505	450	0.89	1030	940	0.91	12.6	12.3	0.97
	SD1	550	490	0.89	1050	910	0.86	16.4	15	0.91
	SD2	880	780	0.88	1400	1330	0.95	7.1	5.6	0.78
	SE1	523	460	0.87	922	840	0.91	15.1	14.2	0.94

Table (4.3) Loads at first crack and ultimate loads for (experimental and numerical) deep beams with openings.

Group no.	Deep beam no.	First Crack load (Pcr.) (kN)			Ultimate load (kN)			Max mid deflection (mm)		
		P_u (Exp.)	P_u (Num.)	$\frac{Pu(Num.)}{Pu(Exp.)}$	P_u (Exp.)	P_u (Num.)	$\frac{Pu(Num.)}{Pu(Exp.)}$	δ Exp.	δ Num.	$\frac{\delta \text{ Num.}}{\delta \text{ Exp.}}$
Group 2	NA1	125	133	0.88	210	205	0.97	2.9	2.54	0.87
	SB1	200	155	0.77	680	601	0.88	9.4	8.8	0.93
	SB2	300	169	0.86	720	670	0.93	12.1	11.65	0.96
	SB3	420	360	0.56	860	756	0.87	14.9	13.8	0.92
	NC1	150	110	0.88	281	207	0.73	2.05	1.45	0.70
	SC2	456	250	0.85	940	871	0.92	13.5	12.23	0.90
	SD1	280	264	0.94	667	640	0.95	15.3	14.33	0.93
	SD2	302	260	0.86	740	684	0.92	13.55	12.7	0.93

4.4 Experimental of Solid Deep Beams

4.4.1 Effect of Steel Fiber Ratios (6%, 7.5% and 9%)

4.4.1.1 Load – deflection curve and crack patterns

The load-deflection curves of SIFCON for typical nonfibrous control specimens (G1NA1) and specimens (G1SB1, G1SB2 and G1SB3) with steel fiber ratios 6%, 7.5%, and 9% respectively, are plotted in fig. (4.1).

The failure of SIFCON deep beams is different from conventional concrete beams during loading stages. This is because of the fact that the opened crack in fibrous concrete is restricted when the load is transferred by the tension in the fibers which cause to bridge the gap between the faces of cracks.

Early crack is appeared in deep beam (G1NA1) with applied small load compared to SIFCON deep beams. The increase in the value of load at first crack and ultimate load with the increase of the steel fiber ratio**.**

Also the increase of the sifcon ratios by 6%, 7.5% and 9% caused an increase in the load at first crack by 275%, 331.25% and 362.5% respectively and increase in the ultimate load by 196%, 206% and 239.4% respectively, where compared to conventional concrete deep beam (G1NA1) as shown in figs. (4.2) and (4.3).

Deep beam (G1NA1) exhibit more brittle behavior but that the increase of steel fiber percentage makes them more ductile with increase ultimate load.

Crack patterns of deep beam (G1NA1) is a combination of shear and flexural crack with small bearing crashing is occurred. The first crack is started in shear zone, and as the load increased, another diagonal cracks appeared on both sides of the deep beams and shear crack progressed upward until failure in shear as shown in plate (4.1).

Deep beam (G1SB1) with increasing applied load, generated flexural crack and another diagonal crack is appeared. Crack in top strut between two point loads is appeared in advanced stages of loading. Flexural failure was appeared when load reached to ultimate value, see plate (4.2). Deep beam (G1SB2) with applied load, combination flexural and shear cracks is appeared. Flexural failure is done at ultimate load, see plate (4.3). In Deep beam (G1SB3) very fine crack in tension zone is began to form when load is applied. Also, one diagonal and crack in top strut is appear but flexural failure is occurred, see plate (4.4).

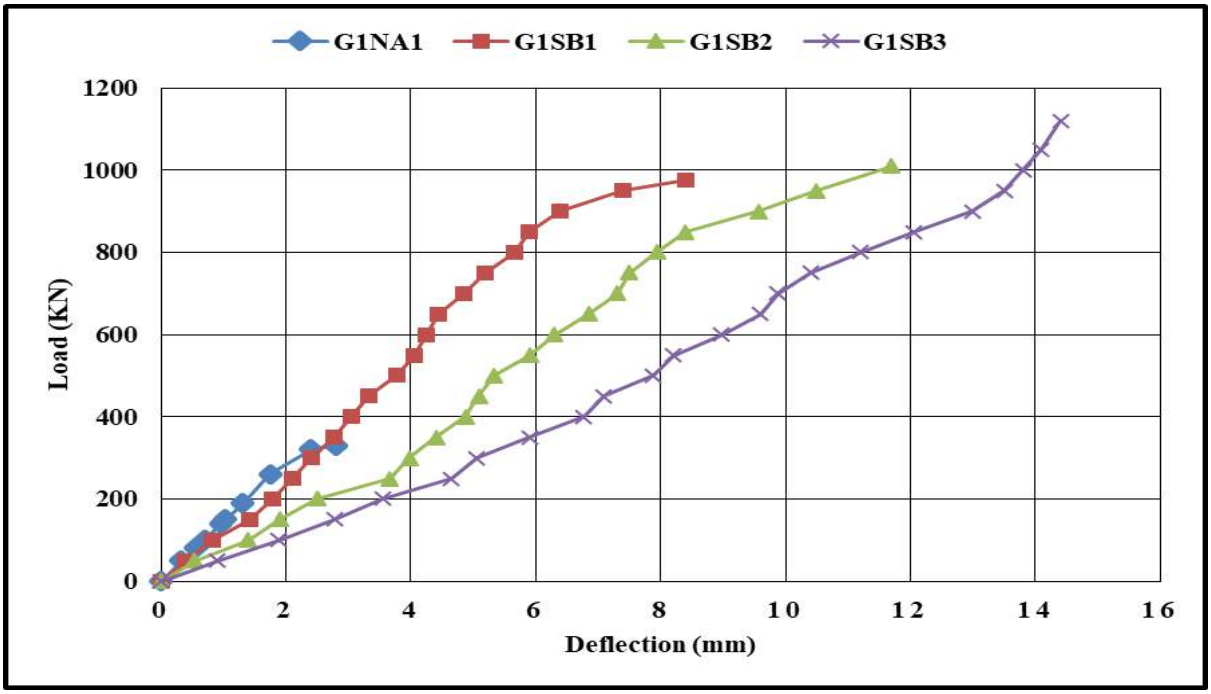

Figure (4.1) Load - Deflection Curve for Deep Beams (G1NA1, G1SB1, G1SB2 and G1SB3) specimens.

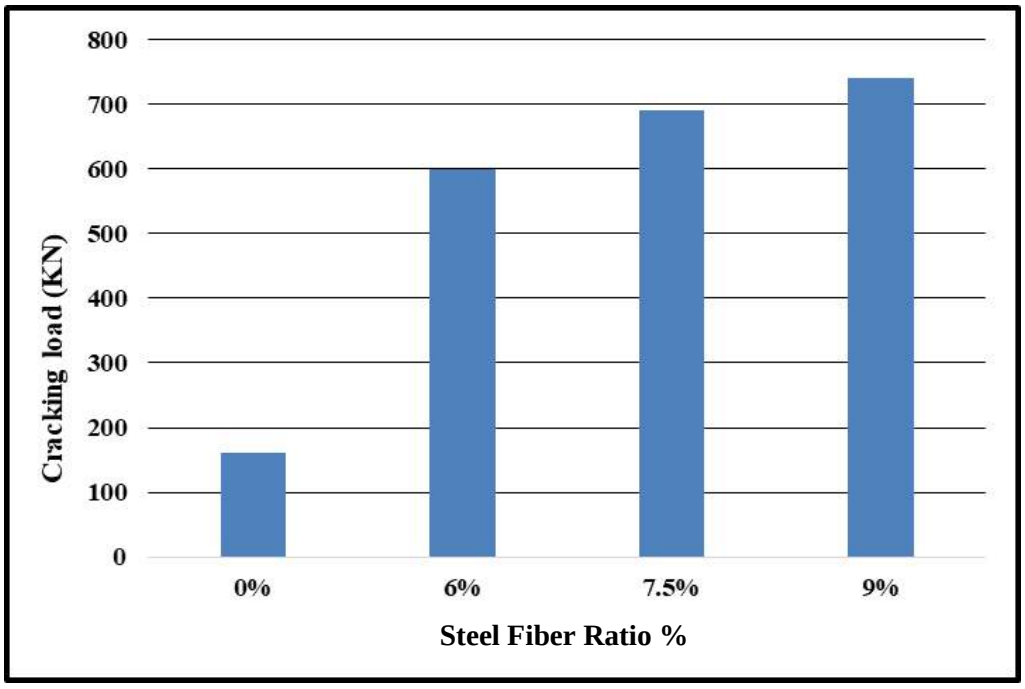

Figure (4.2) Cracking load – steel fiber ratio for deep beams (G1NA1, G1SB1, G1SB2 and G1SB3).

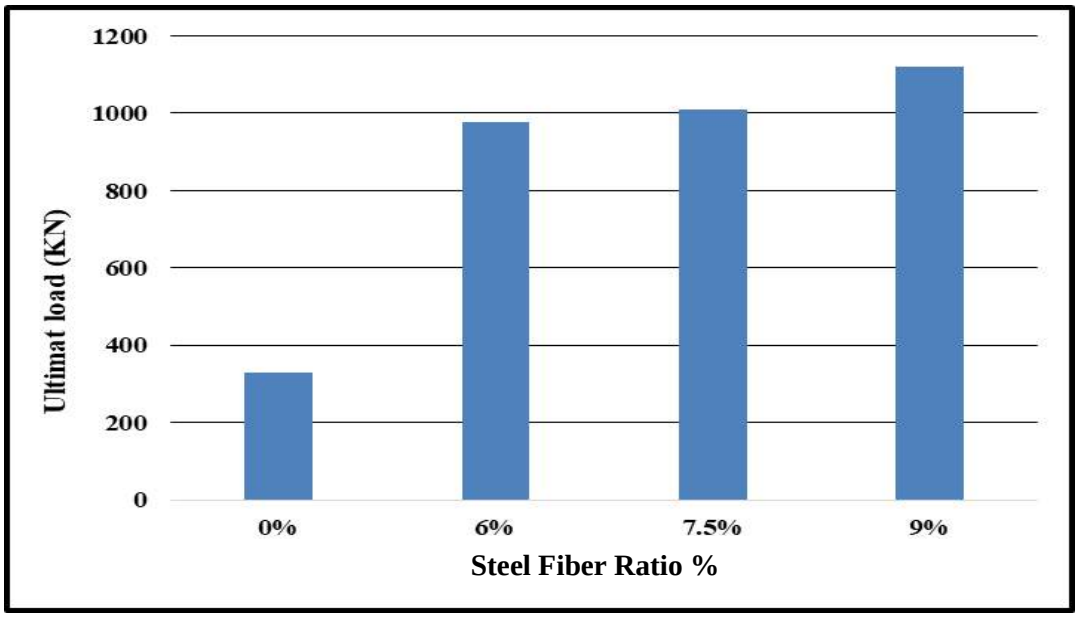

Figure (4.3) Variation of ultimate load – steel fiber ratio for deep beams (G1NA1, G1SB1, G1SB2 and G1SB3).

Plate (4.1) Experimental Deep beam G1AN1 (0%SF) after failure.

Plate (4.2) Experimental deep beam G1SB1 (6%) after failure.

Plate (4.3) Experimental deep beam G1SB2 (7.5%) after failure.

Plate (4.4) Experimental deep beam G1SB3 (9%) after failure.

4.4.1.2 Load – strain curve

Strains were measured in four locations (two levels in the shear zone, one location in the tension zone and one location in the compression zone) across the depth of the deep beam, as shown in chapter three.

Very small strains were recorded at the first stage of loading up to onset of cracks in sifcon deep beams, when a sudden increase in the strains were taken place, thereafter the strains increased almost non-linearly with increasing the load.

In all specimens, except for (G1NA1)), strains larger than (0.003) are measured. The ultimate strains for deep beams (G1NA1, G1SB1, G1SB2 and G1SB3) is (0.0019, 0.0039, 0.0044 and 0.0047) respectively, as shown in Figs (4.4) to (4.7). This coincides with the finding in previous study [62].

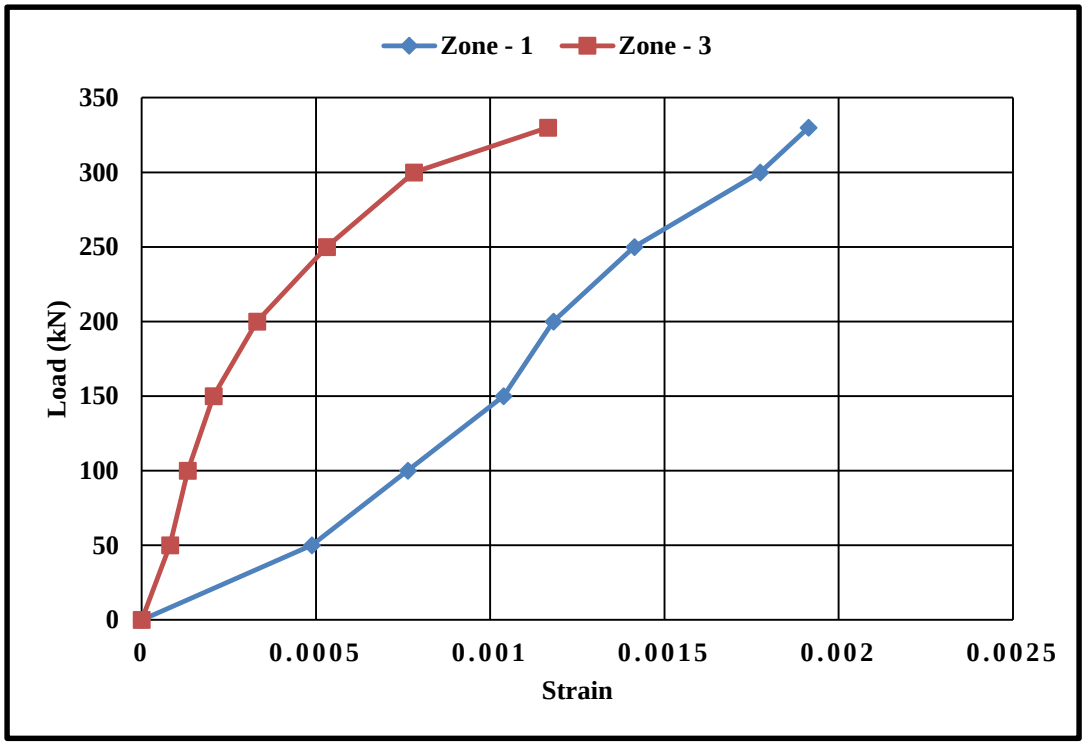

Figure (4.4) Strain distribution of deep beam (G1NA1)

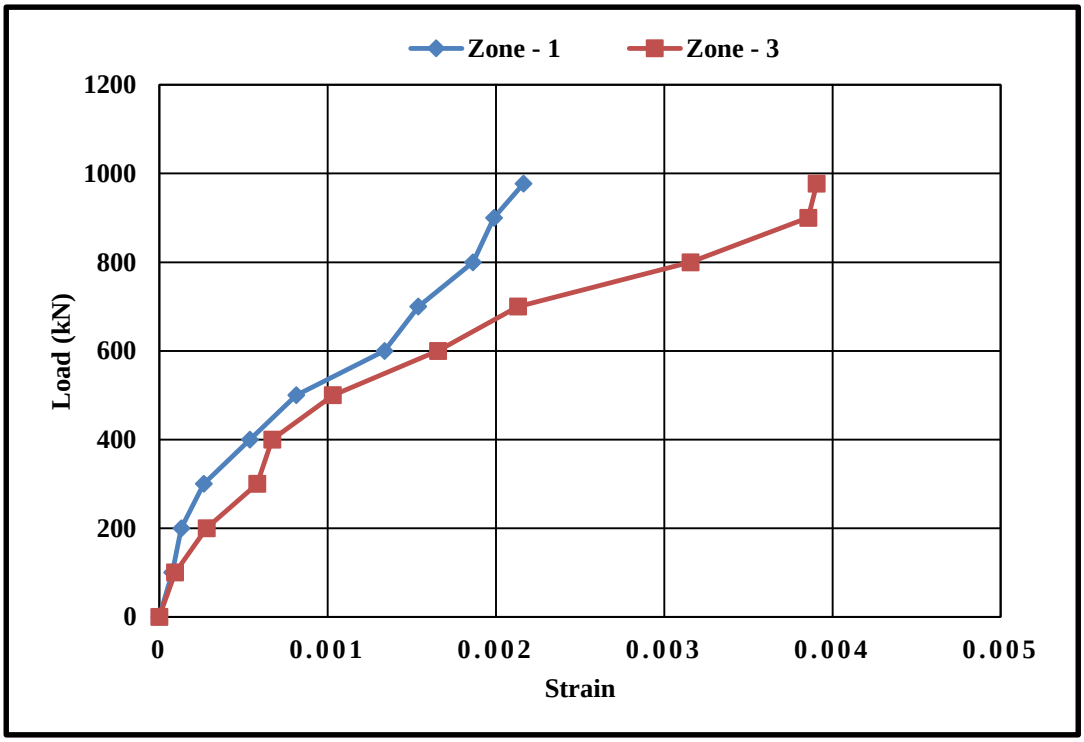

Figure (4.5) Strain distribution of deep beam (G1SB1)

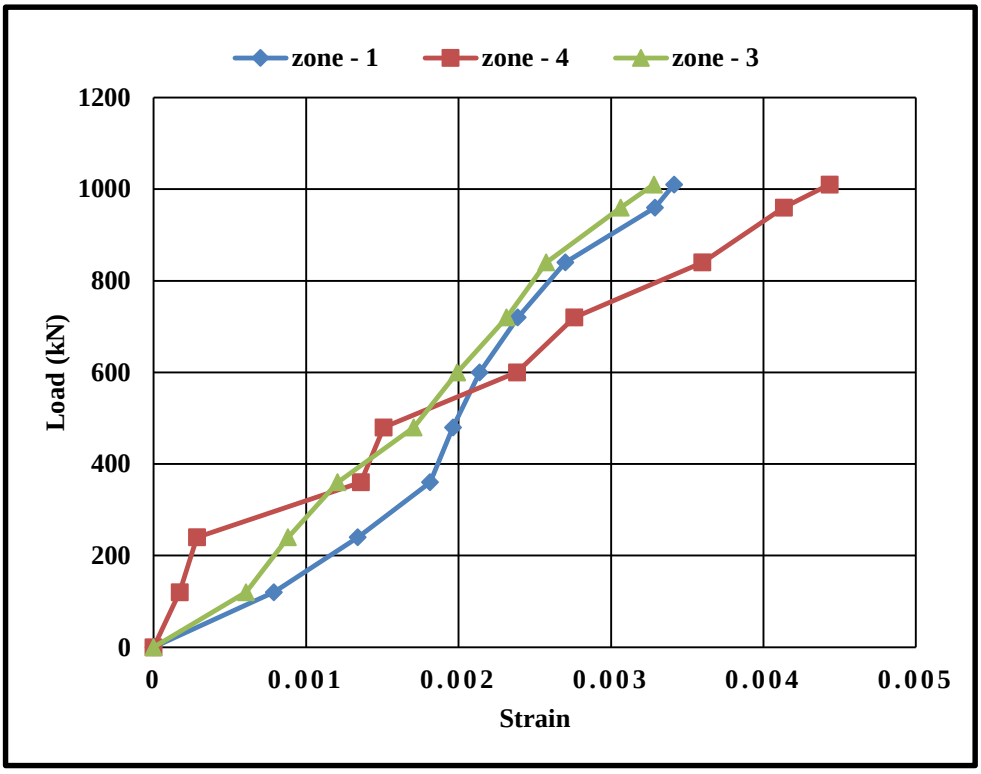

Figure (4.6) Strain distribution of deep beam (G1SB2)

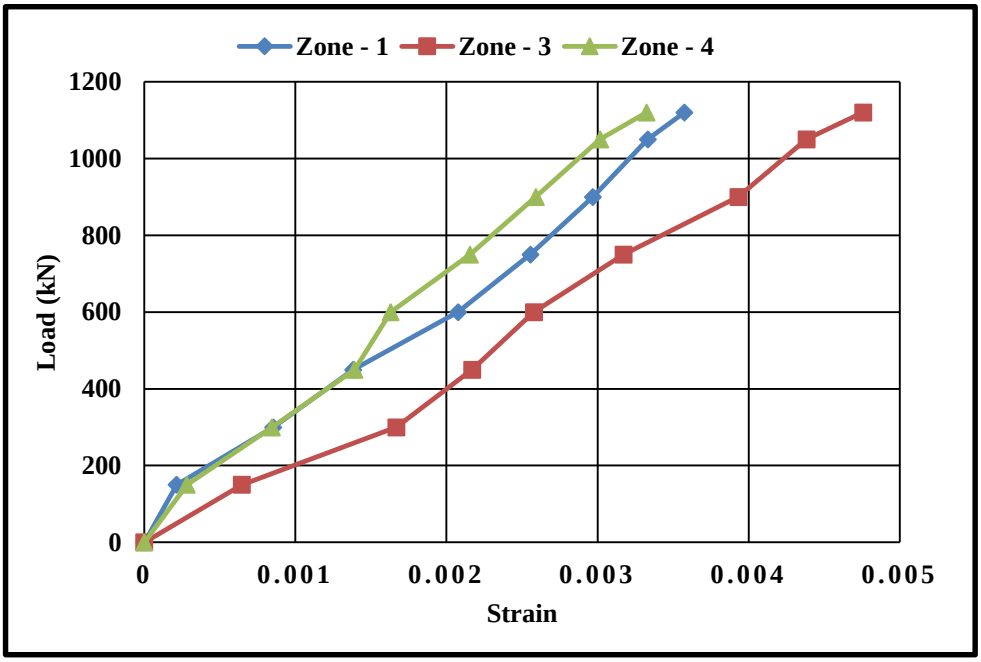

Figure (4.7) Strains distribution of deep beam (G1SB3)

4.4.1.3 Toughness of Solid Deep Beams

In materials science, toughness is the ability of a material to absorb energy and plastically deform without fracturing [63]. One definition of material toughness is the amount of energy per unit volume that a material can absorbed before rupturing so is called by (energy absorption) [63]. The toughness is calculated from load deflection curve [63]. The energy absorption characteristics of SIFCON containing 9% of fiber content performed well among all other SIFCON specimens as in Fig. (4.8). Toughness of beams (G1SB1, G1SB2 and G1SB3) are greater than for beam (G1NA1) by (760%, 1043% and 1173%), respectively.

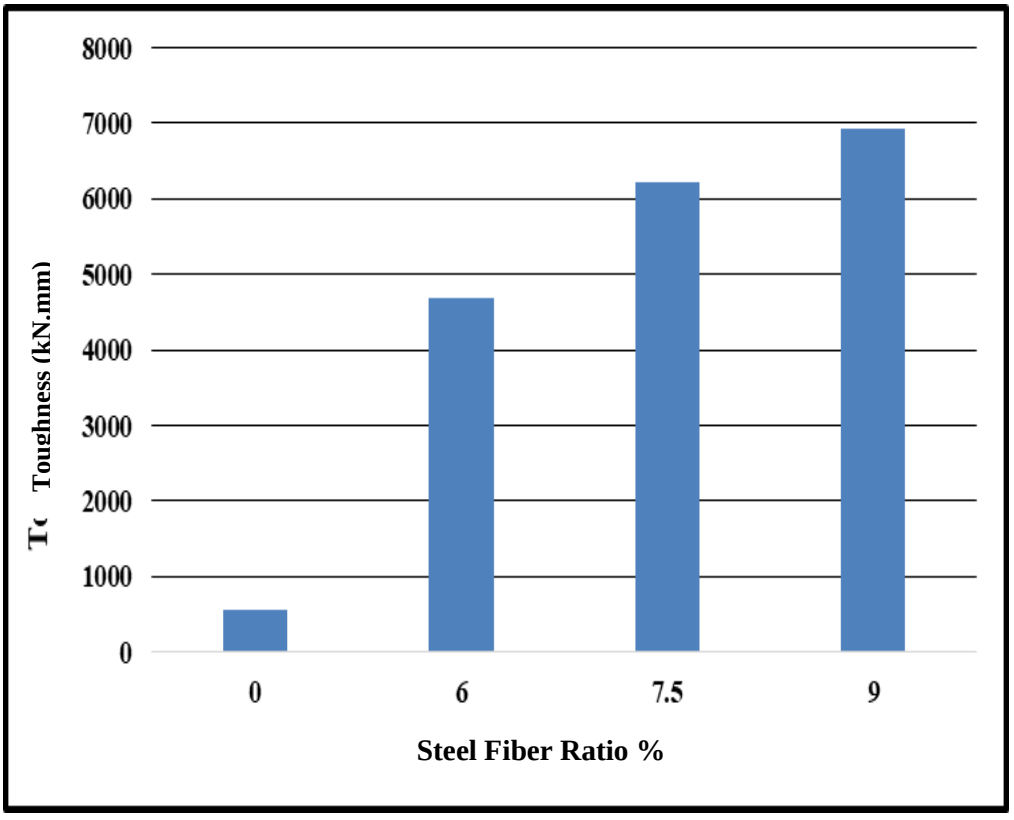

Figure (4.8) Variation toughness of deep beams (G1NA1, G1SB1, G1SB2 and G1SB3) with steel fiber ratio.

4.4.1.4 Ductility of deep beams

Is a measure of a material's ability to undergo significant plastic deformation before rupture, which may be expressed as percent elongation or percent area reduction from a tensile test [63].

Ductility of deep beams (G1SB1, G1SB2 and G1SB3) are greater than for deep beam (G1NA1) by (220%, 380% and 520%) respectively as illustrated in **figure (4.9).**

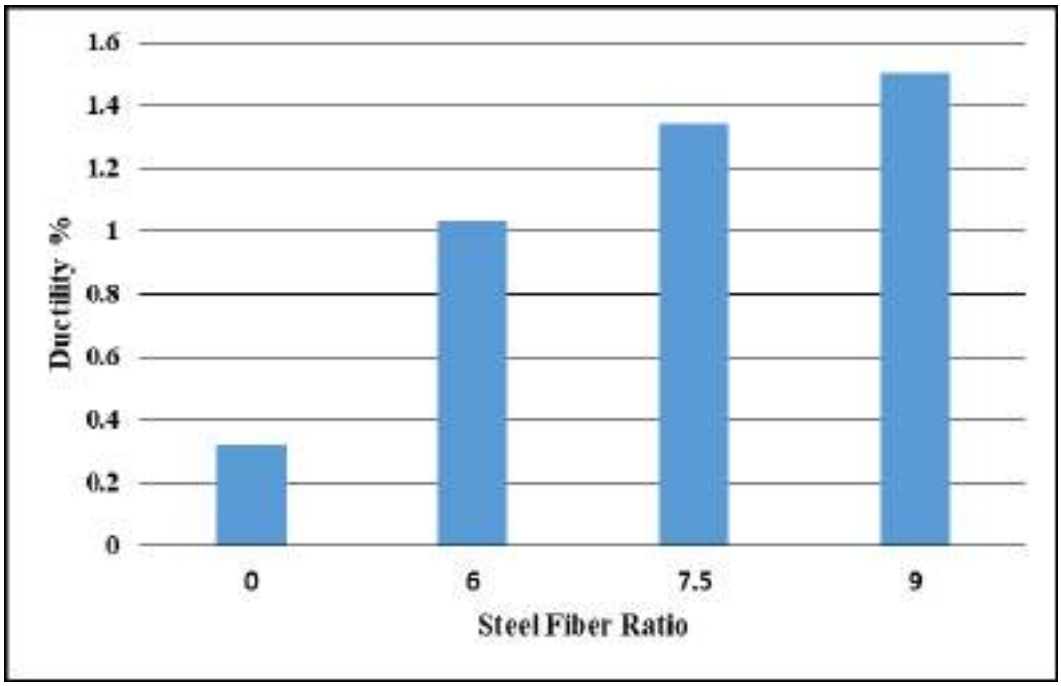

Figure (4.9) Variation ductility of deep beams (G1NA1, G1SB1, G1SB2 and G1SB3) with steel fiber ratio.

4.4.2 Effect of Presence vertical web reinforcement

4.4.2.1 Load – deflection curve and crack pattern

Fig. (4.10) shows that the load verses the deflection curves of SIFCON deep beams G1NA1, G1SB3, and G1SC1 with removing vertical web reinforcement.

The results showed that the SIFCON deep beam (G1SC1) when removing vertical web reinforcement gave a decrease by about 31.7% from deep beam (G1SB3) and increase of about 215.6% compared with deep beam (G1NA1) in cracking load as shown in fig. (4.11).

The ultimate load of deep beam (G1SC1) is reduction by 8% compared with (G1SB3) and increasing by 212.12% from (G1NA1), as shown in fig. (4.12).

In general, remove of vertical web reinforcement in the SIFCON deep beam which showed that the effect is very little on the ultimate load capacity compared to cost. This is due to the presence of SIFCON in the shear and flexural zones which showed good resistance to shear and flexural strengths.

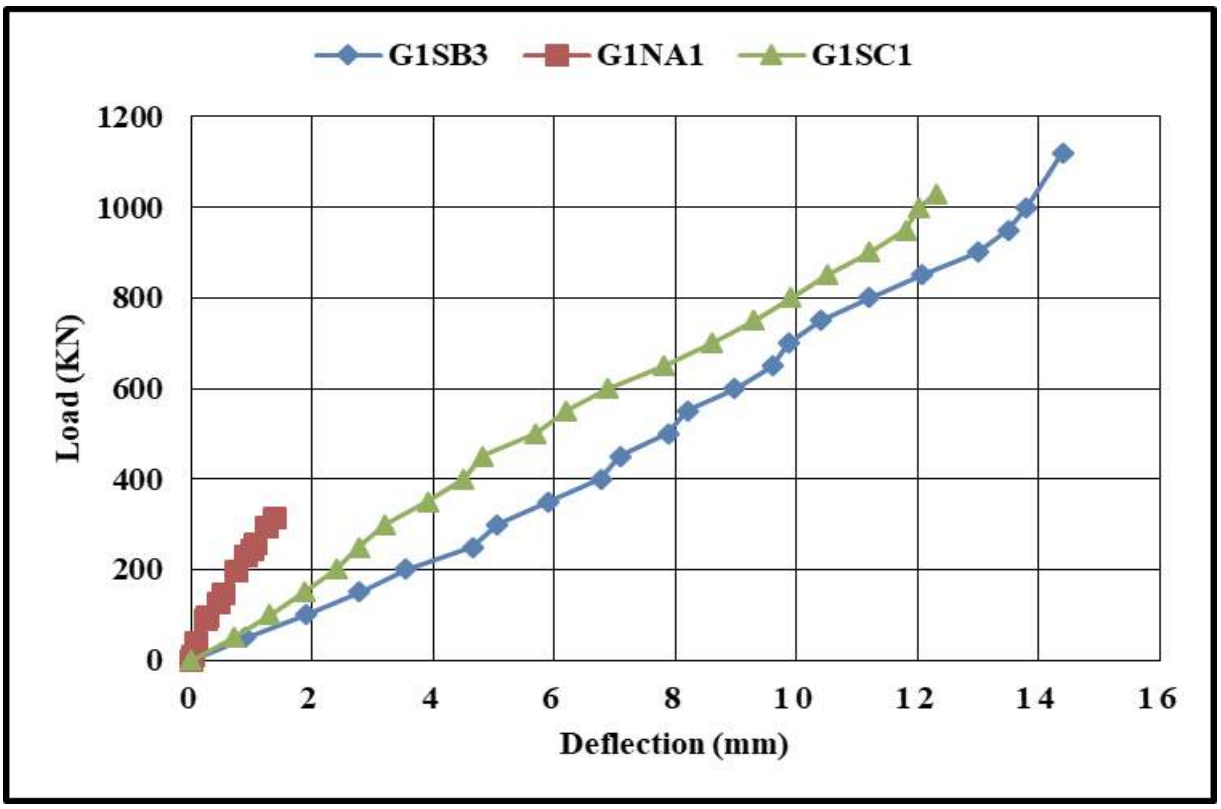

Figure (4.10) Load - Deflection Curve for Deep Beams (G1NA1, G1SB3 and G1SC1) specimens.

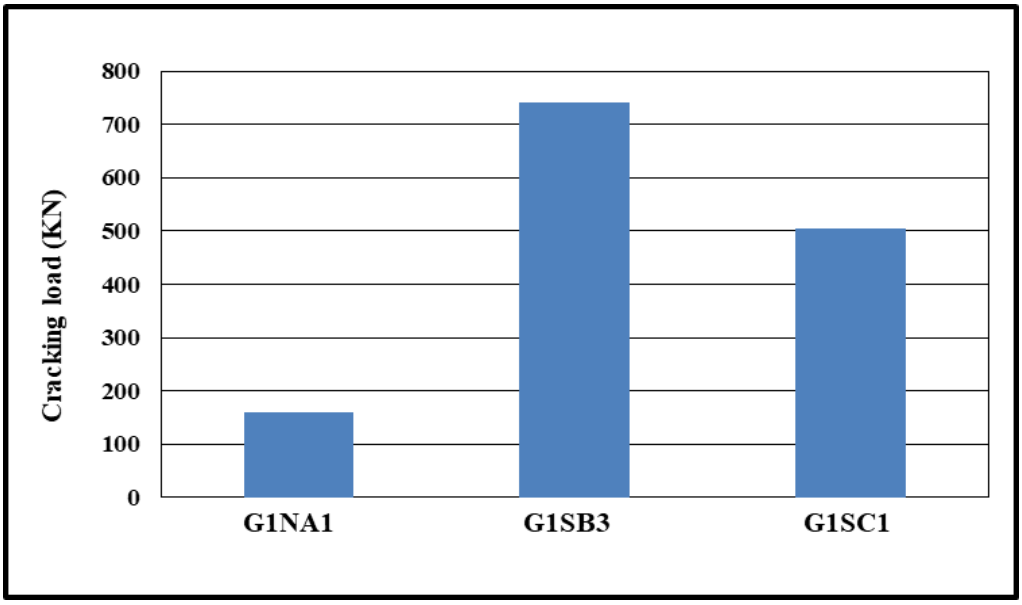

Figure (4.11) Variation of cracking load with solid deep beams (G1NA1, G1SB3, and G1SC1).

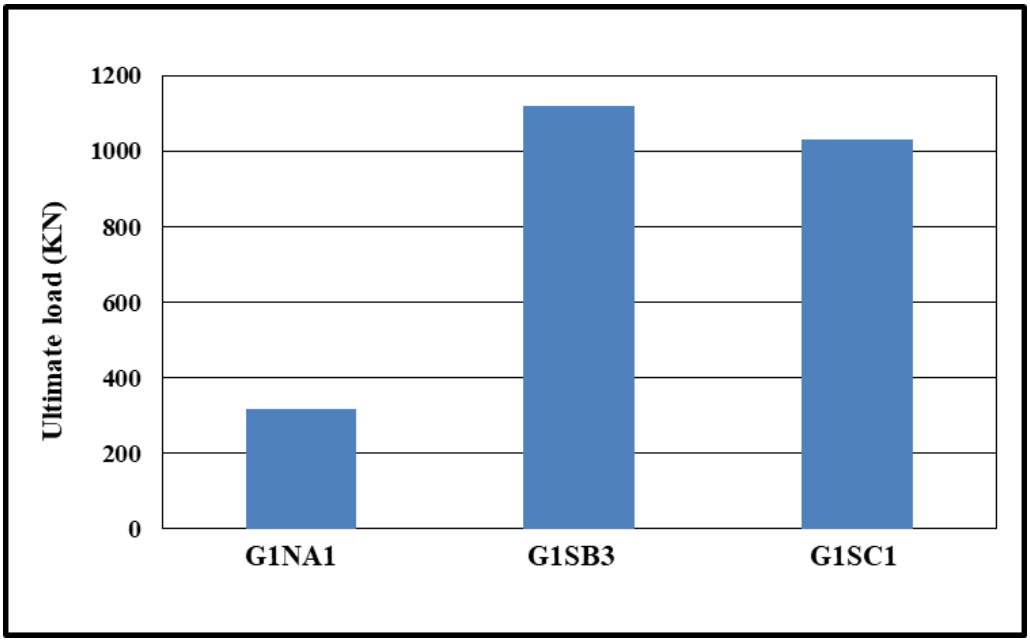

Figure (4.12) Variation of ultimate load with solid deep beams (G1NA1, G1SB3, and G1SC1).

The crack patterns of specimen (G1SC1) are shown in **plate (4.5).** The cracks of the deep beam (G1SC1) are similar to the deep beam (G1SB3). The increase of load

generated cracks in the tensile area. Small number of Cracks were also observed in the shear area and top strut. The failure was in the tensile area when reaching the ultimate load despite the removal of the vertical web reinforcement due to the high strength of the SIFCON in shear zone.

Plate (4.5) Experimental deep beam G1SC1 after failure.

4.4.2.2 Load – strain curve

The strain concrete is decreased by removing vertical web reinforcement. The value of ultimate strains was (0.0035) for zone 1, (0.0044) for zone 2 and (0.003) for zone 3. Higher value of strain recorded in tension zone, **as in fig. (4.14)**.

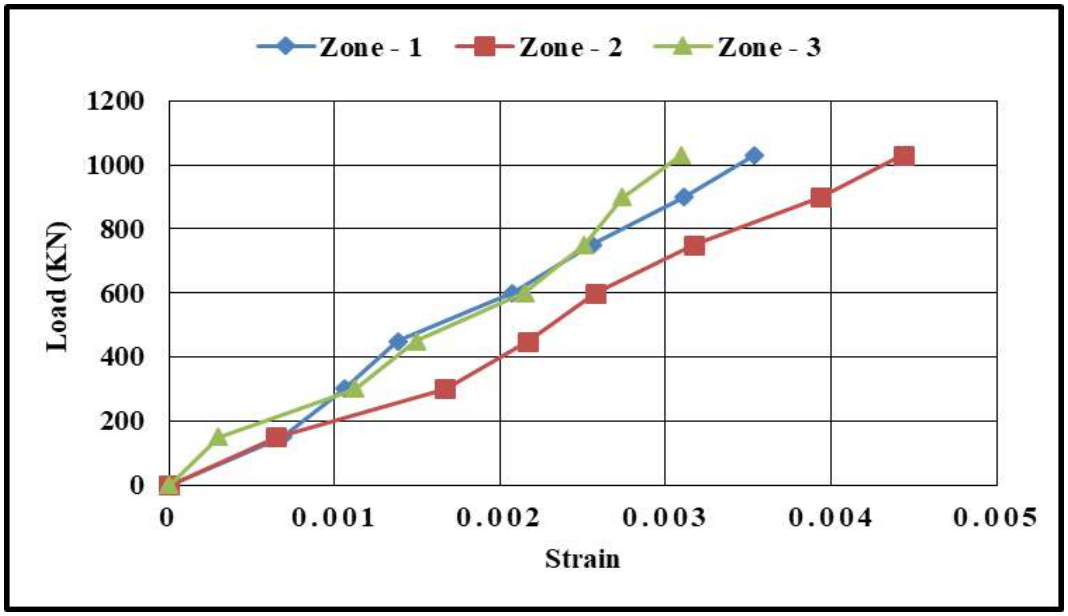

Figure (4.13) Strains distribution of deep beam (G1SC1).

4.4.2.3 Toughness of deep beam

The calculation area under curve of load – deflection of deep beam (G1SC1), the value of toughness is 6338.3 kN.mm. Toughness decreased with removing vertical web reinforcement by 8.5% from deep beam (G1SB3) but it is greater than deep beam (G1NA1) by (1065%), so this lead to fact that SIFCON mix give very high energy absorption, see **Fig. (4.15)**.

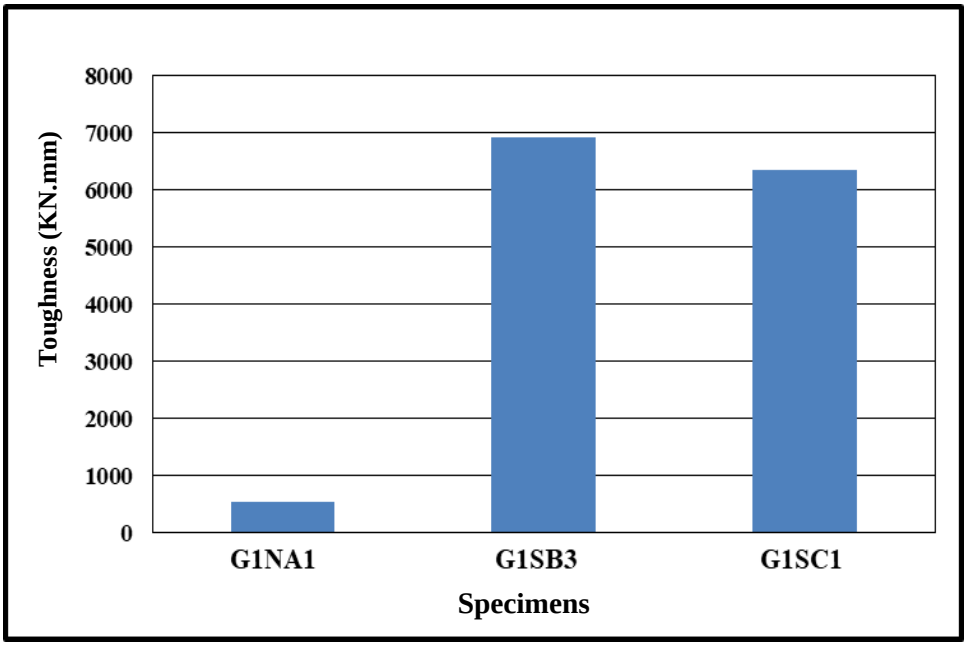

Figure (4.14) Variation toughness of deep beams (G1NA1, G1SB3 and G1SC1).

4.4.2.4 Ductility of deep beam

The value of ductility characteristics of SIFCON deep beam (G1SC1) is 2.9 %. Ductility decrease with removing vertical web reinforcement by percentage 6.45%. However, the value of ductility increased from the conventional deep beam (G1NA1) by 480% see **Fig. (4.15)**

.

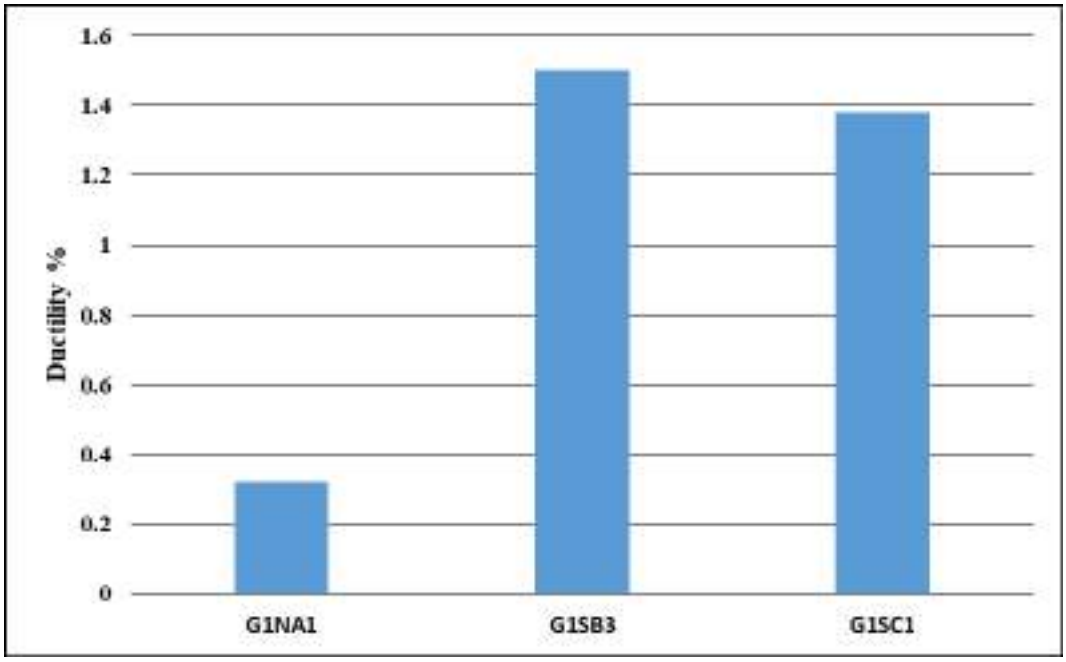

Figure (4.15) Variation ductility of deep beams (G1NA1, G1SB3 and G1SC1).

4.4.3 Effect of Shear Span (a/d effect)

4.4.3.1 Load – deflection curve and crack pattern

The influence of varying shear span to the effective depth ratio a/d on the behavior of SIFCON solid deep beams is investigated. Two deep beams having a/d ratios 1.08 and 0.727 are examined in addition to a/d ratio 0.9 tested in group B (deep beam G1SB3).

The load-deflection relationship for deep beams (G1SD1 and G1SD2) are presented in **Fig. (4.16)**.

The crack load is decreased in deep beam (G1SD1) by 25.7% and (G2SD2) increased by about 18.9% if compared with deep beam (G1SB3) as shown in **fig. (4.17)**.

While, the ultimate load of beam (G1SD1) is decreased by about 6.25% and (G1SD2) is increased by about 25% from deep beam (G1SB3), as shown in **fig. (4.18)**. The reason is due to the decrease in the ratio of (a/d) lead to increase in the arching action.

The crack patterns of these deep beams are depicted in **plate (4.6) and (4.7)**. At the deep beam (G1SD1), multiple cracks are beginning to form in tension zone when load is applied in start of test. It was observed diagonal cracks when load is continuing to applying. The cracks in the tensile area stopped near to neutral axis although reaching to ultimate load.

At the deep beam (G1SD2), multiple diagonal cracks is began to form in shear zone when load is applied. By observing tensile area, all cracks is vanished as a result of the shifting of the loads to the supports.

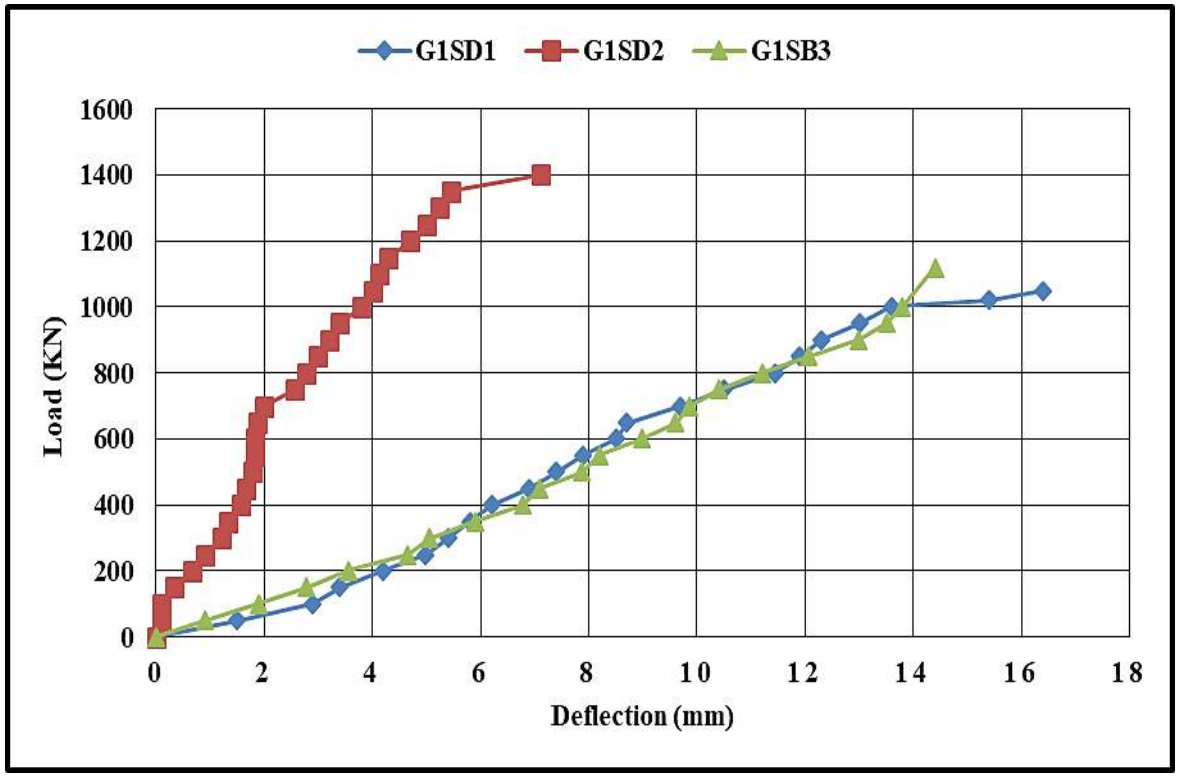

Figure (4.16) Load - Deflection Curve for Deep Beams (G1SB3, G1SD1 and G1SD2) specimens.

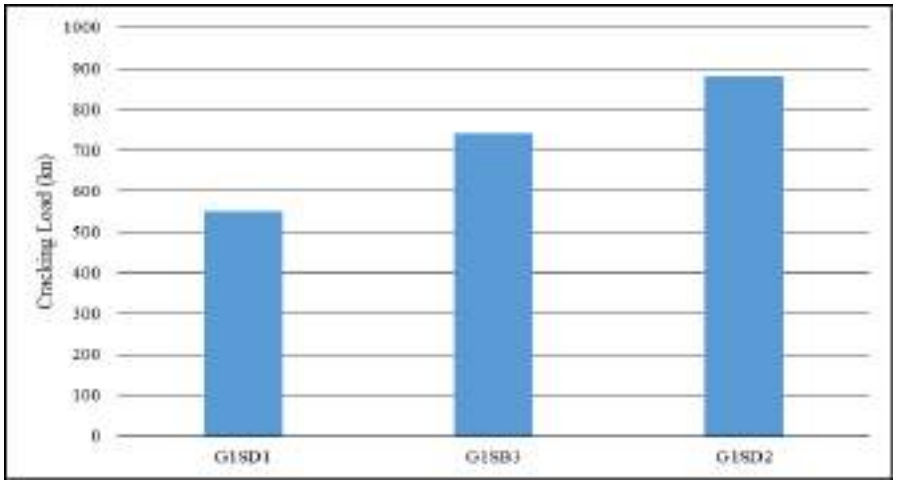

Figure (4.17) Variation of cracking load with solid deep beams (G1SD1, G1SB3 and G1SD2).

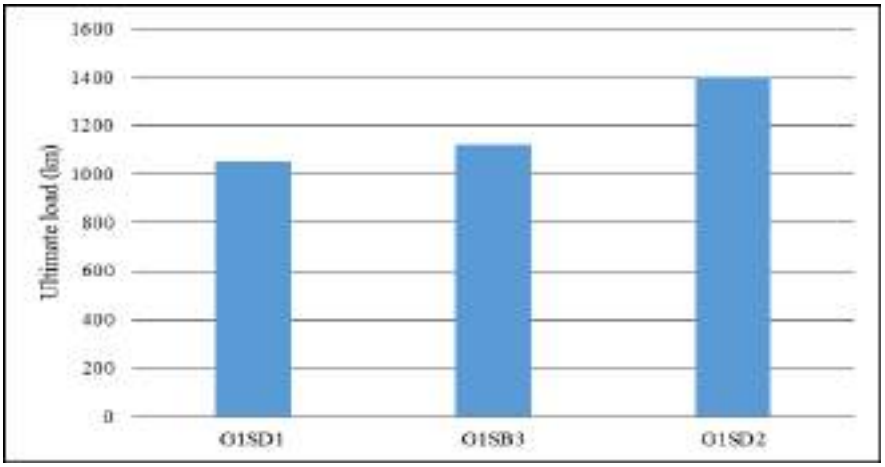

Figure (4.18) Variation of ultimate load with solid deep beams (G1SD1, G1SB3 and G1SD2)

Plate (4.6) Experimental deep beam (G1SD1) after failure.

Plate (4.7) Experimental deep beam (G1SD2) after failure.

4.4.3.2 Load – strain curves of deep beams

Figures (4.19) and (4.20), it can be observed that the strain increased in the zone (2) more than in zones (1) and (3) for the deep beam (G1SD1). This is because the increasing the ratio (a/d), in which loads are close to the middle of the beam, causing the flexural in the beam more than shear and thus increase of strains in the middle. And vice versa for the deep beam (G1SD2)

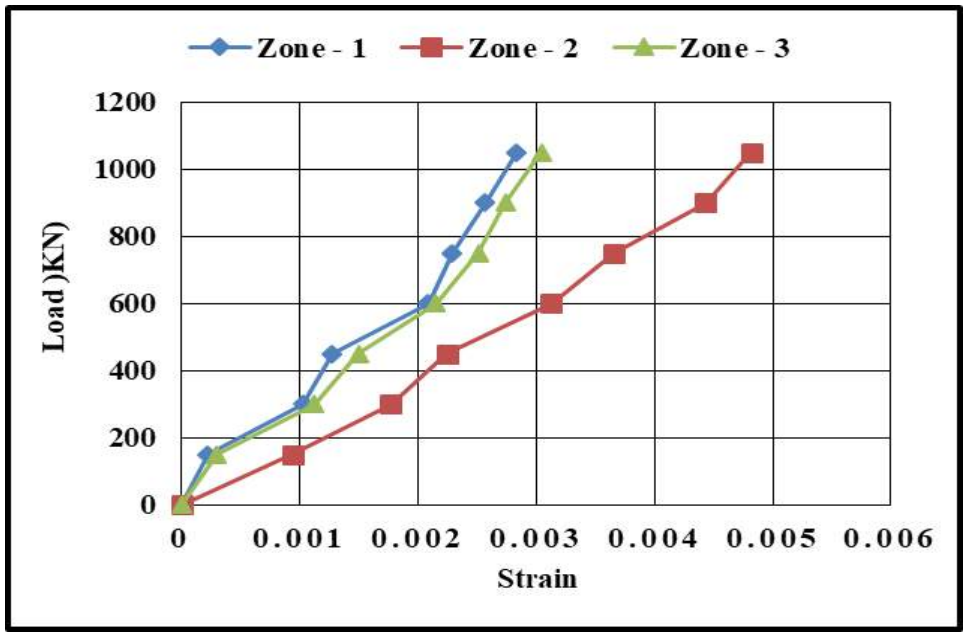

Figure (4.19) Strains distribution of deep beam (G1SD1).

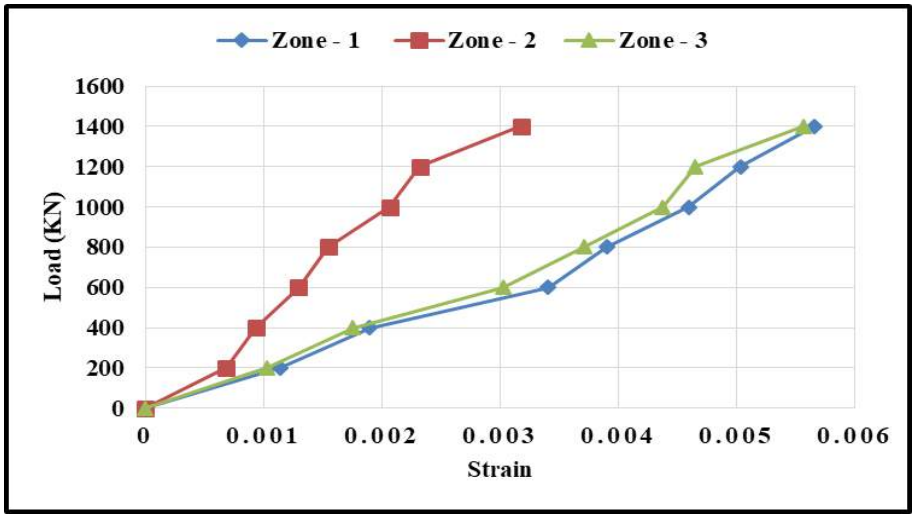

Figure (4.20) Strains distribution of deep beam (G1SD2).

4.4.3.3 Toughness of deep beams

The value of toughness characteristics of SIFCON deep beam (G1SD1 and G1SD2) is (7558 and 4265.5) kN.mm, respectively. Toughness decreased with decrease a\d ratio, see **figure (4.21)**.

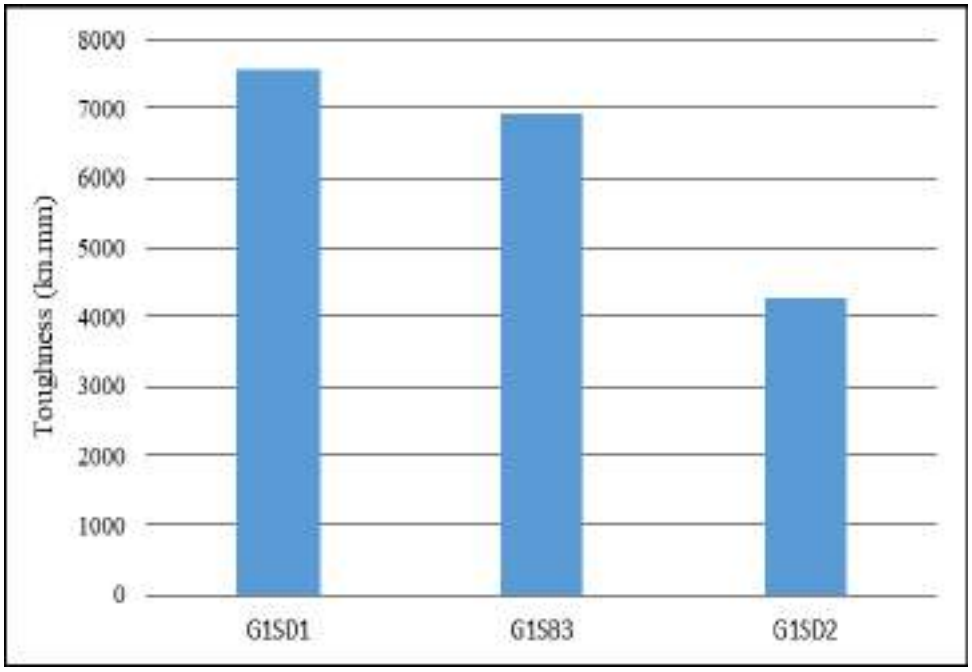

Figure (4.21) Variation toughness of deep beams (G1SB3, G1SD1 and G1SD2).

4.4.3.4 Ductility of deep beams

The values of ductility characteristics of SIFCON deep beams (G1SD1 and G1SD2) is 4.31% and 0.8 %. Note that the ductility is decrease with decrease a\d ratio., see **figure (4.22)**:

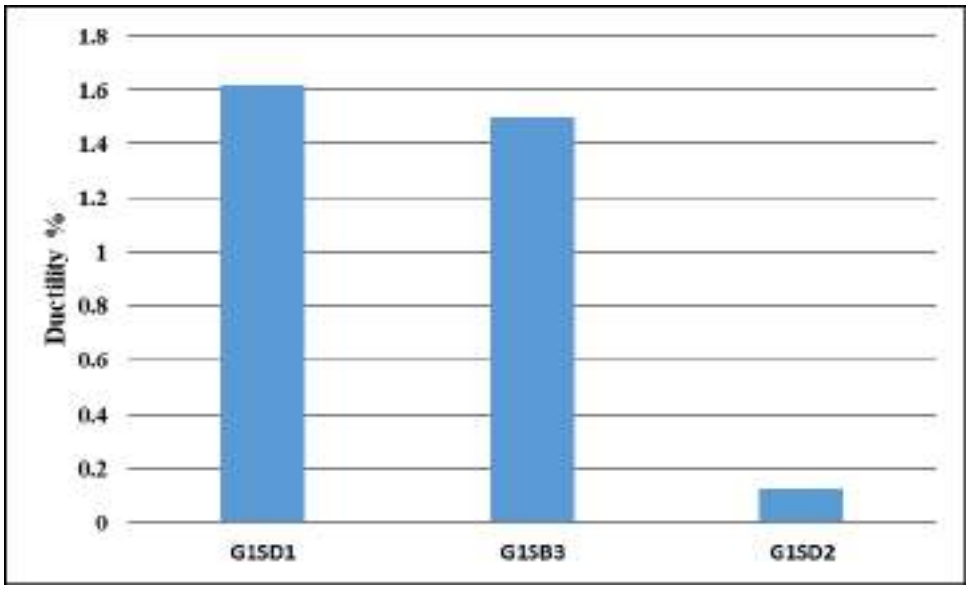

Figure (4.22) Variation ductility of deep beams (G1SB3, G1SD1 and G1SD2).

The reason that the ductility dropped in the deep beam (G1SD2) had a small deflection and therefore produced a little elongation.

4.4.4 Effect of Removing Main and Web Reinforcement

The purpose of this study is to determine the efficiency of the Sifcon at deep beams without the use of vertical reinforcement.

4.4.4.1 Load – deflection curve and crack pattern

Experimental load-deflection response of deep beam (G1SE1) is shown in fig. (4.23). In general, the relationship is approximately linear in this deep beam prior to failure, it can be observed that the removal of mesh reinforcement caused increasing in deflection and ductility.

The crack patterns of this deep beam are depicted in plate (4.8)**.** At load of (460 kN), the crack propagation of deep beam G1SE1 started with the formation of flexural cracks at mid span and extending upwards at limit level of depth. And then followed by small cracks in shear zone. As the load increased, another diagonal cracks appeared on both sides of the deep beams and multi flexural crack progressed to upward.

Also, high cracking load was about 523 KN in tension zone, see figure (4.24).

The ultimate load capacity for deep beam (G1SE1) is recorded about (922 KN). It was decrease about 17.6% from deep beam (G1SB3) and increase about 179.4% from deep beam (G1NA1), see figure (4.26).

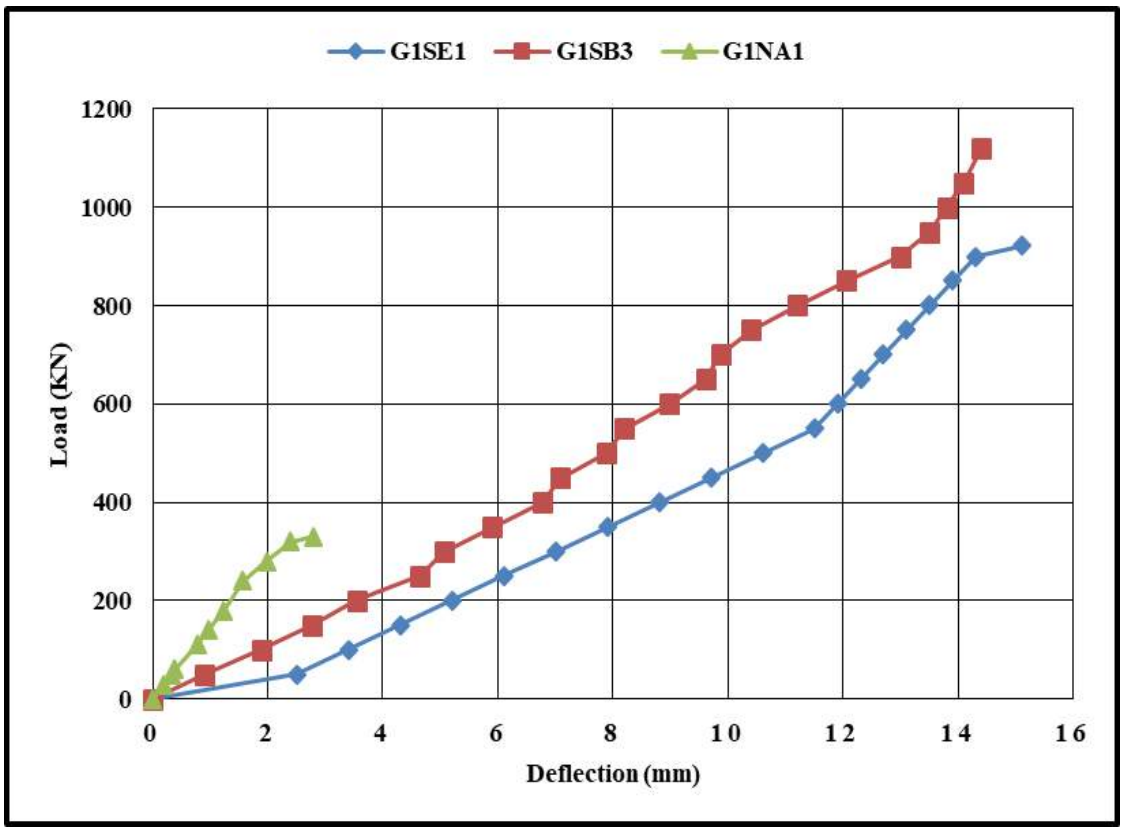

Figure (4.23) Load - Deflection Curve for Deep Beams (G1NA1, G1SB3 and G1SE1) specimens.

Plate (4.8) Experimental deep beam (G1SE1) after failure.

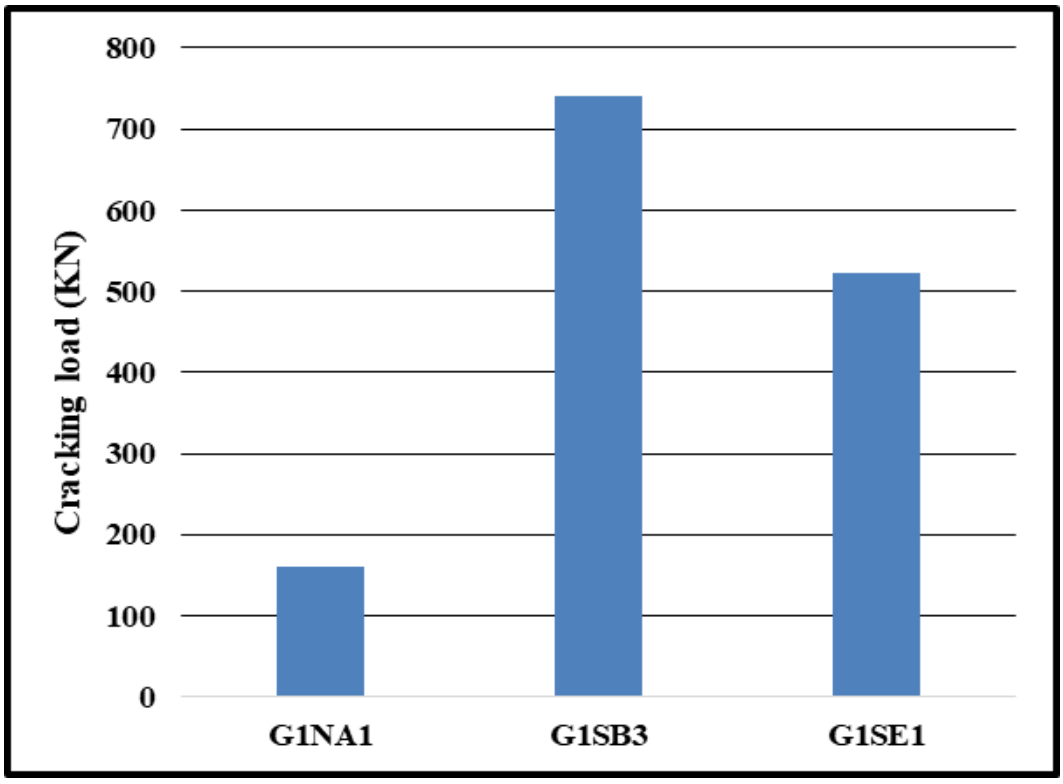

Figure (4.24) Variation of cracking load with solid deep beams (G1NA1, G1SB3 and G1SE1).

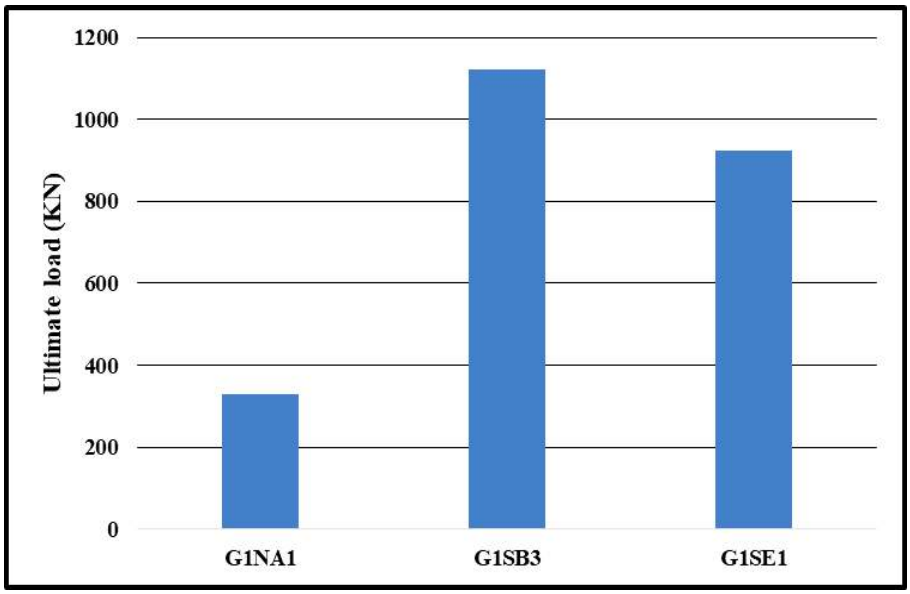

Figure (4.25) Variation of ultimate load with solid deep beams (G1NA1, G1SB3 and G1SE1).

4.4.4.2 Load – strain curves of deep beams

Strains of deep beam (G1SE1) is listed in **figures (4.26).** Higher strain is recorded in tension zone (0.0041).

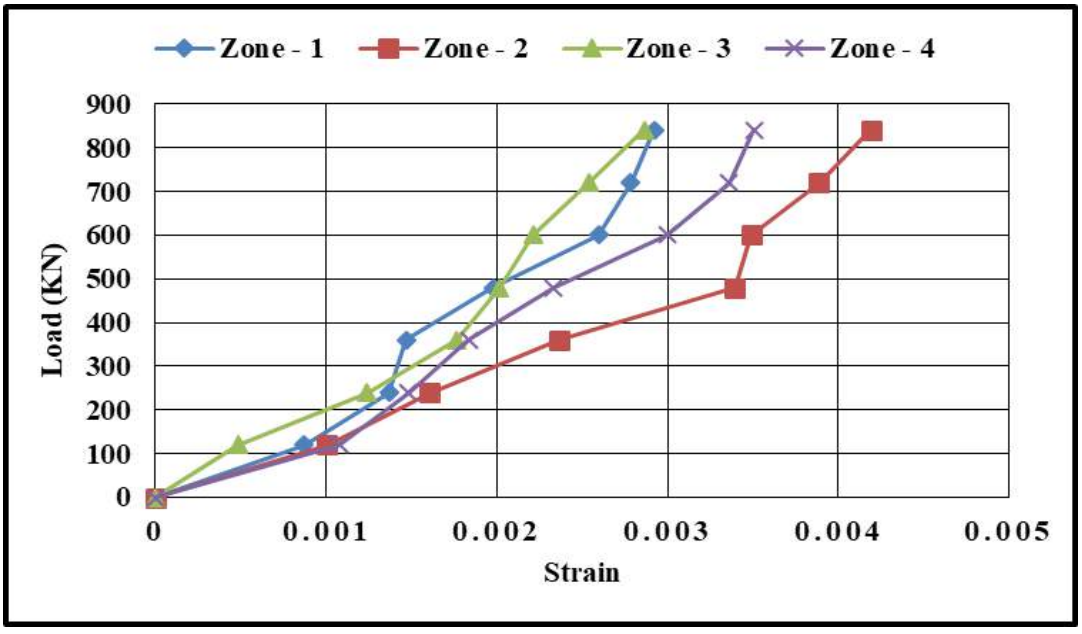

Figure (4.26) Strains distribution of deep beam (G1SE1).

4.4.4.3 Toughness of deep beam (G1SE1)

Energy absorption value is 5981.5 KN.mm. It should be noted that the energy absorption of SIFCON deep beam (G1SE1) without main and web reinforcement exhibited small toughness value if they compared with Sifcon solid deep beam (G1SB3), it is about of 13.62%. This means that the removal of the reinforcement mesh had little effect and gave high results compared to the conventional deep beam as shown in **figure (4.27).**

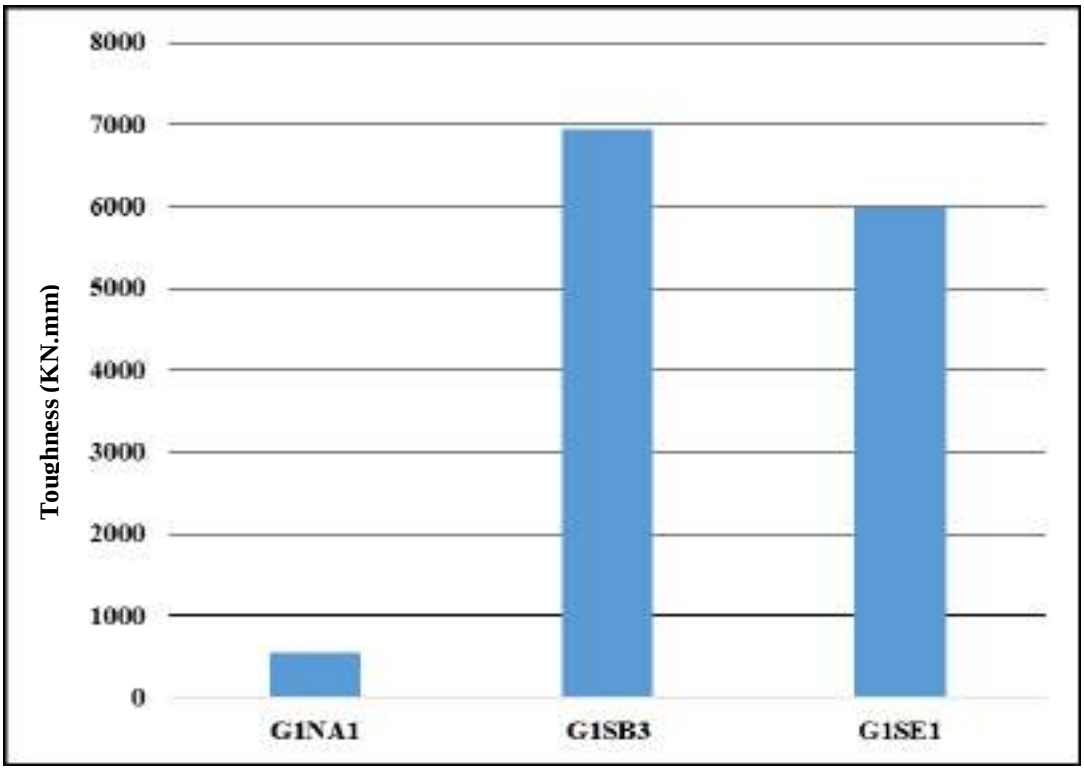

Figure (4.27) Variation toughness of deep beams (G1NA1, G1SB3 and G1SE1).

4.4.4.4 Ductility of deep beam (G1SE1)

Higher ductility is recorded (4.6%) in deep beam (G1SE1) by increasing percentage 48.4%, see **figure (4.28)**. The reason that the ductility increased in deep beam (G1SE1) due to increase in deflection.

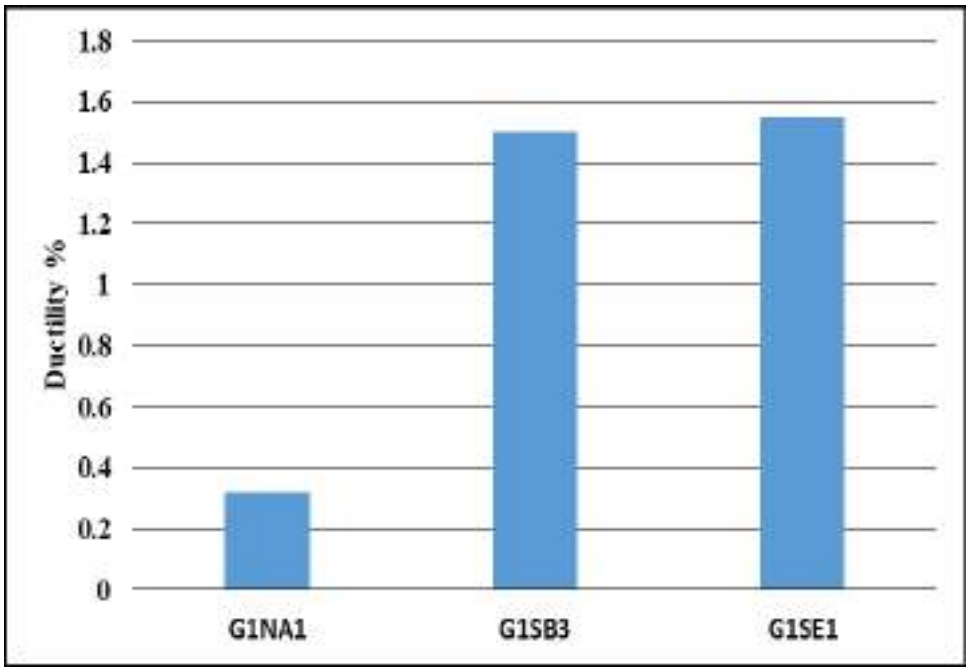

Figure (4.28) Variation ductility of deep beams (G1NA1, G1SB3 and G1SE1).

4.5 Experimental of deep beams with openings

4.5.1 Effect of Steel Fiber ratio (6%, 7.5% and 9%)

4.5.1.1 Load – deflection curve and crack pattern

The load-deflection relationship for this group of deep beam is presented in **Figure (4.29)**. This group consisted of four deep beams (G2NA1, G2SB1, G2SB2 and G2SB3), the first deep beam is casted for comparison purposes. All deep beams of this group failed in shear.

The increasing in cracks loads for sifcon deep beams (G2SB1, G2SB2 and G2SB3) were 60%, 140% and 236% respectively compared with the beam (G2NA1), see figure (5.30).

And the increasing in ultimate loads for sifcon deep beams (G2SB1, G2SB2 and G2SB3) were 223.8%, 242.8% and 309.5% respectively compared with the beam (G2NA1) see figure (4.31).

The crack of deep beam of conventional concrete G2NA1 started with the formation of shear cracks followed by flexure cracks. The appearance and distribution of cracks in the shear span area were considerably affected by the presence of the openings, while the crashing in concrete occurs when the load increases. At earlier loads, inclined shear cracks were formed from the diagonal edges of the opening and then propagated toward the support and load points as the load increased. These cracks simultaneously initiated above and below the openings in both sides of the deep beam. With a few increments, flexure cracks started to form from the deep beam soffit, as in plate (4.9).

Deep beam (G1SB1) with applied load, generated diagonal shear crack in two edge of circular opening is appear without flexural crack. As observe, no crack in top strut between two point loads with high load. Shear failure is done at ultimate load, as shown in **plate (4.10)**. Deep beam (G1SB2) with applied load, shear cracks are appearing without any flexural cracks. Shear failure is done at ultimate load, as shown in **plate (4.11).** In Deep beam (G1SB3) very fine crack in tension zone is began to form when load is applied. Also, one diagonal is developing to failure on the two edge side of circular openings, as shown in **plate (4.12)**.

Eventually, the failure occurred by splitting the deep beams along the line joining the bearing edges and openings tangents opposite to it, followed by crushing of concrete at the edge bearings at the load positions for conventional concrete and without crashing for sifcon deep beams.

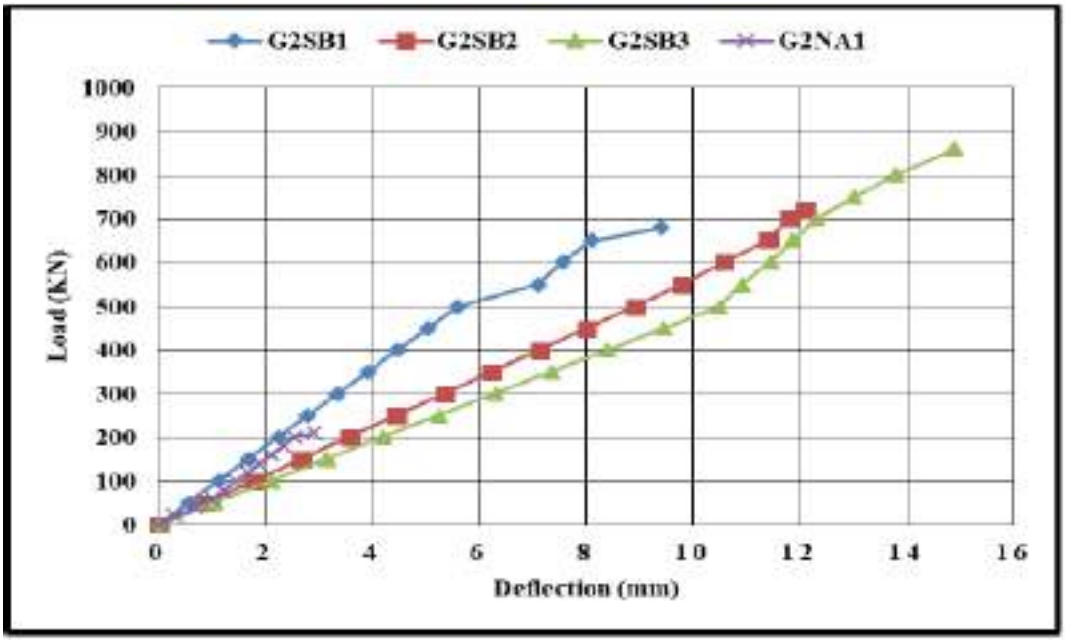

Figure (4.29) Load - Deflection Curve for Deep Beams (G2NA1, G2SB1, G2SB2 and G2SB3) beams.

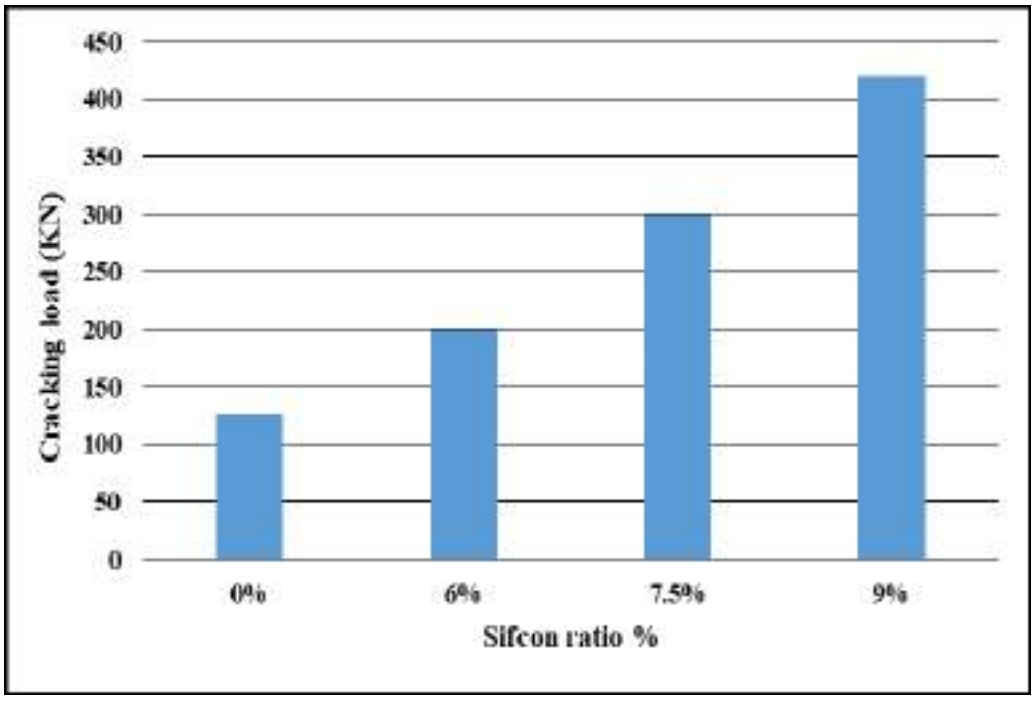

Figure (4.30) Variation of Crack load with Sifcon ratio of openings deep beams.

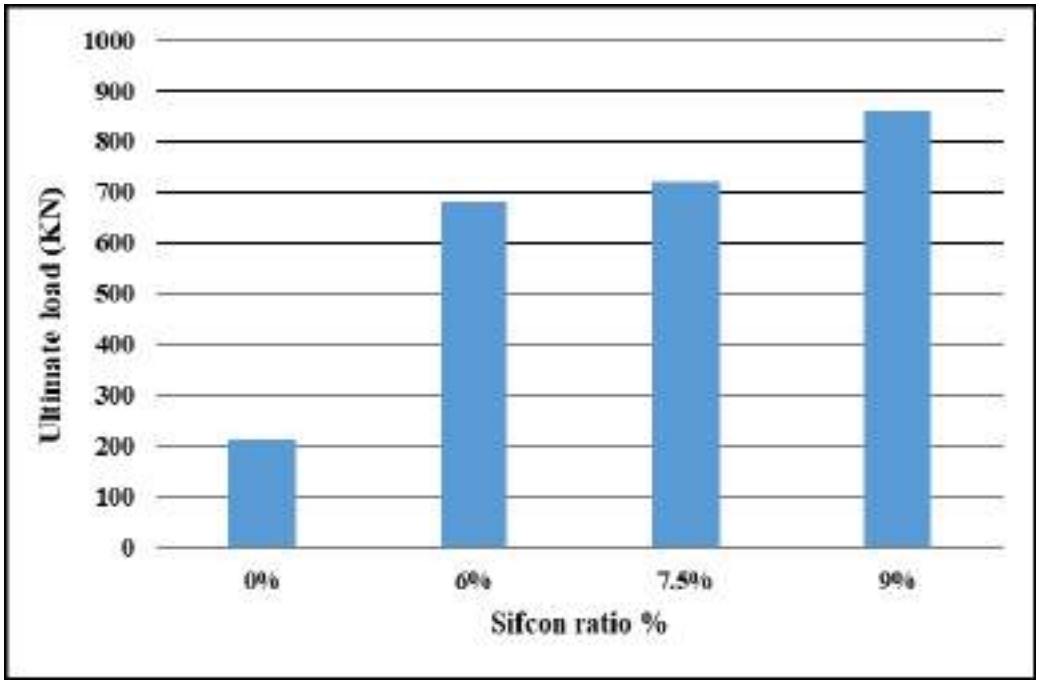

Figure (4.31) Variation of ultimate load with Sifcon ratio for opening deep beams.

Plate (4.9) Experimental Deep beam G2NA1 (0%SF) after failure.

Plate (4.10) Experimental Deep beam G2SB1 (6%SF) after failure.

Plate (4.11) Experimental Deep beam G2SB2 (7.5%SF) after failure.

Plate (4.12) Experimental Deep beam SB3 (9%SF) after failure.

4.5.1.2 Load – strain curves of deep beams

In specimens (G2SB1, G2SB2 and G2SB3) of Sifcon exhibit large strain (0.006, 0.0092 and 0.01) respectively, more than (0.003) with increase load in failure regions and conventional concrete deep beam with strain (0.003). The presence of opening in deep beam increasing strain close to openings due to concentration stresses around openings, see **figures (4.32) to (4.35).**

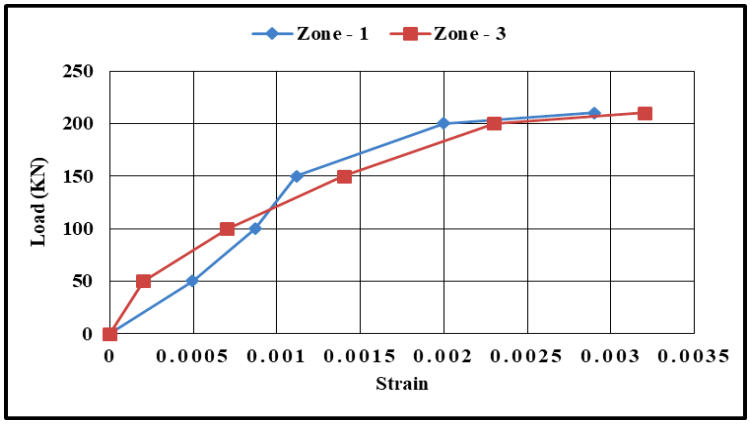

Figure (4.32) Strains distribution of deep beam (G2NA1).

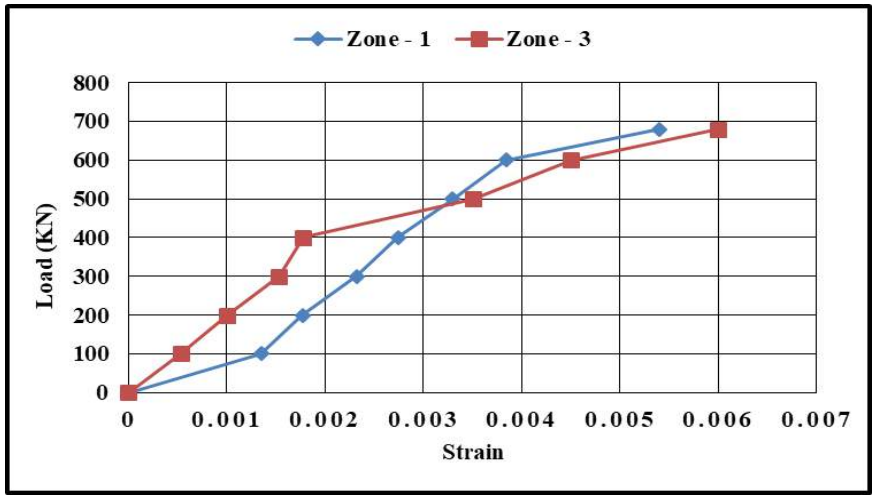

Figure (4.33) Strains distribution of deep beam (G2SB1).

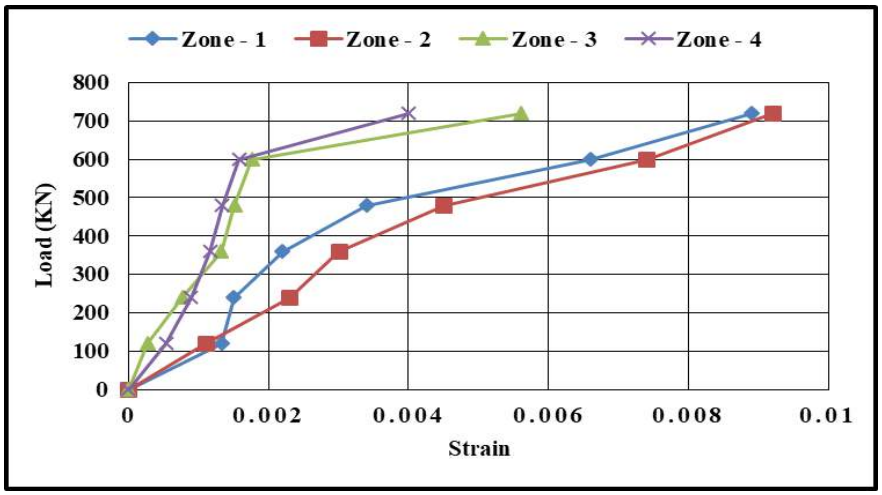

Figure (4.34) Strains distribution of deep beam (G2SB2).

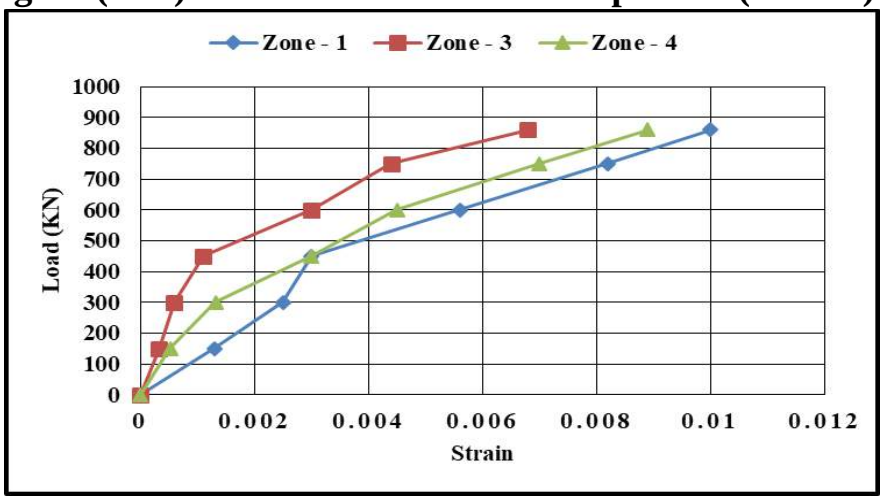

Figure (4.35) Strains distribution of deep beam (G2SB3).

4.5.1.3 Toughness of deep beams

Toughness increases with increase sifcon ratio by about (888.26%, 1270% and 1799.8%) compared with the deep beam (G2NA1), see **figure (4.36).**

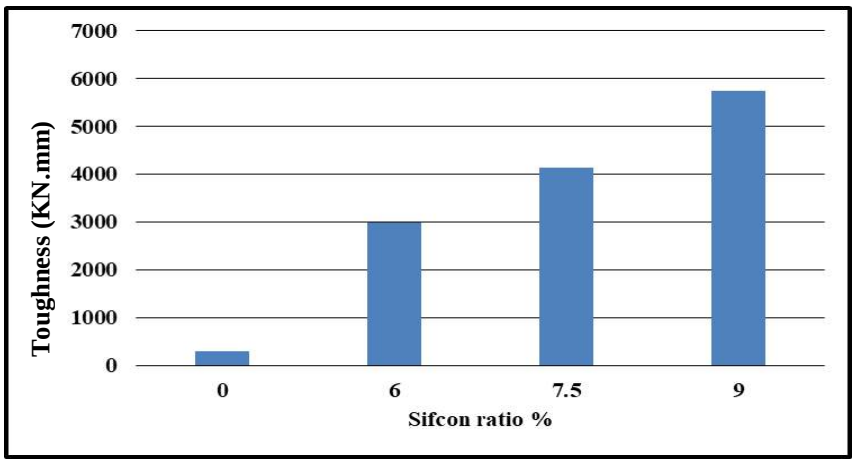

Figure (4.36) Variation toughness of deep beams (G1NA1, G1SB3 and G1SE1).

4.5.1.4 Ductility of deep beams

Ductility of deep beams with openings (G2SB1, G2SB2 and G2SB3) increases by about (147.43%, 348.71% and 402.56%) compared with the deep beam (G1NA1). ductility in deep beam with openings increase if comparison with solid deep beams, see **figure (4.38)**

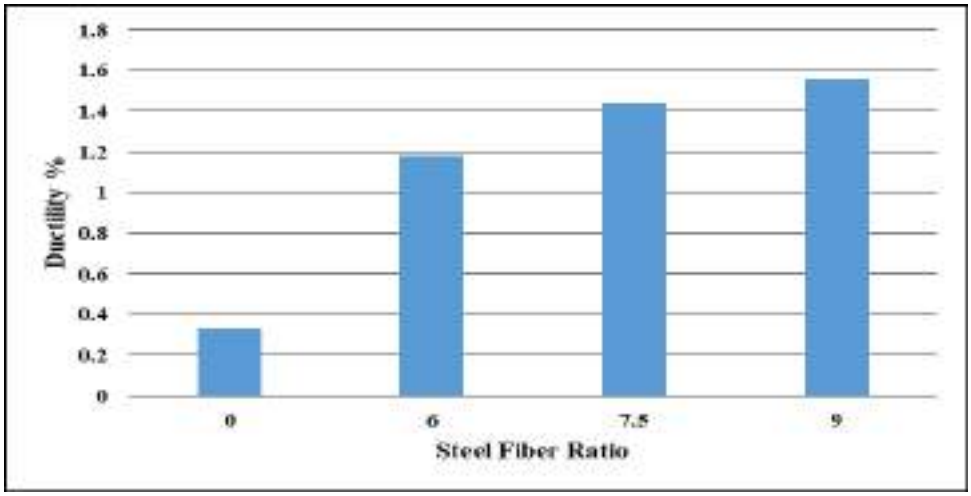

Figure (4.37) Experimental ductility of deep beams (G2NA1, G2SB1, G2SB2 and G2SB3).

4.5.2 Opening Reinforcement Effect

The incorporation of the inclined reinforcement around openings is found very effective in improving the shear strength and the deflection of the tested RC deep beam [29]. Thus, it's good to examine the effect of the inclined reinforcement around openings on the behavior of slurry infiltrated fibrous (SIFCON) and normal concrete. Therefore, in this group two deep beams (G2NC1 and G2SC2) had inclined reinforcement around their openings were tested. One of them was cast with normal concrete and the other from slurry infiltrated fibrous concrete (SIFCON).

4.5.2.1 Load – deflection curve and crack pattern

Figure (4.40) explains the load-deflection relationship of this group. It can be noted that, for deep beam G2NC1 the deflection values decreased when adding inclined reinforcement with increasing load as a result of restricting the crack width in the shear zone. Cracking load is listed in **figure (4.39)**:

Eventually, in shear zone deep beam G2NC1 failed with load greatly larger than the failure load of deep beam G2NA1 by about 33.8%, also deep beam G2SC2 failed with load greatly a little than the failure load of deep beam G2SB3 by about 9.3%, as shown in **Figure (4.38)**. This a little increment is expected due to the positive influence of Sifcon mix. The two beams failed in shear. The shear failure occurred by the same way observed in deep beam G2NA1. The deep beam G2SC2 failed at load greater than deep beam G2NC1 by about 234.5 % and without the crushing of concrete at the edge bearings at the load and support positions. Due to the behavior of Sifcon mix. Also, it can be seen that the ultimate load of deep beam G2SC2 is significantly increased when compared with the normal concrete deep beam G2NA1 by about 347.62%, this increment is because of the behavior of Sifcon with the existence of inclined reinforcement around the openings.

The crack patterns of deep beam G2NC1 were characterized by the formation of inclined cracks in a similar way to that occurred in deep beam G2NA1 at the same load level. While, for deep beam G2SB3, the inclined cracks appeared on the load level greater than that of deep beams G2NA1 and G2NC1. Shear crack without flexural crack followed them as the load increased in deep beam G2SC2, while in deep beam G2NC1 appeared at the load level slightly smaller from deep beam G2NA1. Other diagonal cracks formed with the increasing of the loads until they stopped to appear in flexural region. **Plates (4.13) and (4.14)** show the crack patterns of the tested deep beams.

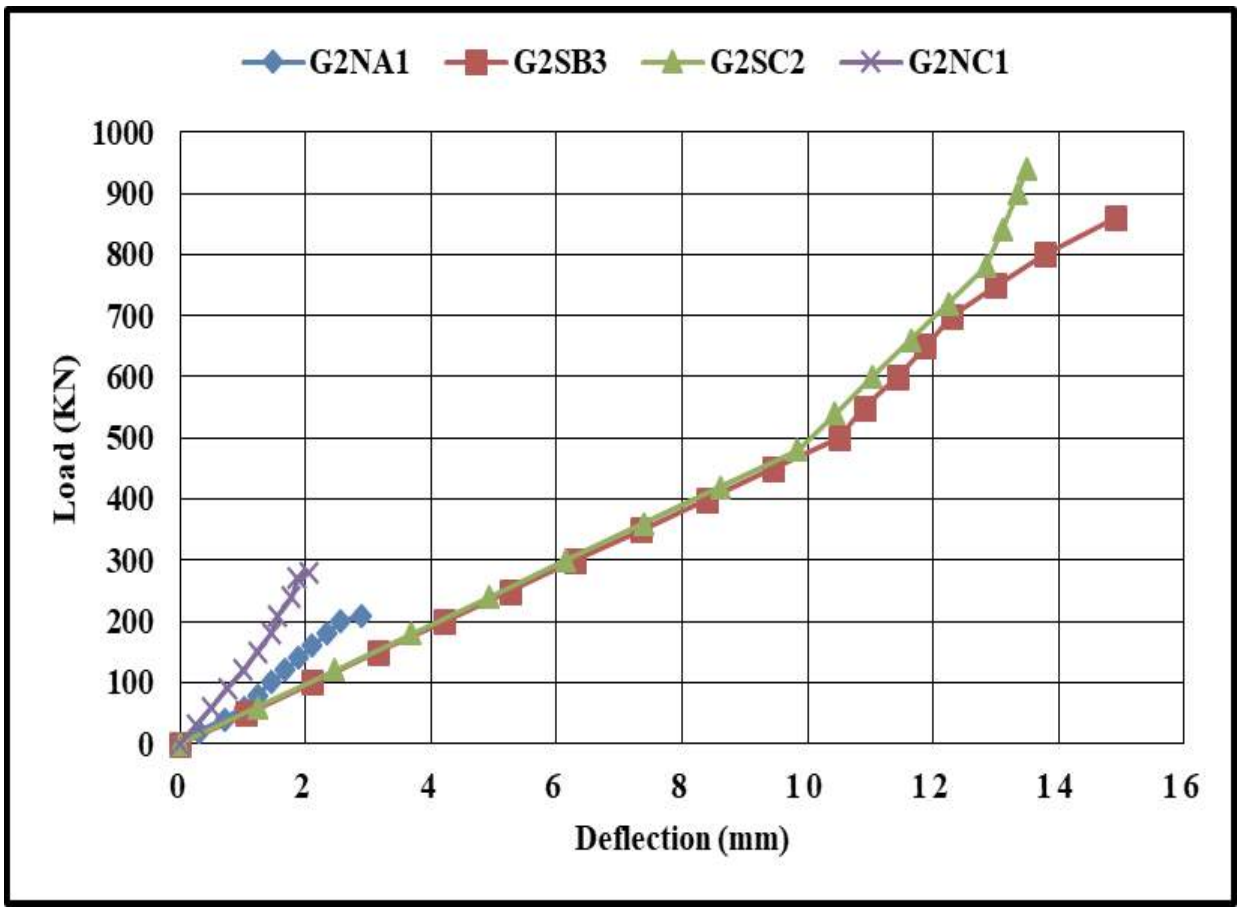

Figure (4.40) Load - Deflection Curve for Deep Beams (G2NA1, G2SB3, G2SC2 and G2NC1) specimens.

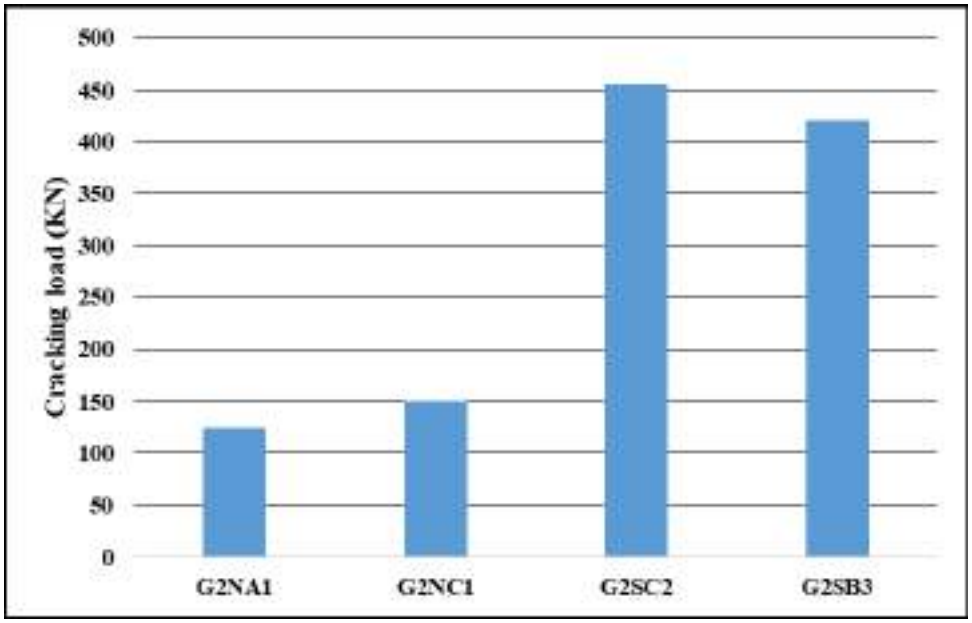

Figure (4.39) Variation of cracking load with openings deep beams (G2NA1, G2NC1, G2SC2 and G2SB3).

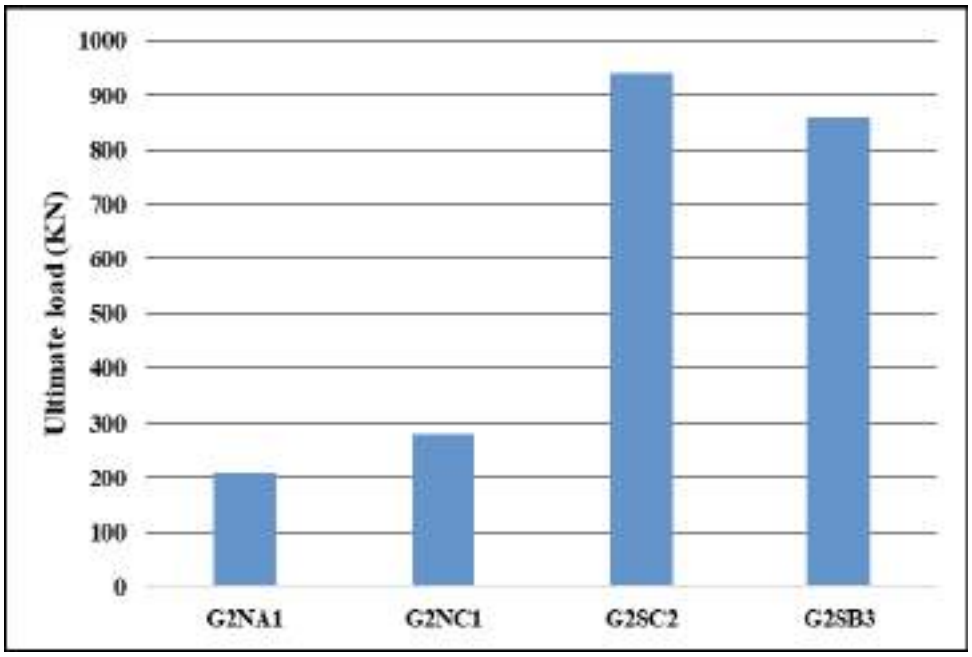

Figure (4.38) Variation of ultimate load with openings deep beams (G2NA1, G2NC1, G2SC2 and G2SB3).

Plate (4.13) Experimental Deep beam G2NC1 (0%SF) after failure.

Plate (4.14) Experimental Deep beam G2SC2 (9%SF) after failure.

4.5.2.2 Load – strain curves of deep beams

Strains of deep beams (G2NC1 and G2SC2) is illustrated in **figures (4.42) and (4.43).** High strain recorded in deep beam (G2SC2) as about (0.015).

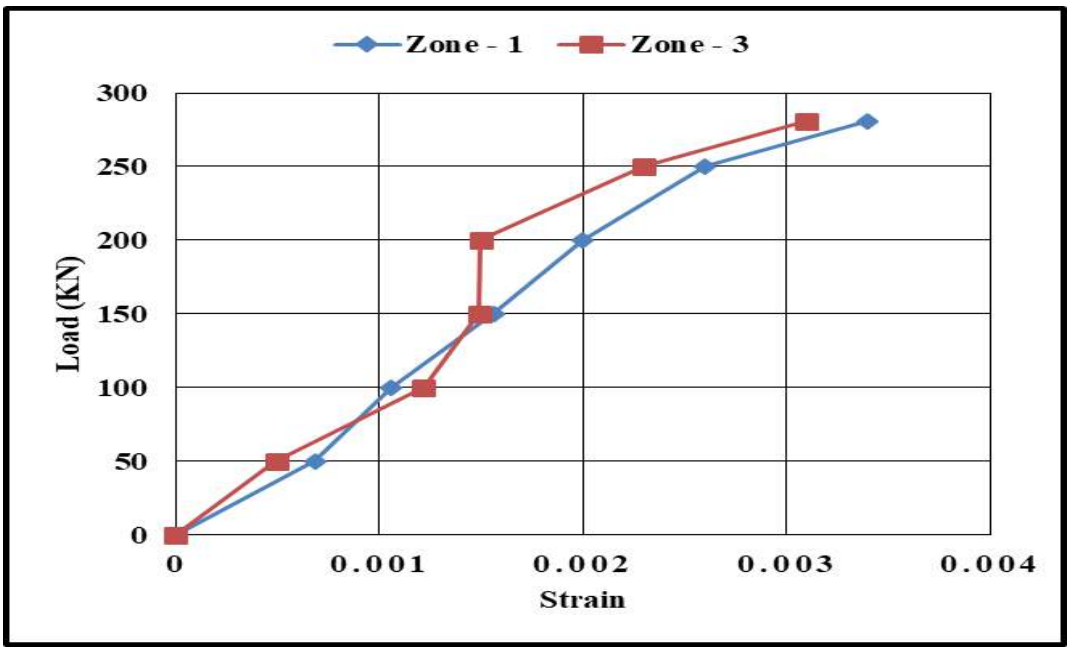

Figure (4.41) Strains distribution of deep beam (G2NC1).

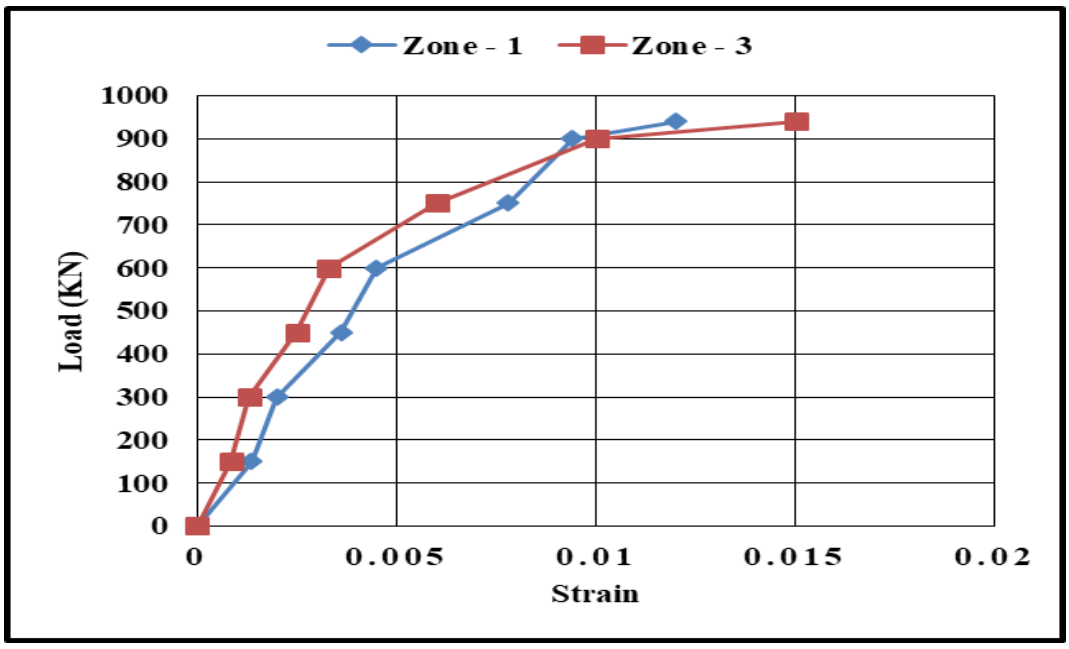

Figure (4.42) Strains distribution of deep beam (G2SC2).

4.5.2.3 Toughness of deep beams

It can be noted that the energy absorption of Sifcon deep beam (G2SC2) exhibit decrease in toughness value if compared with Sifcon deep beam (G2SB3) by about 16.14% and increasing about 1677% from (G2NC1), see **figure (4.43)**.

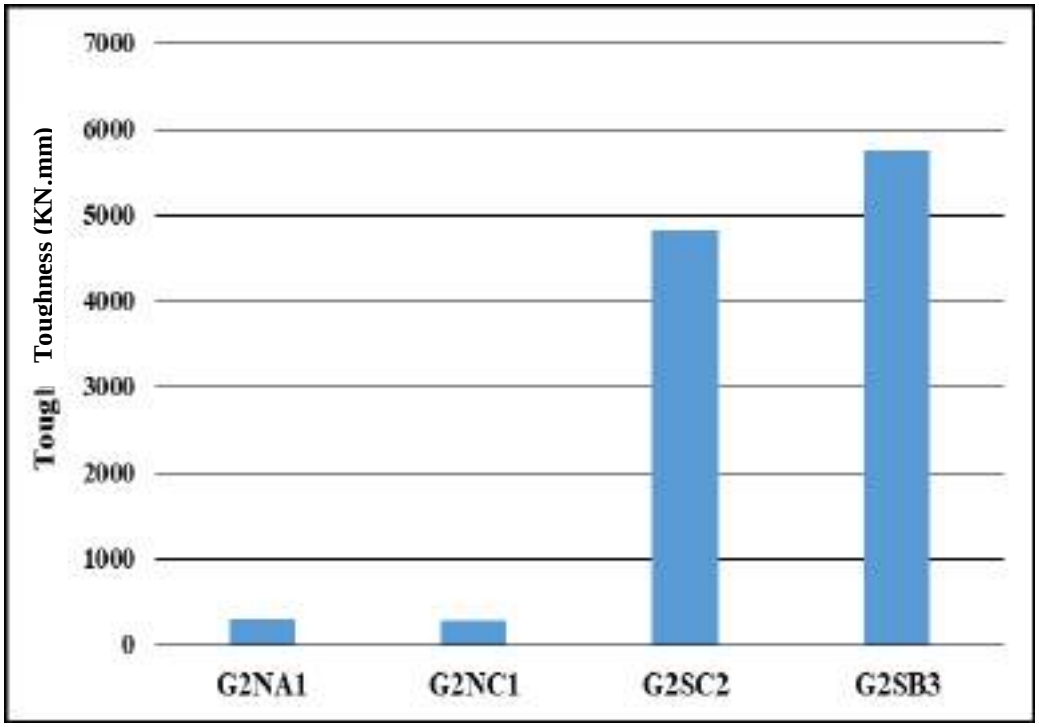

Figure (4.43) Variation toughness of deep beams (G2NA1, G2NC1, G2SC2 and G2SB3).

4.5.2.4 Ductility of deep beams

It can be noted that ductility of Sifcon deep beam (G2SC2) increased in ductility if compared with normal deep beam (G2NC1) by about 873.6% and decrease in ductility by about 37.9% if compared with deep beam (G2SB3), see figure (4.44).

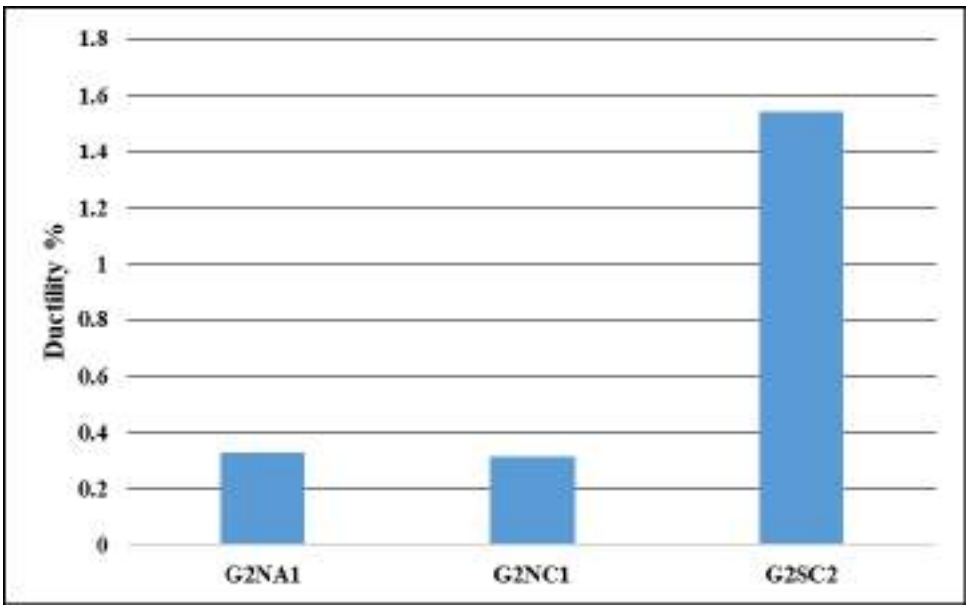

Figure (4.44) Variation ductility of deep beams (G2NA1, G2SB1, G2SB2 and G2SB3).

4.5.3 Effect of opening shape

For the purpose of studying the effect of the openings shapes on the behavior of deep beams, the shape of openings has been changed to a square for beam G2SD1 and a triangular for beam G2SD2).

4.5.3.1 Load – deflection curve and crack pattern

The deep beams with square and triangular openings appeared a difference in both load and deflection compared with the beams with circular openings as cleared in figure (4.45). This might be due to more concentration of stress at corners zone of the square and triangular openings. The cracking loads for the beams G2SD1 and G2SD2 were decreased by about 33.33% and 28% respectively than the beam G2SB3), see figure (5.46). While the ultimate loads for the beams G2SD1 and G2SD2 were decreased by about 22.44% and 13.95% respectively than the beam

G2SB3), see figure (4.47).

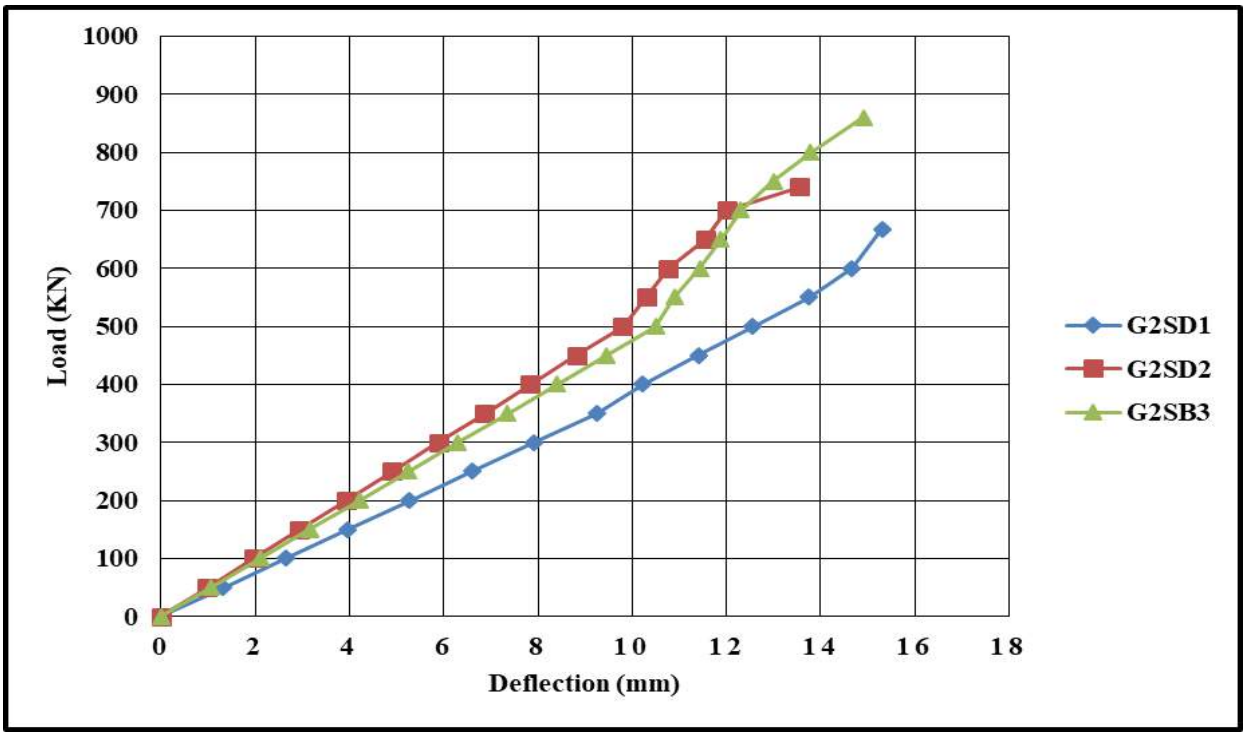

Figure (4.45) Load - Deflection Curve for Deep Beams (G2SB3, G2SD1 and G2SD2) specimens.

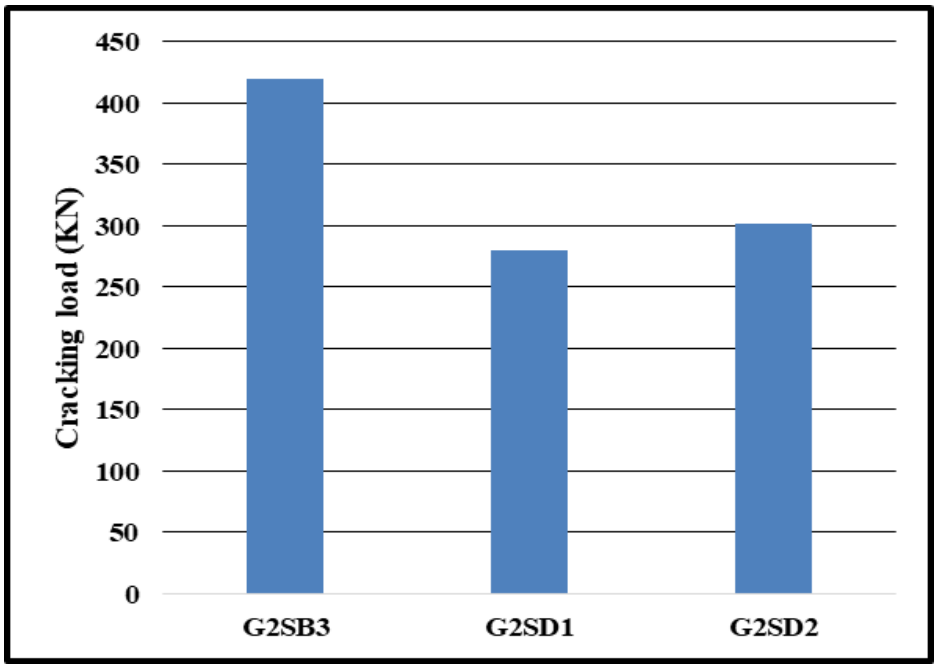

Figure (4.46) Variation of cracking load with openings deep beams (G2SB3, G2SD1 and G2SD2).

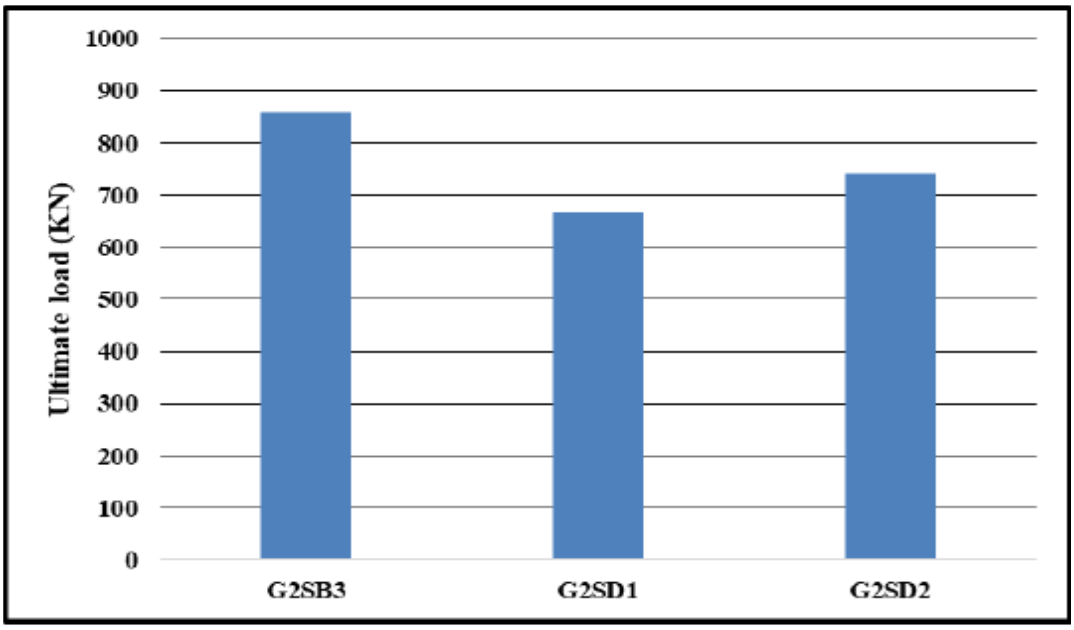

Figure (4.47) Variation of ultimate load with openings deep beams (G2SB3, G2SD1 and G2SD2).

The crack pattern is shown in **plate (4.33a and b) and (4.34).** The first crack is started in shear zone for two beams. The failure is occurred without any flexural cracks.

Plate (4.33a) Experimental Deep beam (front view) G2SD1 (9%SF) after failure.

Plate (4.33b) Experimental Deep beam (rear view) G2SD1 (9%SF) after failure.

Plate (4.34) Experimental Deep beam G2SD2 (9%SF) after failure.

4.5.3.2 Load – strain curves of deep beams

Load – strain of this group is illustrated in **figures (4.48) to (4.49).** Deep beam (G2SD1) had higher strain by about (0.0145).

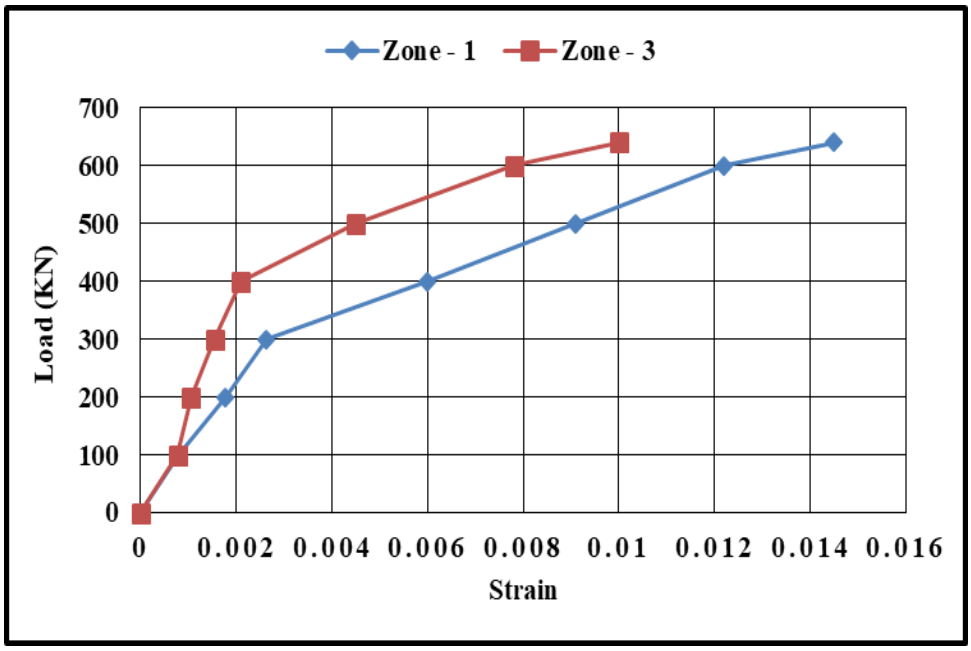

Figure (4.48) Strains distribution of deep beam (G2SD1).

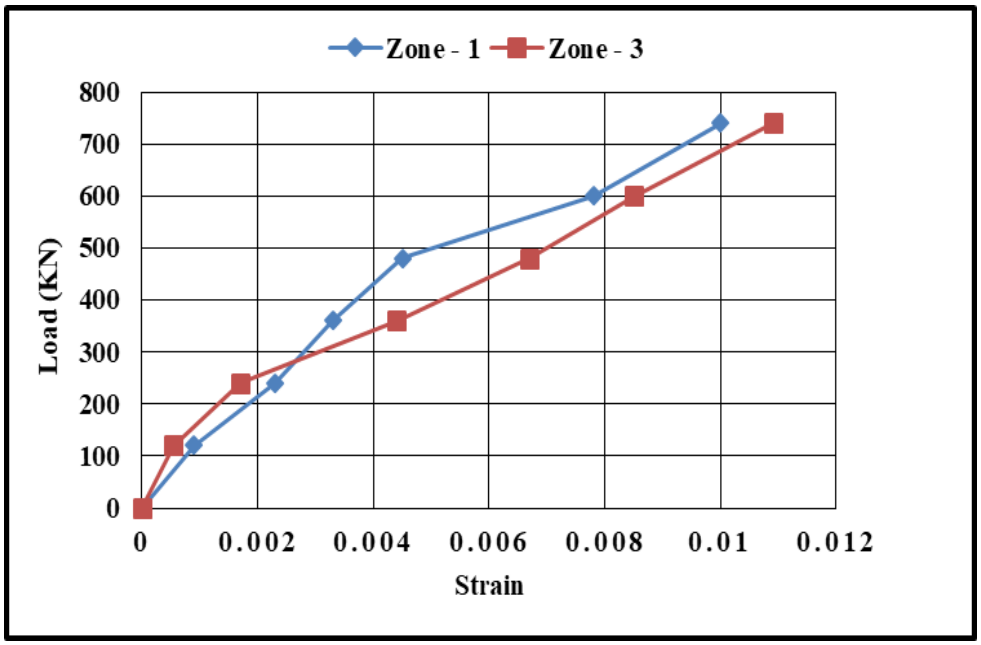

Figure (4.49) Strains distribution of deep beam (G2SD2).

4.5.3.3 Toughness of deep beams

It was noted that the energy absorption of Sifcon deep beams (G2SD1 and G2SD2) exhibit decrease in toughness value if compared with Sifcon deep beam (G2SB3) by about 20.3% and 25.5% , see **figure (4.50)**.

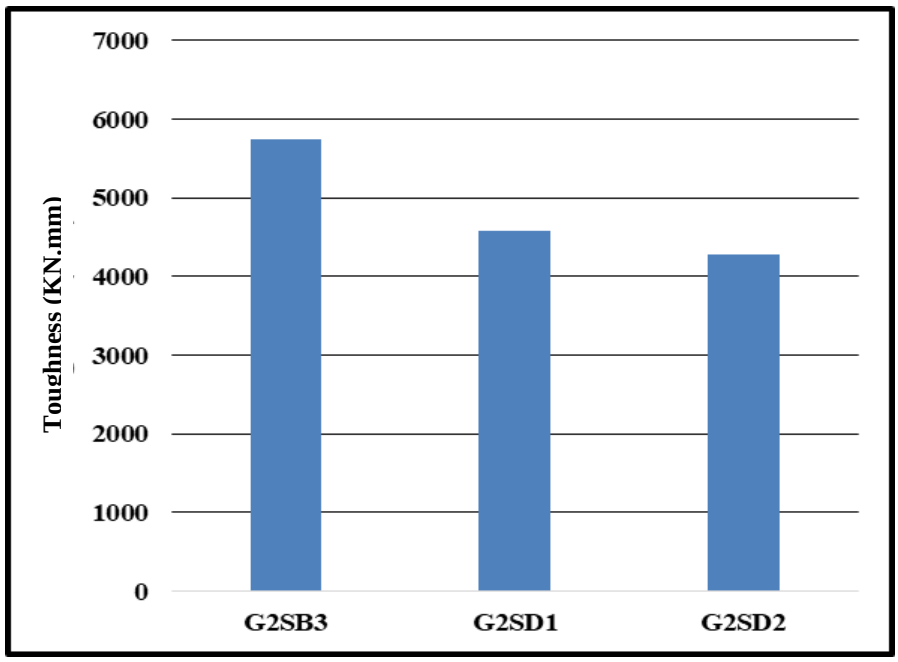

Figure (4.50) Variation toughness of deep beams (G2SD1, G2SD2 and G2SB3).

4.5.3.4 Ductility of deep beams

It can be noted that ductility of Sifcon deep beam (G2SD1 and G2SD2) increased in ductility value if compared with Sifcon deep beam (G2SB3) by 27.8% and 11.6%, see **figure (4.51)**.

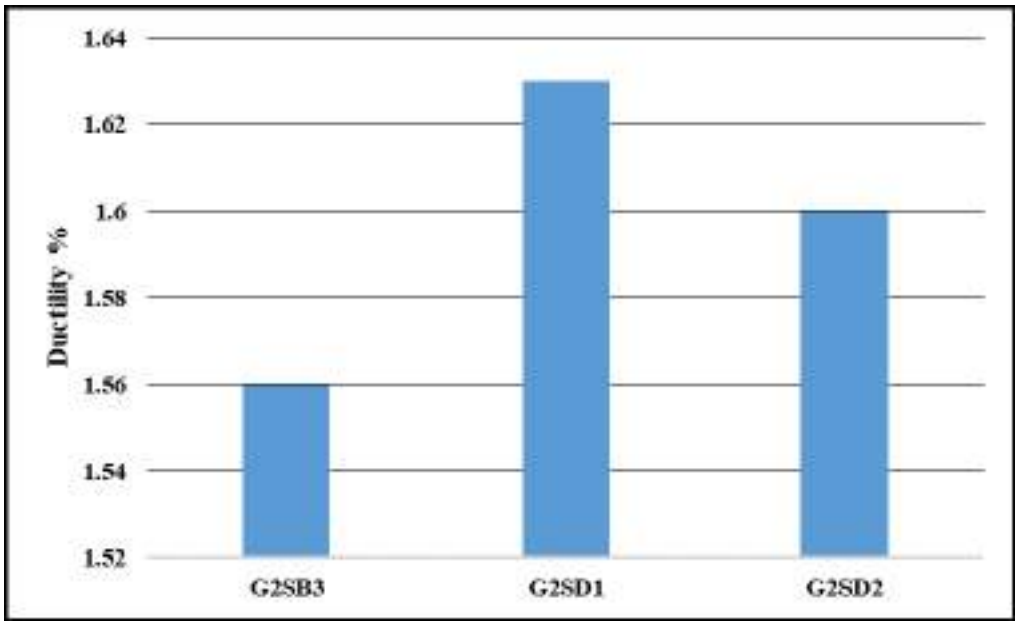

Figure (4.51) Variation ductility of deep beams (G2SD1, G2SD2 and G2SB3).

CHAPTER FIVE

FINITE ELEMENT ANALYSIS AND NUMERICAL MODELING

Chapter Five

Finite Element Analysis and Numerical Modeling

5.1 General

The nonlinear response of RC structures can be computed using the finite element method (FEM). This analytical method, gives the interaction of different nonlinear effects on RC structures. The success of analytical simulation is in selecting suitable elements, proper material models and in selecting proper solution method. The FEM is well suited for modeling composite materials with material models. The various finite element software packages are available. ANSYS (Analysis System), is an efficient finite element package available for the nonlinear analysis. This software becomes the most popular software in mechanical engineering, civil construction and science of materials namely with composite material and hybrid-materials structures. This chapter discusses the procedure for developing analysis model and materials simulations of SIFCON deep beams in ANSYS Ver.15. The necessary steps to create the calibrated model are explained in detail and the steps taken to generate the analytical load-deformation response of the member are discussed.

This chapter presents a suitable models and compares the results from the ANSYS finite element analyses with the experimental data for the sixteen tested deep beams.

5.2 The Finite Element Method

Now days, a numerical solution of FEM are widely utilized in solving of the structural problems. The large systems of algebraic equations were firstly assembled and then solved using computer abilities. Many of commercial finite element programs ANSYS, NASTRAN, SAP and ABAQUS are used. The selection of the ANSYS software was due to many advantage modeling the concrete material, steel

reinforcement element, stress-strain curve for concrete and reinforced bars, concrete crack/crush and failure criterion.

5.3 Finite Element Formulation

5.3.1 Basic Finite Element Relationships

To form the element equations, the principle of virtual work is used in the equilibrium equation for a nonlinear structure in a static equilibrium. The principle states that " if a general structure in equilibrium is subjected to a system of small virtual displacements within a compatible state of deformation, the virtual work due to the external action is equal to the virtual strain energy due to the internal stress [64], thus:

$$W_{int.} = W_{ext.} \qquad \text{..... (5.1)}$$

where,

$W_{int.}$ = internal work (strain energy)

$W_{ext.}$ = external work (work done by the applied force)

The virtual internal work is:

$$W_{int.} = \int_v \{\partial\varepsilon\}^T \{\sigma\}.\, dv \qquad \text{..... (5.2)}$$

where,

$\{\varepsilon\}$ = elements of virtual strain vector.

$\{\sigma\}$ = elements of real stress vector.

dV = infinitesimal volume of the element.

By using the general stress-strain relationship, stresses, $\{\sigma\}$ can be determined from the corresponding strains $\{\varepsilon\}$ as:

$$\{\sigma\} = [C].\ \{\varepsilon\} \qquad \text{..... (5.3)}$$

Where,

$[C]$= constitutive matrix

After substituting equation (4.3) into (4.2), the virtual internal work can be written as:

$$W_{int.} = \int_v \{\partial\varepsilon\}^T [C] \{\varepsilon\}. dV \quad \ldots\ldots\ldots\ldots (5.4)$$

The displacements $\{U\}$ within the element are related by interpolation to nodal displacements $\{a\}$ by:

$$\{U\} = [N].\{a\} \quad \ldots\ldots\ldots\ldots (5.5)$$

Where,

$[N]$ = shape function matrix

$\{a\}$ =unknown nodal displacements vector (local displacements)

$\{U\}$= body displacements vector (global displacements).

By differentiating equation (4.5), the strains for an element can be related to its nodal displacements by:

$$\{\varepsilon\} = [B] .\{a\} \quad \ldots\ldots\ldots (5.6)$$

where,

$[B]$ = strain-nodal displacement relation matrix, based on the element shape functions.

Assuming that all effects are in the global Cartesian system, and then combining equation (4.6) with equation (4.4) yields:

$$W_{int.} = \{\partial a\}^T \int_v \{B\}^T [C] \{B\}. dv. \{a\} \quad \ldots\ldots\ldots (5.7)$$

The external work, which is caused by the nodal forces applied to the element, can be accounted for by:

$W_{ext.} = \{a\}^T.\{F\}$ …… (5.8)

Where:

$\{F\}$= nodal forces applied to the element

Finally, equations (4.1), (4.7) and (4.8) may be combined to give:

$\{\partial a\}^T.\{F\} = \{\partial a\}^T \int_v \{B\}^T [C]\{B\}.dv.\{a\}$ …….. (5.9)

Noting that $\{\partial a\}^T$ vector is a set of arbitrary virtual displacements, the condition required to satisfy equation (4.9) can be reduced to:

$[K^e] . \{a\} = \{F\}$ …… (5.10)

Where, $[K^e] = \int_v \{B\}^T [C]\{B\}.dv$ …… (5.11)

$[K^e]$ = Element stiffness matrix

$dV = dx . dy . dz$

Equation (4.10`) represents the equilibrium equation on a one-element basis. For all elements, the overall stiffness matrix of the structure [K] is built up by adding the element stiffness matrices (adding one element at a time), after transforming from the local to the (overall) global coordinates, this equation can be written as:

$[K] . \{a\} = \{F^a\}$ …… (5.12)

Where:

$[K] = \sum_n [K^e]$ = overall structural stiffness matrix.

$\{F^a\}$= {F} vector of applied loads (total external force vector).

n = total number of elements.

5.4 Finite Element Representation

In structural analysis, the finite element method has been used as a general method of stress and deformation analysis. A three dimensional solid element is an alternative way to finite element representation of the structures. These elements that are used in ANSYS program are shown in **Table (5.1)** [64].

Table (5.1): Finite element representation of structural components.

Structural component	Finite element representation	Element designation in ANSYS
Concrete or Mortar	8-node brick element (3 translation DOF per node)	SOLID 65
Steel reinforcement bars	2-node discrete element (3 translation DOF per node)	LINK 180
Steel plate and supports	8-node brick element	LINK 185

5.4.1 Finite Element Representation of Concrete or Sifcon

The finite element idealization of SIFCON deep beams should be able to represent the concrete cracking, crushing, the interaction between concrete and reinforcement, the interaction between concrete and steel fibers to reduce crack

growth and the capability of concrete to transfer shear after cracking by aggregate interlock [65].

In the current study, a three-dimensional brick element with 8 nodes (SOLID-65) was used to model the concrete. The element has eight corner nodes, and each node has three degrees of freedom (u, v and w in x, y and z direction, respectively). The steel fiber reinforcement modeling is done by assuming steel fiber embedded in solid 65 elements. The element is capable of plastic deformation, cracking in three orthogonal directions, and then crushing. The geometry and node locations for this element type are shown in **Fig. (5.1)** [64]**.**

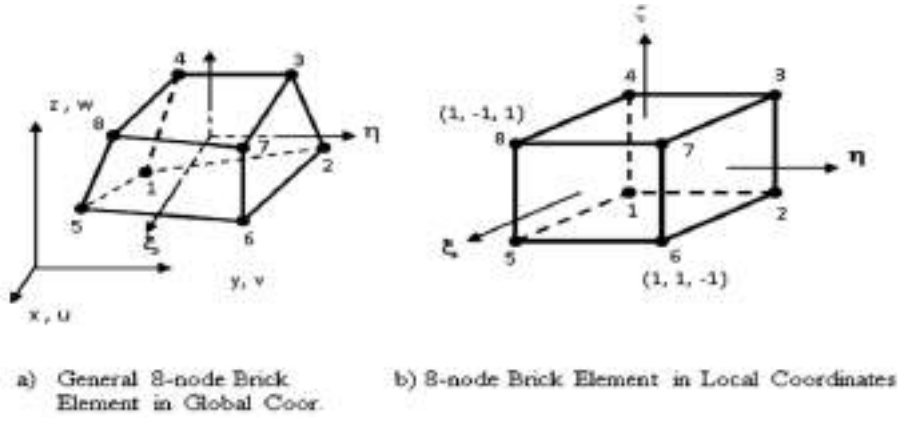

a) General 8-node Brick Element in Global Coor b) 8-node Brick Element in Local Coordinates

Figure (5.1): Three-dimensional 8-node brick (SOLID 65) element.

5.4.2 Finite Element Model of Reinforcement

Three techniques exist to model steel reinforcement in finite element models for reinforced concrete [65], these are: -

5.4.2.1 Discrete Representation

In the discrete representation which has been widely used the reinforcement is modeled as one dimensional bar or beam elements that are connected to concrete mesh nodes as shown in **Fig. (5.2a)**. Therefore, the concrete and the reinforcement mesh share the same nodes and the same occupied regions.

Full displacement compatibility between the reinforcement and concrete is a significant advantage of the discrete representation. The disadvantages are the restriction of the mesh and the increase in the total number of elements.

5.4.2.2 Embedded Representation

The embedded representation is often used with high order isoperimetric elements. The bar element is built in a way that keeps reinforcing steel displacements compatible with the surrounding concrete elements as shown in **Figure (5.2b)**. In the case of steel reinforcement is complex, this model is significant.

5.4.2.3 Smeared (Distributed) Representation

The stiffness matrix of the reinforcing steel is evaluated separately and then added to that of the concrete to obtain the global stiffness matrix. The smeared model assumes that reinforcement is uniformly spread in a layer throughout the concrete element in a defined region of the finite element mesh as shown in **Figure (5.2c)**. This approach is used for large scale models where the reinforcement does not significantly contribute to the overall response of the structure.

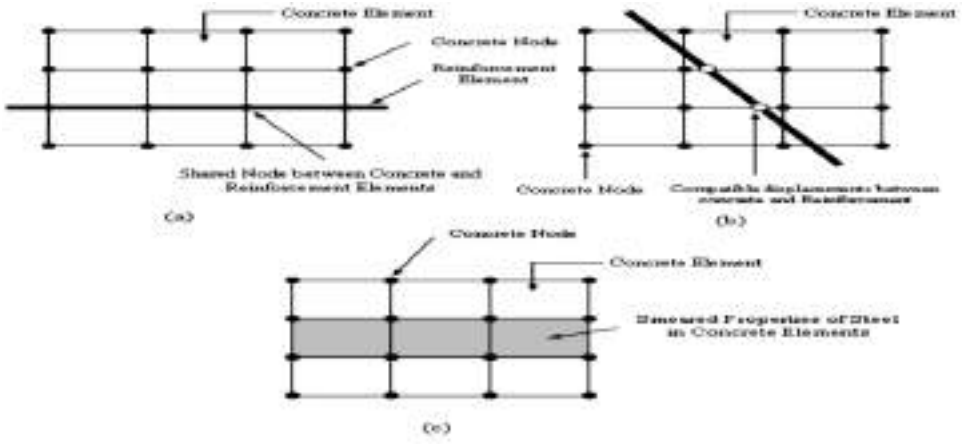

Fig. (5.2): Models for reinforcement in reinforced concrete: (a) discrete ;(b) embedded; and (c) smeared.

In the present study, the main bars reinforcement is represented by using 2- node discrete representation (LINK180 element in ANSYS V.15) as shown in **fig. (5.3)**. The steel reinforcement is assumed to be capable of transmitting axial forces only. Perfect bond is assumed to exist between the concrete and the reinforcing bars. To provide the perfect bond, the link element for the steel reinforcing bar is connected between nodes of each adjacent concrete solid element, so the two materials share the same nodes.

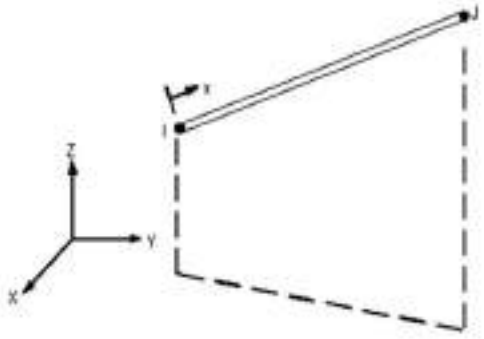

Figure. (5.3) LINK180 Element

The steel plates of supports and steel plate of the applied load were modeled by a Solid185 element. This element has eight nodes. Each node has three translational degrees of freedom x, y, and z directions. The geometry of this element is shown in **Figure (5.4)**

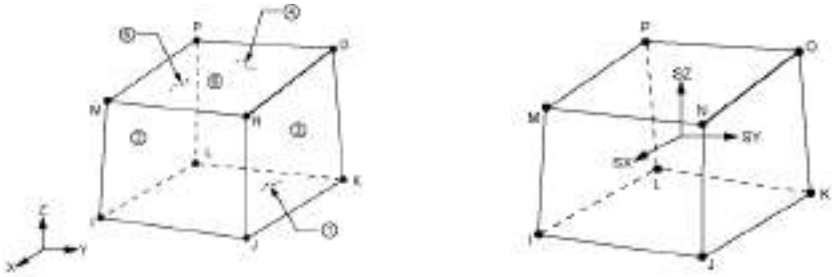

(a) Element's Geometry **(b) Stress Output**

Figure (5.4) Configuration of SOLID185.

5.5 Nonlinear Solution Techniques

Most phenomena in solid mechanics are nonlinear. However in many applications, it is convenient and practical to use linear formulation for problems to obtain engineering solutions. On the other hand, some problems definitely require nonlinear analysis if realistic results are to be obtained such as post yielding and large deflection behavior of structures.

For reinforced concrete members, the nonlinear finite element analysis yields a wide range of useful information about displacements, strains, distribution of normal and shear stresses in concrete, crack pattern at different stages of loading.

Nonlinear structural behavior arises from a number of cases, which can be grouped into these principal categories [66]:

1. Geometric Nonlinearities: These arise when a structure experiences large deformations in geometric configuration that are sufficient to change the way by which the load is applied.

2. Material Nonlinearities: These arise when the properties of the material suffer from nonlinearity changes during the load history.

3. Changing status: many common structural features exhibit nonlinear behavior that is status – dependent. For example, a tension – only cable is either slack or taut.

In the analysis of reinforced concrete and reactive powder concrete, the behavior of a nonlinear material is due to the continual and sudden change in the element stiffness which arises from cracking, crushing of concrete, fiber deboning, yielding of steel reinforcement and the plastic deformation of concrete and reinforcement. These represents the main sources of the nonlinearity. In the present study, the material nonlinearity is considered.

In the finite element analysis, the structural response to loading can be followed relatively easily in linear problems. While, in nonlinear problems, more sophisticated solution techniques should be employed. Usually, a nonlinear solution

is obtained by making successive linear approximations until the constitutive laws and equilibrium conditions are satisfied within an acceptable error [66].

The solution of equation (4.12) for a linear elastic structural problem can be obtained directly. In nonlinear problems, a direct solution is no longer possible since the stiffness matrix [K] depends on the displacement level ([K] = [K (a)], and therefore, it cannot be exactly calculated before the determination of the unknown nodal displacements {a}. For a nonlinear solution, the state of equilibrium of a structural system corresponding to the applied load must be found. These equilibrium equations can be derived by applying equilibrium conditions to the structural system. The equilibrium equations can be expressed as:

$$\{r\}= \{p\}-\{F^a\} \qquad \ldots\ldots\ldots\ldots (5.13)$$

Where

$\{r\}$=out of balance force vector.

$\{p\}$= vector of the nodal forces equivalent to the internal stress level, which is given by:

$$[p] = \int_v \{B\}^T [\sigma] . dv \qquad \ldots\ldots\ldots\ldots (5.14)$$

The equivalent internal forces also depend on the displacement level, {P} = {p (a)}, and have to be approximated in successive steps until equation (5.12) is satisfied.

The solution of nonlinear problems by the finite element method is usually attempted by one of the following three basic techniques:

1-Iterative techniques

2-Incremental techniques

3- Incremental- Iterative techniques

In the present work Incremental-Iterative techniques were utilized.

5.5.1 Incremental-Iterative Techniques

This technique, **Figure (5.5)**, is usually carried out by applying the external loads as a sequence of sufficiently small increments, and within each increment of loading, iterations are performed until equilibrium is satisfied according to some selected convergence criterion. This mixed method is widely used in the analysis of reinforced concrete structures because of its accuracy and capability to provide information throughout the loading history. The incremental-iterative solution procedures, which have been used in the present study, use the following procedures [63]:

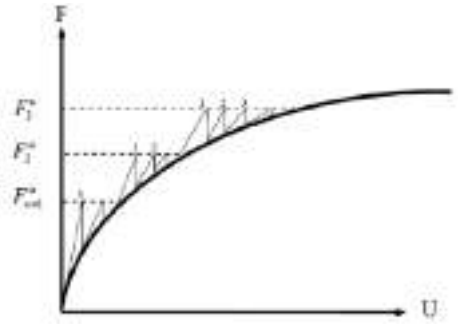

Figure (5.5): Incremental-iterative techniques.

5.5.1.1 Full Newton-Raphson Procedure

In this procedure, the stiffness matrix is updated at every equilibrium iteration, thus a large amount of computation may be required to form and solve the stiffness matrix, **Fig. (5.6)** [64].

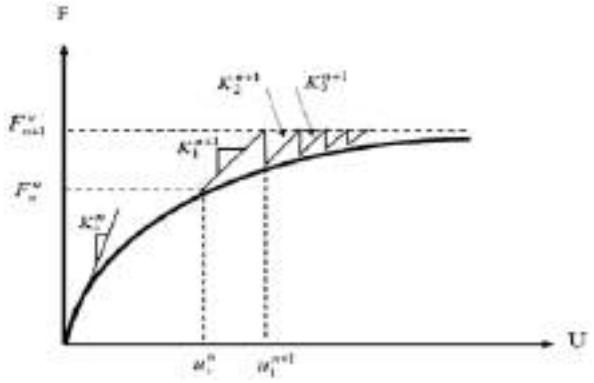

Figure (5.6): Full Newton-Raphson method.

5.5.1.2 Modified Newton-Raphson Procedure

The modified forms of the Newton-Raphson method are most common. In one the stiffness matrix is updated at the beginning of the first iteration of every load increment (KT1 method). In case of two modifications, the stiffness matrix is calculated at the beginning of the second iteration (KT2 method), so that the nonlinear effects are more accurately represented in the stiffness matrix.

These methods are more economical than the full Newton-Raphson method because they involve fewer stiffness matrix reformulations, but the convergence is slower and a large number of iterations is required to achieve a converged solution, **Fig. (5.7)** [64].

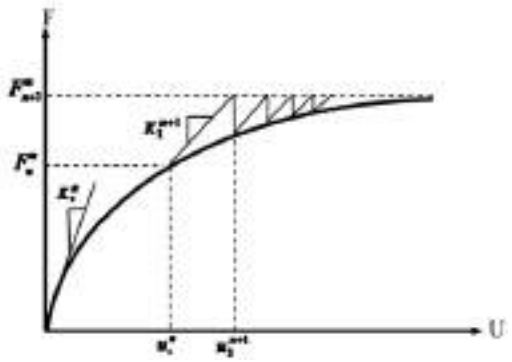

Figure (5.7): Modified Newton-Raphson.

5.5.1.3 Initial-Stiffness Procedure

In this procedure, the stiffness matrix is formed and solved only once at the beginning of the analysis, and the program uses this initial stiffness matrix at every equilibrium iteration. For this procedure, the computation cost per iteration is significantly reduced, but in case of strong nonlinearities (such as large deformation analyses), the method often fails to converge**, Figure (5.8)**. In the present study, ANSYS Version.15 uses the full Newton-Raphson method with the finite element method in analyzing the tested specimens [64].

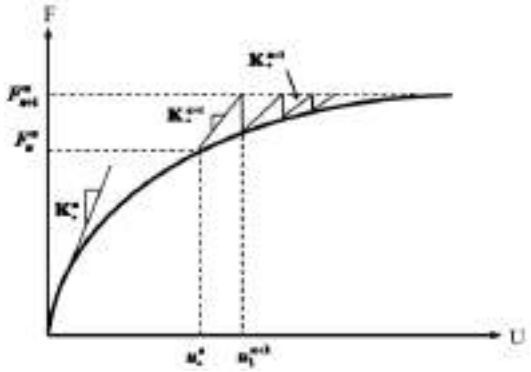

Figure (5.8): Initial stiffness method.

5.5.2 Convergence Criterion

For the incremental-iterative solution method, the progress of the iterative procedure is monitored with reference to a specified convergence criterion. Convergence is assumed to occur when the difference between the external and internal forces becomes negligibly small, and the iterative process is then terminated. Selecting a suitable convergence tolerance usually specifies accuracy of the approximate solution. If the convergence tolerance is too loose, inaccurate results may be obtained, and if the tolerance is too tight, additional computational effort is spent to obtain needless accuracy.

However, nonlinear structural analysis with several convergence criteria can be used to monitor equilibrium. These criteria are usually based on out of balance forces, displacement or internal energy. The convergence criterion, adopted in the present study, uses the out of displacement convergence. The incremental displacements at iteration (i) relative to the total displacement are considered in the criterion. When the incremental displacements are within a given tolerance of the total displacements the solution is considered to have converged. The criterion can generally be written in the form [61]:

$$\|\{\Delta D_i\}\| = \left(\sum \Delta D_i^2\right)^{0.5} \le T_n \left(\sum D_i^2\right)^{0.5} \quad \ldots\ldots\ldots\ldots (5.15)$$

Where:

T_n = tolerance [varied between (0.0005-0.01) in this study].

$\{\Delta D_i\}$ = incremental displacement vector at (i) iteration.

n = total number of degrees of freedom.

5.5.3 Equilibrium Iteration (Analysis Termination Criterion)

The nonlinear finite element analysis used in simulating the response of reinforced concrete structures must include as well a criterion to terminate the analysis when failure of the structure is reached. In a physical test under load control, collapse of a structure takes place when no further loading can be sustained; this is usually indicated in the numerical tests by successively increasing iterative displacements and a continuous growth in the dissipated energy. Hence, when the convergence of the iterative process cannot be achieved and then it is necessary to specify a suitable criterion to terminate the analysis.

In the present study, a maximum number of iterations for each increment of load is specified to stop the nonlinear solution if the convergence tolerance has not been achieved. A maximum number of iterations in the range of (100) is used, because it is observed and found that this range is generally sufficient to predict the solution's divergence or failure **[65]**.

5.6 Modeling of Materials Properties

Behavior of concrete extensively depends on the properties of each of its components; cement mortar, aggregates and air voids. In case of SIFCON, additional variables also influence its properties, such as the steel fiber volume fraction, silica fume and superplasticizer.

In many cases, the analysis and design of reinforced concrete structures encounters practical difficulties due to the complex material behavior involving phenomena

such as inelasticity, cracking and interaction between concrete and reinforcement. These complexities have led to the development of many models for the analysis of plain and reinforced concrete.

The reinforcing steel can be considered as a homogeneous material and its properties are generally well defined.

On the other hand, plain concrete and fibrous concrete are heterogeneous materials having completely different properties in compression and in tension. Because of this heterogeneity, it is difficult to define their properties accurately.

5.6.1 Modulus of Elasticity

Modulus of elasticity is strongly influenced by the concrete materials and their proportions. It is a function of modulus of elasticity of each component and its content ratio in the composite. An increase in the modulus of elasticity of concrete is expected with an increase in the compressive strength since the slope of the ascending branch of the stress-strain diagram becomes steeper. From test of modulus of elasticity in experimental work that shown value is 43531 MPa for mix 3.

5.6.2 Poisson's Ratio (υ)

Experimental data on values of Poisson's ratio (υ) (i.e., the ratio of lateral to longitudinal strain) for SIFCON under uniaxial compressive stress were very limited. Poisson's ratio of SIFCON may not differ too much from other concretes. Within the elastic range the Poisson's ratio for all investigated is about 0.2.

5.7 Material Modeling of Deep Beams

5.7.1 Real constants

Two real constants used, concrete and steel bars are used to define the geometry of the target surface elements [67] see **Table (5.2)** below:

Table (5.2) Real constants for ANSYS V.15 Models.

Real constant set	Element type	constants			
1	LINK 180	Cross section area (mm^2) – Ø4 mm	12.56		
2	LINK 180	Half Cross section area (mm^2) – Ø10 mm	39.27		
3	LINK 180	Cross section area (mm^2) – Ø16 mm	201		
4	LINK 185	without real constant			
5	Solid 65	Properties	**Real constants**		
			Rebar 1	Rebar 1	Rebar 1
		Material number	4	4	4
		Volume ratio	0.03	0.03	0.03
		Orientation angle THETA (Horizontal angle)	0	90	135
		Orientation angle PHI (vertical angle)	90	0	135

5.7.2 Material models

Parameters needed to define the material models are illustrated in **Fig. (5.9)**. As seen below, there are multiple parts of the material model for each element. Material number (1) refers to the solid 65 elements, material number (2, 3 and 4) refers to the LINK 180 element, material number (5) refers to the LINK 185 element and material number (6) refers to the LINK 180 element (steel fiber). The solid 65 element requires linear isotropic and multilinear isotropic material properties for proper model concrete. The multilinear isotropic material uses the von mises failure criterion along with the willam and warnke (1974) model to define the failure of the

concrete. EX is the modulus of elasticity of concrete (E_c), and PRXY is the poisson's ratio (υ). The modulus was based on the experimental values presented in table. poisson's ratio was assumed to be 0.2 for concrete and 0.3 for steel.

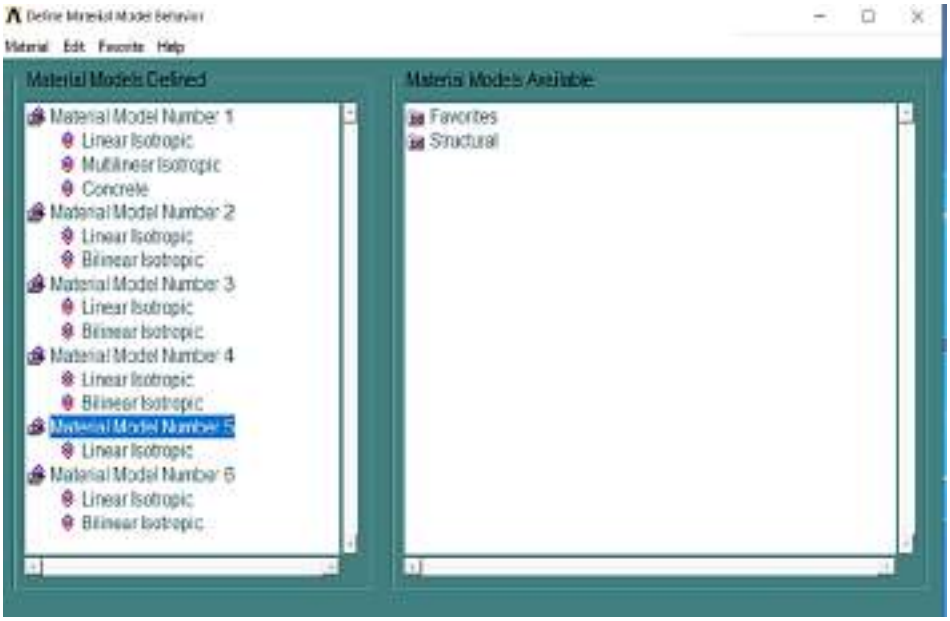

Figure (5.9) Material properties' numbers.

5.7.3 Boundary Conditions and Loading

In order to get a unique solution, constrains should be carried out. The applied of boundary conditions was used in ANSYS 15 as applied specific displacement with zero value. To keep the model behaves like the experimental beam, the boundary conditions need to be applied along the axis of symmetry. All nodes of the vertical plane of symmetry must be constrained in the perpendicular directions (UZ = 0) and allow the vertical movement.

The roller support was modeled by constrained, in the Y direction, the nodes that lie in mid-line of plate. The rotational movement was allowed to complete the modeling of the roller. The applied force was modeled as a lumped at the steel plate. The force applied at each internal node of the actual force and has a magnitude a twice that applied at each of the two external nodes on the plate, see **Figure (5.10).**

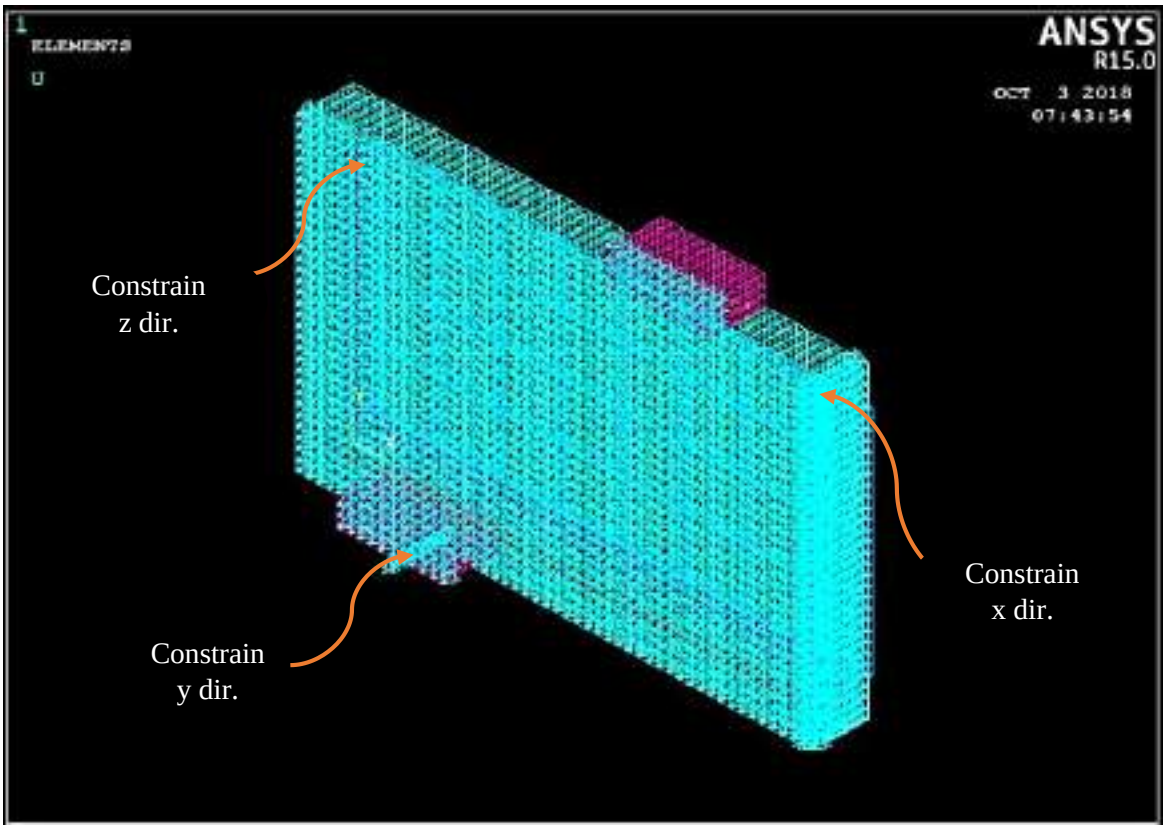

Figure (5.10) Quarter deep beam boundary conditions.

Due to symmetry, it was used quarter of the beam to represent the model.

5.8 Finite Element of Deep Beams Results

In the present section, the tested beams have been analyzed using three dimensional finite element models. The main objectives of the analysis are to check the accuracy of the adopted finite element models to predict the overall behavior of the tested beams, and to get more information about load – deflection, toughness and ductility of deep beams.

In nonlinear analysis, the total load applied to a finite element model is divided into a series of load increments called load steps. At the completion of each incremental solution, the stiffness matrix of the model is adjusted to reflect nonlinear changes in structural stiffness before proceeding to the next load increment. The ANSYS program (ANSYS version 15.0) uses Newton-Raphson equilibrium iterations for updating the model stiffness.

5.8.1 Load-Deflection Relationship

Figures (5.11) to (5.26) illustrate the load-deflection relationships and the contours for vertical displacement of the tests and numerical deep beams. These figures show that the predicted behavior concerning the load-deflection curve is approximately similar to the experimental results. The relationships start linear and then become nonlinear. Good agreement between the experimental and theoretical results is achieved.

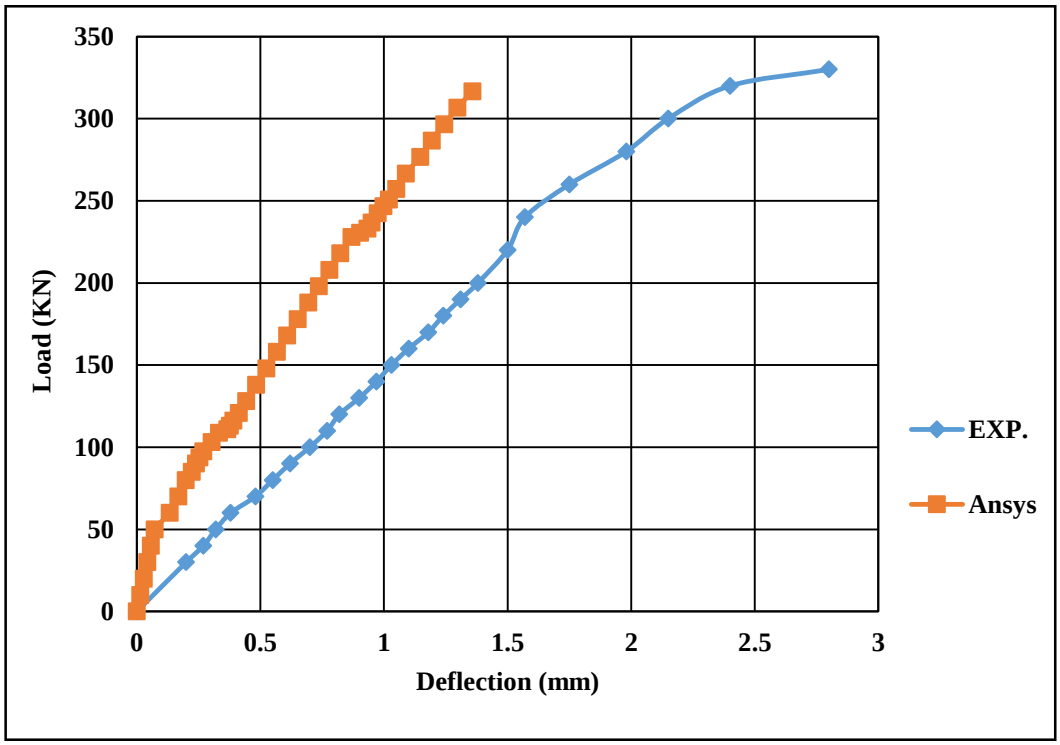

Figure (5.11) Load-Deflection Response (exp. – ansys) of deep beam G1AN1.

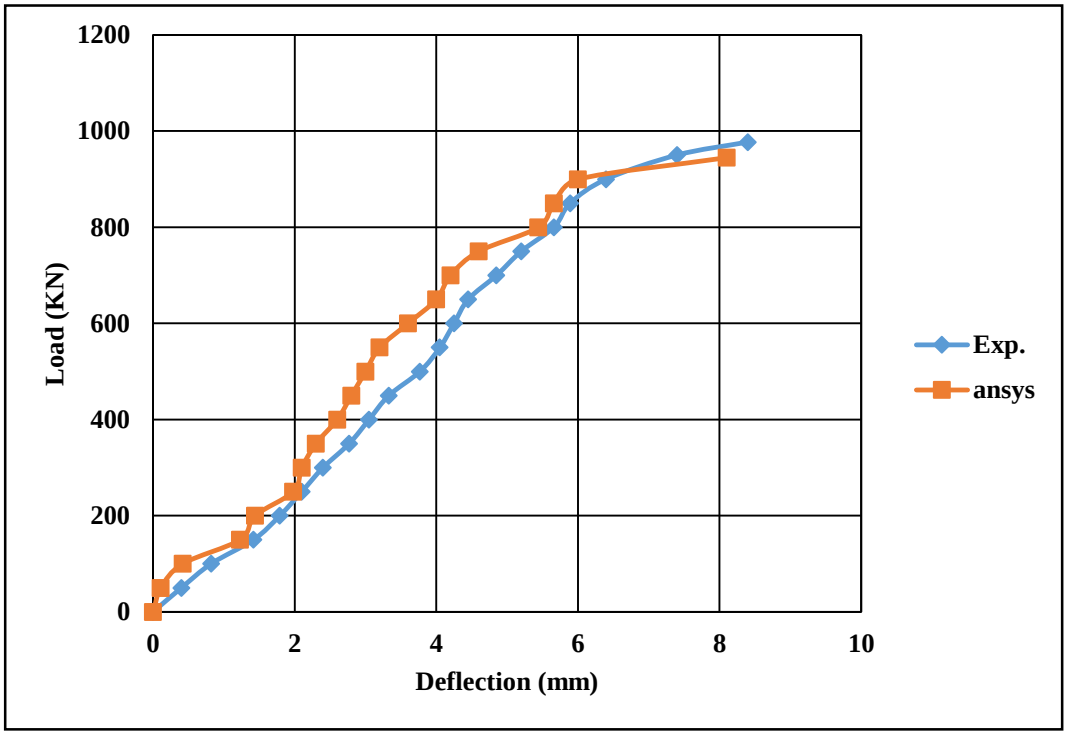

Figure (5.12) Load-Deflection Response (exp. – ansys) of deep beam G1SB1.

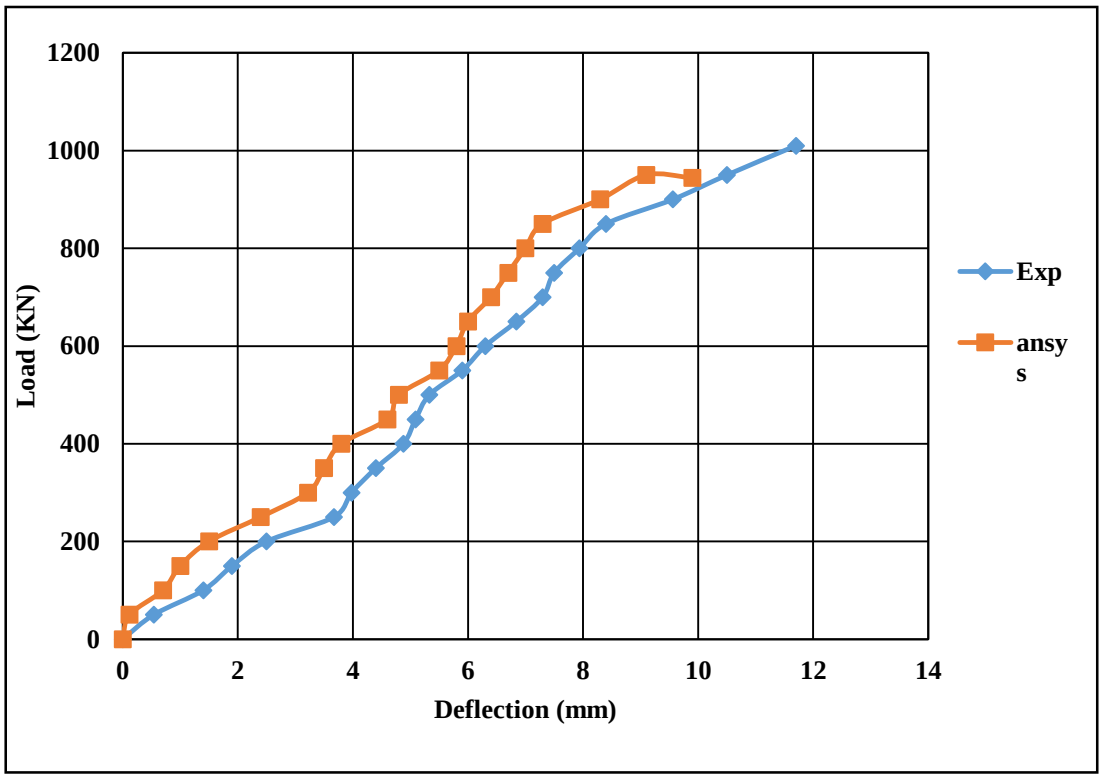

Figure (5.13) Load-Deflection Response (exp. – ansys) of deep beam G1SB2.

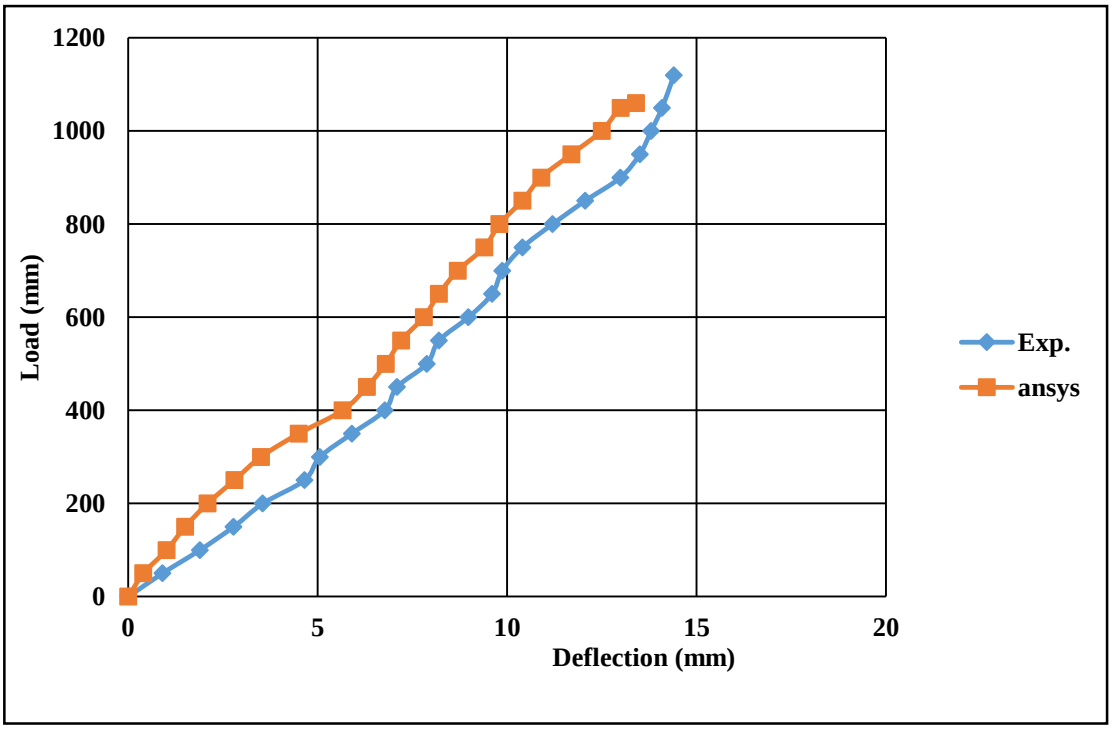

Figure (5.14) Load-Deflection Response (exp. – ansys) of deep beam G1SB3.

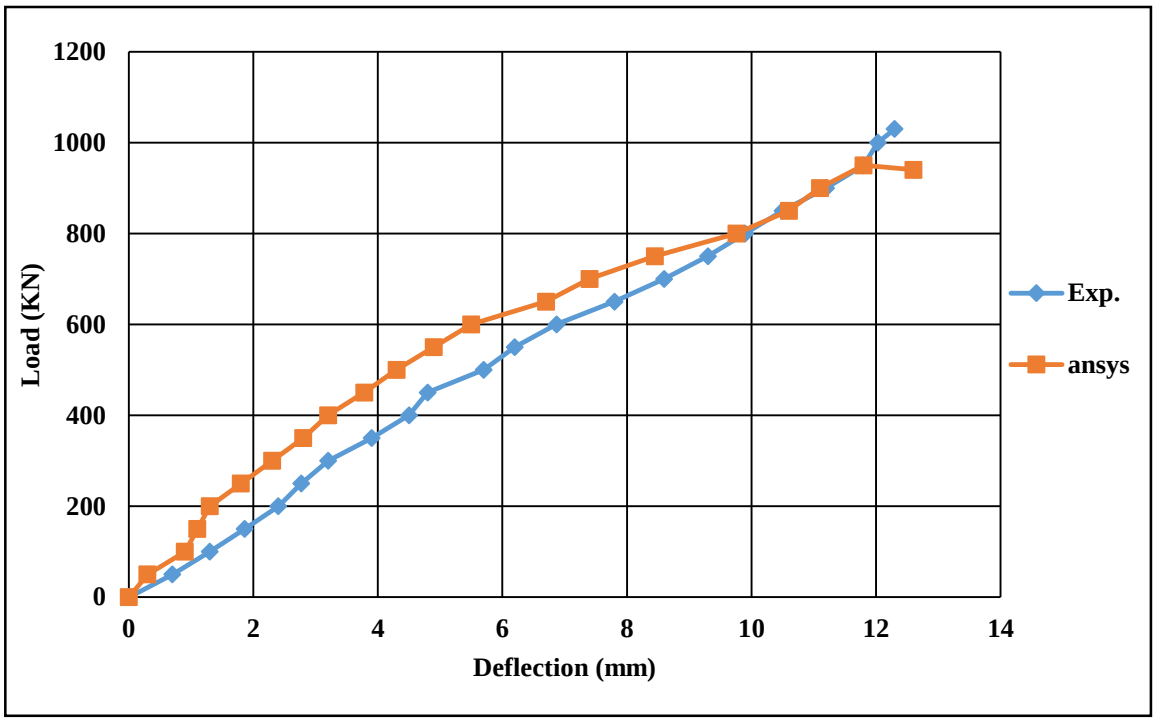

Figure (5.15) Load-Deflection Response (exp. – ansys) of deep beam G1SC1.

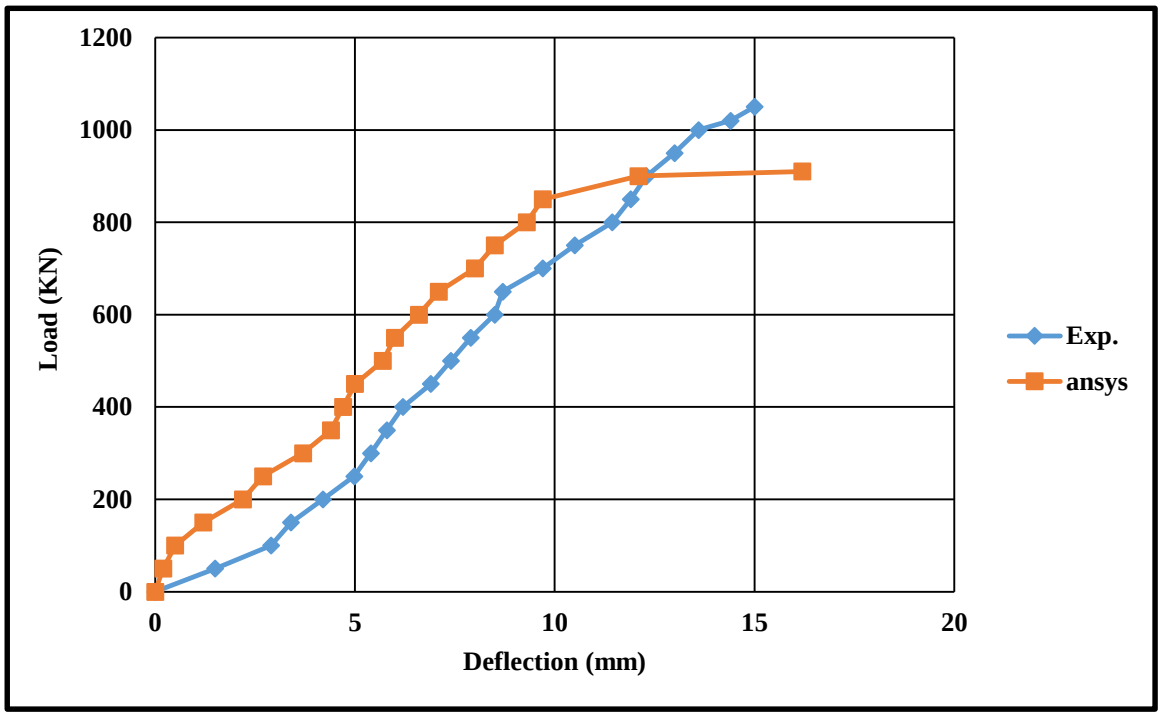

Figure (5.16) Load-Deflection Response (exp. – ansys) of deep beam G1SD1.

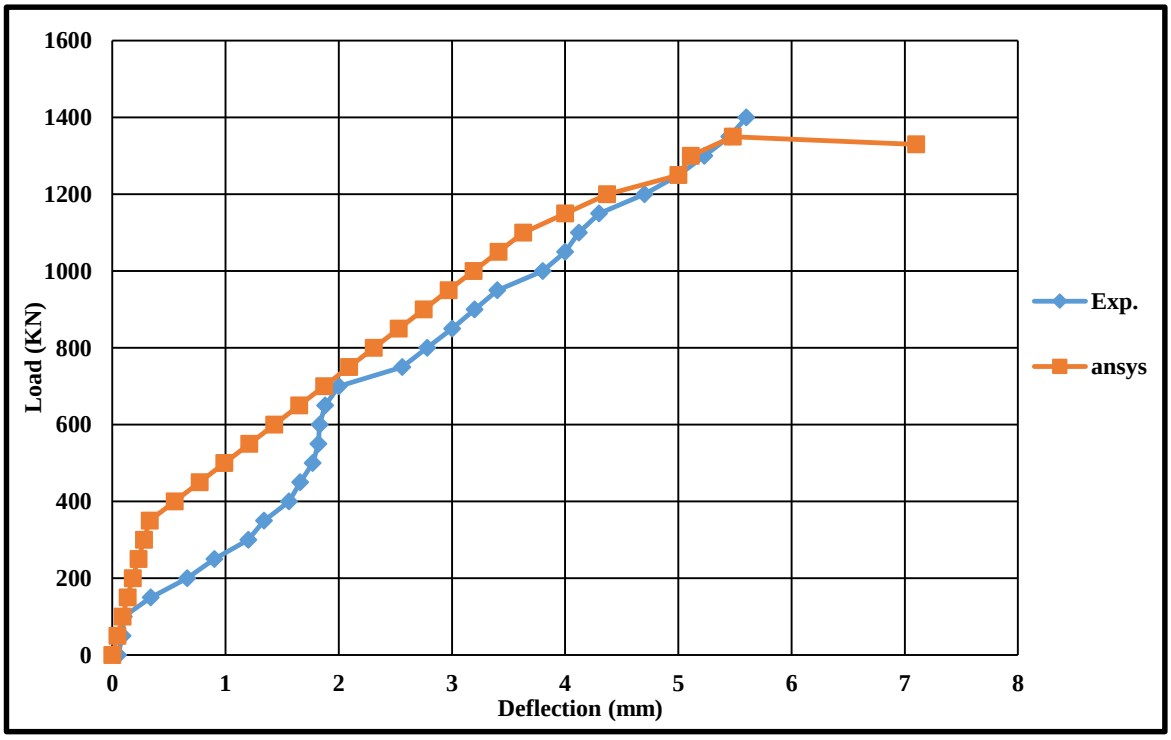

Figure (5.17) Load-Deflection Response (exp. – ansys) of deep beam G1SD2.

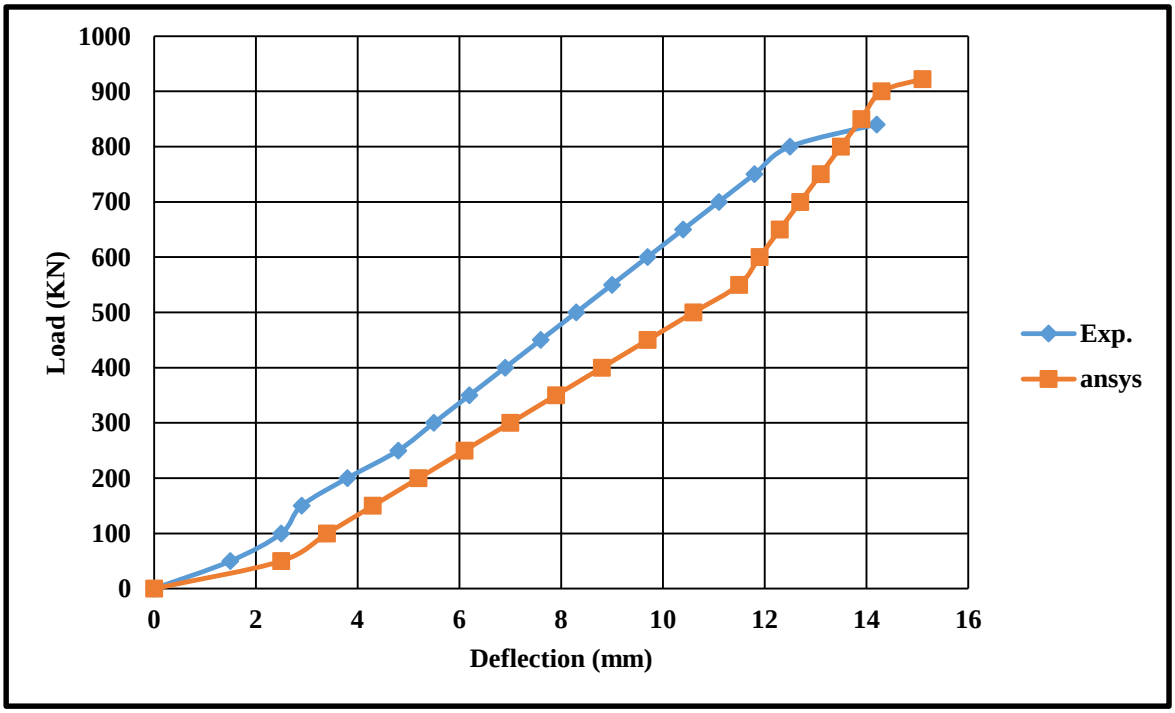

Figure (5.18) Load-Deflection Response (exp. – ansys) of deep beam G1SE1.

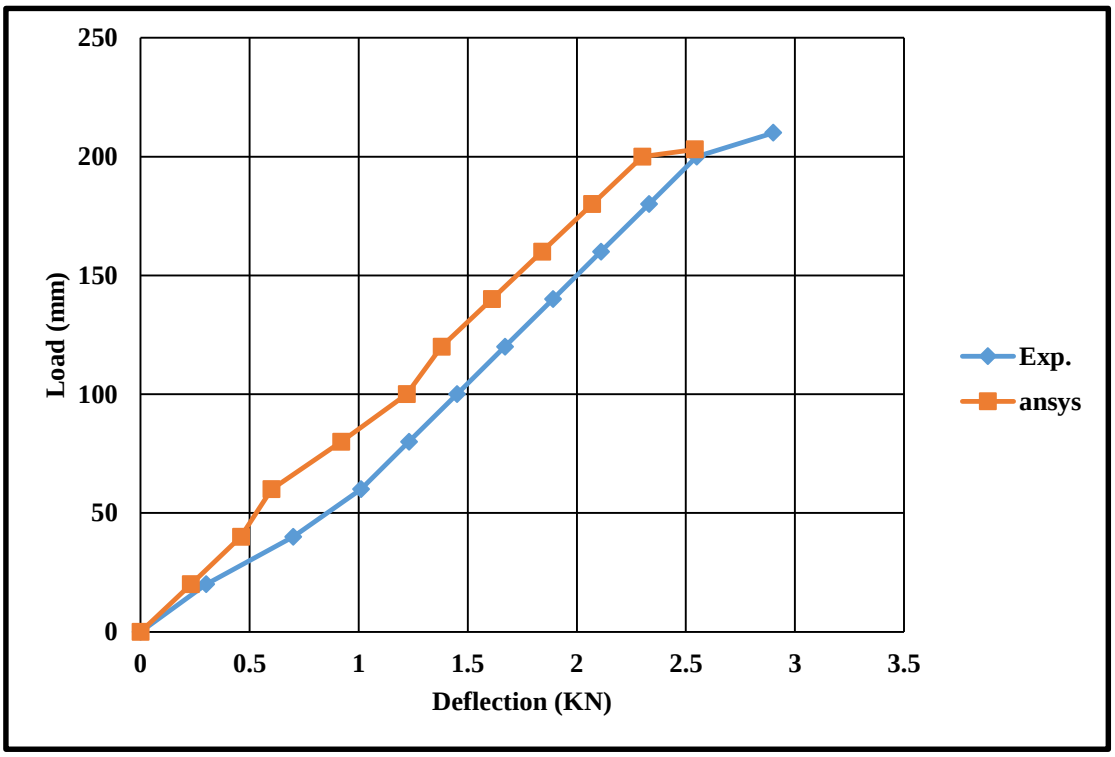

Figure (5.19) Load-Deflection Response (exp. – ansys) of deep beam G2NA1.

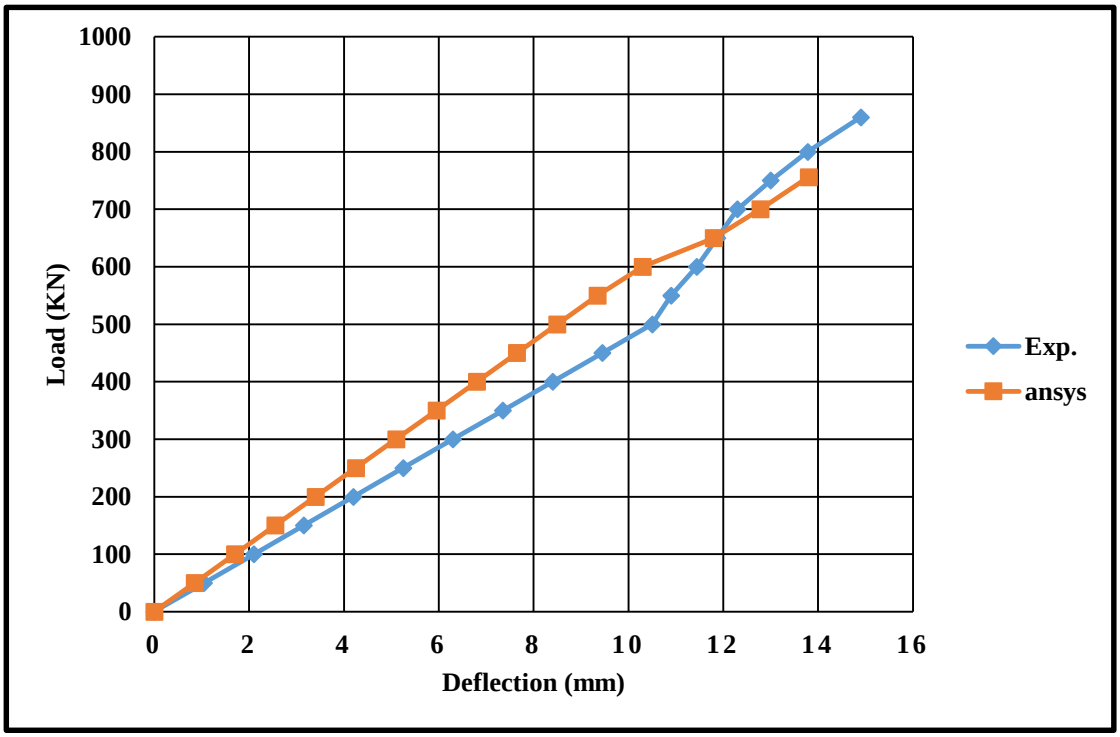

Figure (5.20) Load-Deflection Response (exp. – ansys) of deep beam G2SB1.

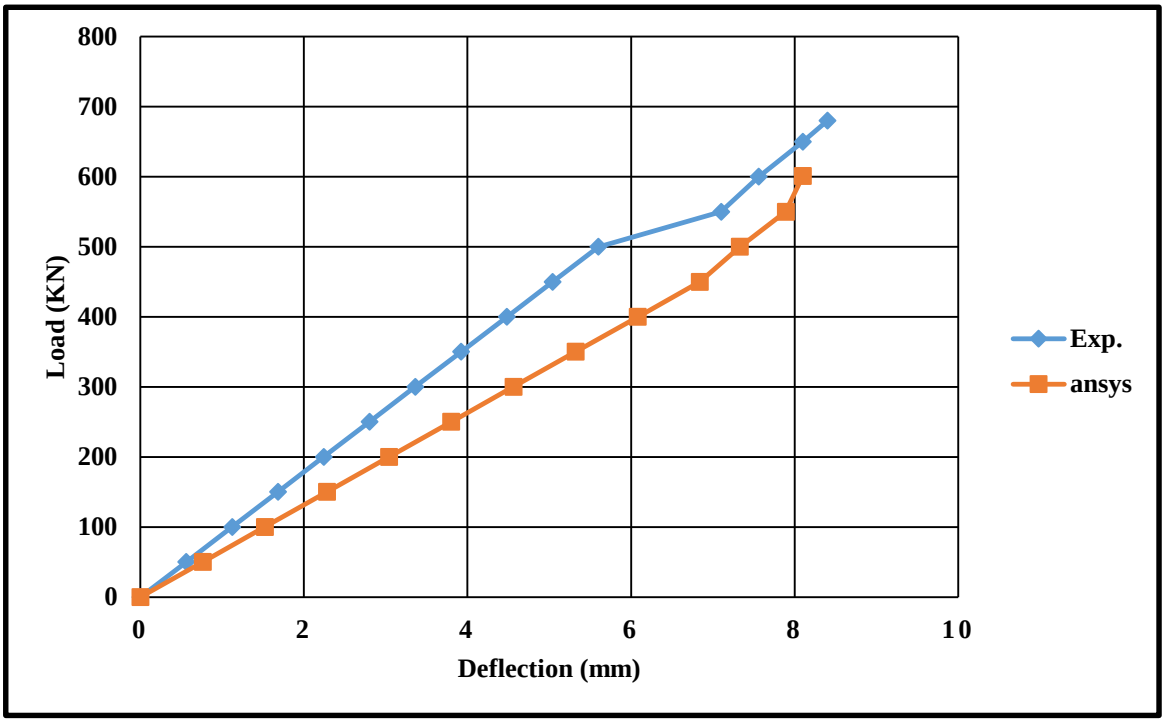

Figure (5.21) Load-Deflection Response (exp. – ansys) of deep beam G2SB2.

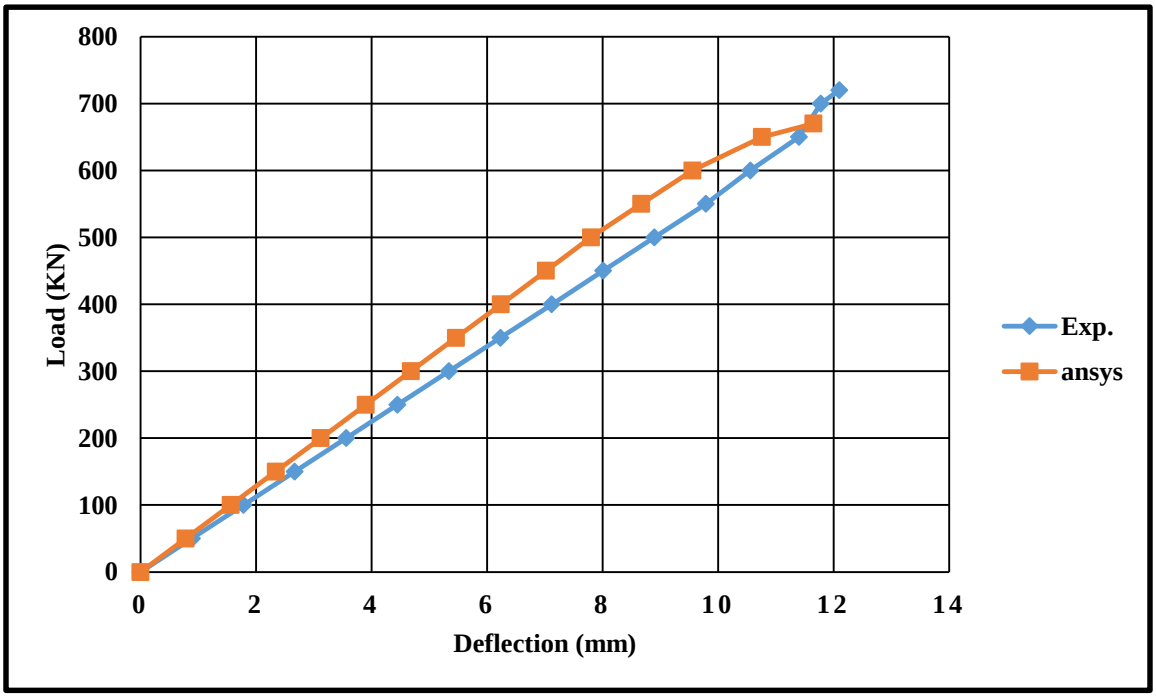

Figure (5. 22) Load-Deflection Response (exp. – ansys) of deep beam G2SB3.

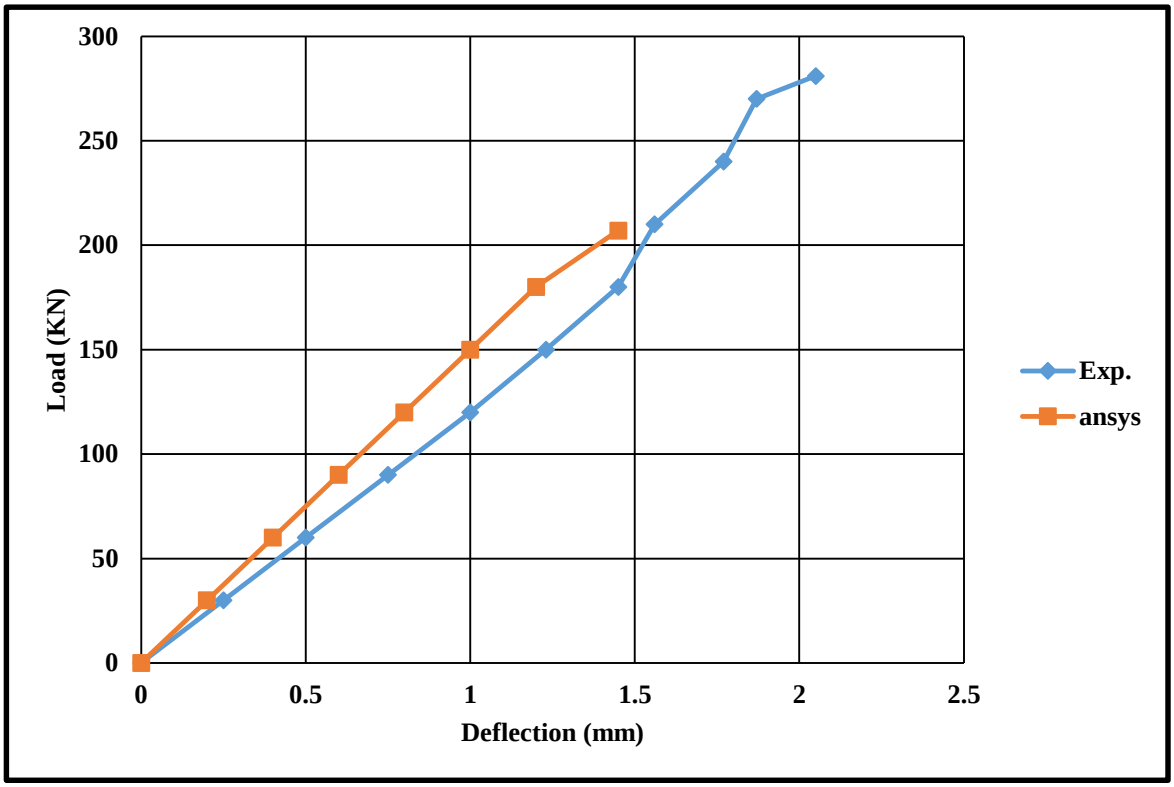

Figure (5.23) Load-Deflection Response (exp. – ansys) of deep beam G2NC1.

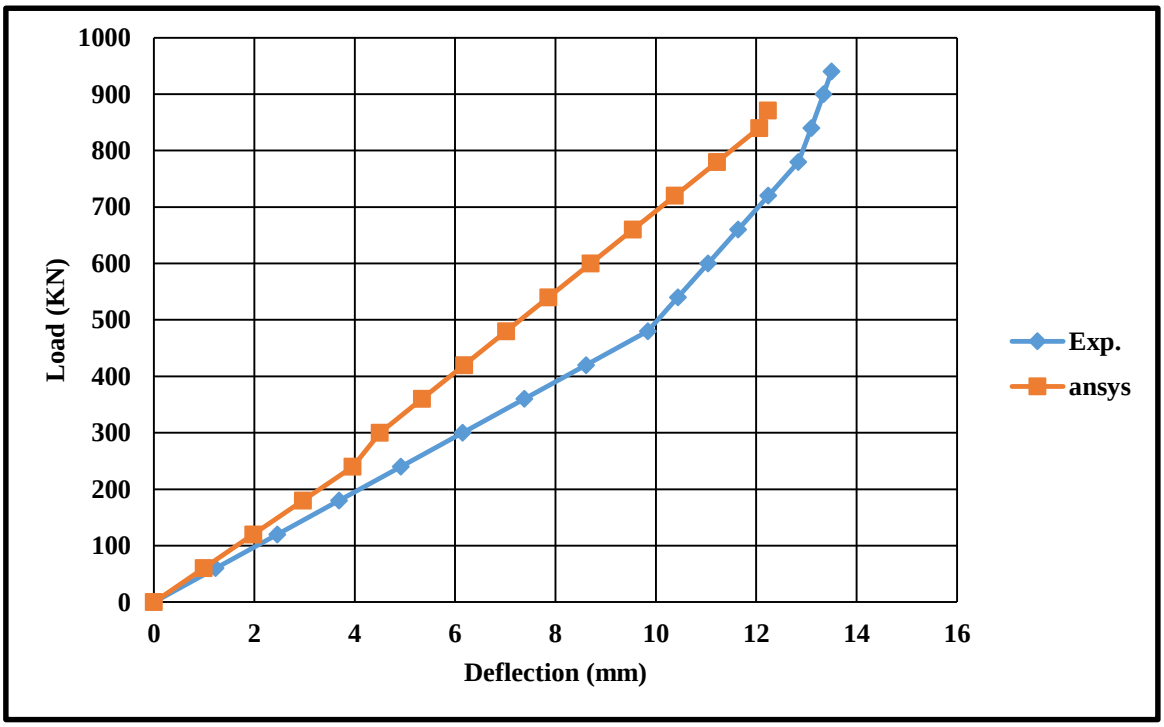

Figure (5.24) Load-Deflection Response (exp. – ansys) of deep beam G2SC2.

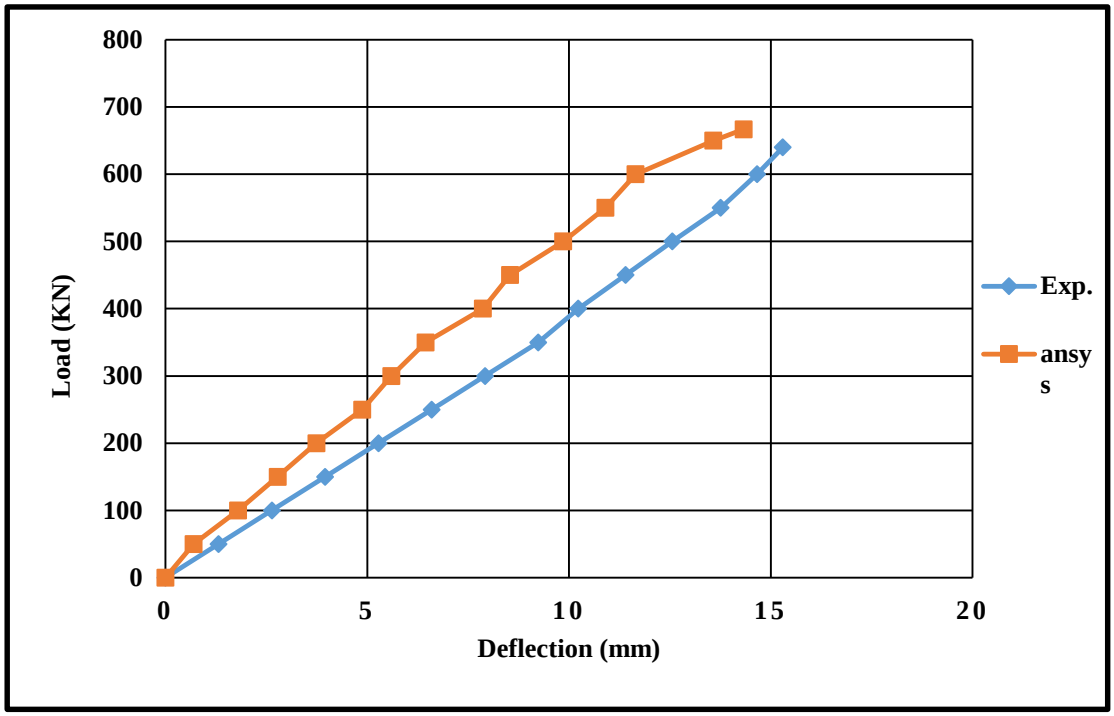

Figure (5.25) Load-Deflection Response (exp. – ansys) of deep beam G2SD1.

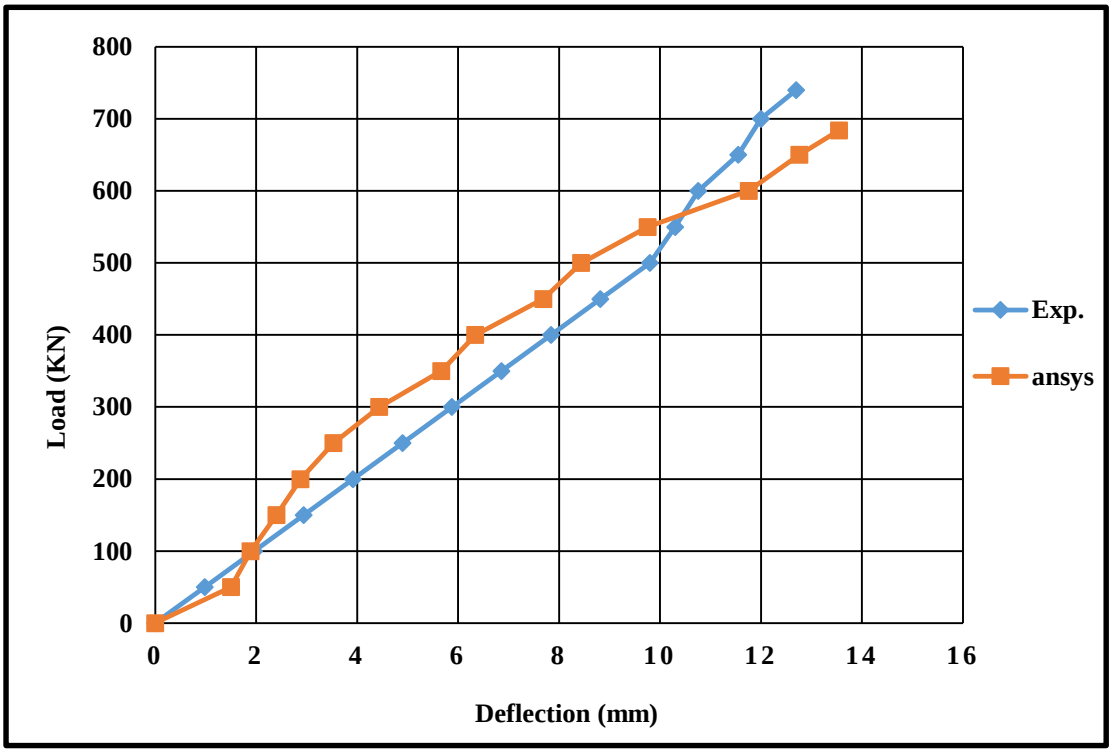

Figure (5.26) Load-Deflection Response (exp. – ansys) of deep beam G2SD2.

5.8.2 Toughness

Tables (5.4) and (5.5) listed experimental and numerical toughness of group one and group two. Good agreement between the experimental and theoretical results is achieved.

Table (5.4) Experimental and Numerical toughness of solid deep beams.

Items	Experimental Toughness KN.mm	Numerical Toughness KN.mm
G1NA1	544	243
G1SB1	4678	4753
G1SB2	6217	5789
G1SB3	6925	7189
G1SC1	6338	7361
G1SD1	7558	10023
G1SD2	4265	6876
G1SE1	5981	5521.

Table (5.4) Experimental and Numerical toughness of deep beams with openings.

Items	Experimental Toughness KN.mm	Numerical Toughness KN.mm
G2NA1	302	279
G2SB1	2989	2186
G2SB2	4143	4256
G2SB3	5746	5459
G2NC1	271	156
G2SC2	4818	5075
G2SD1	4580	5243
G2SD2	4278	5187

Figures (5.27) and (5.28) show variation of steel fiber ratio with toughness for group one and two:

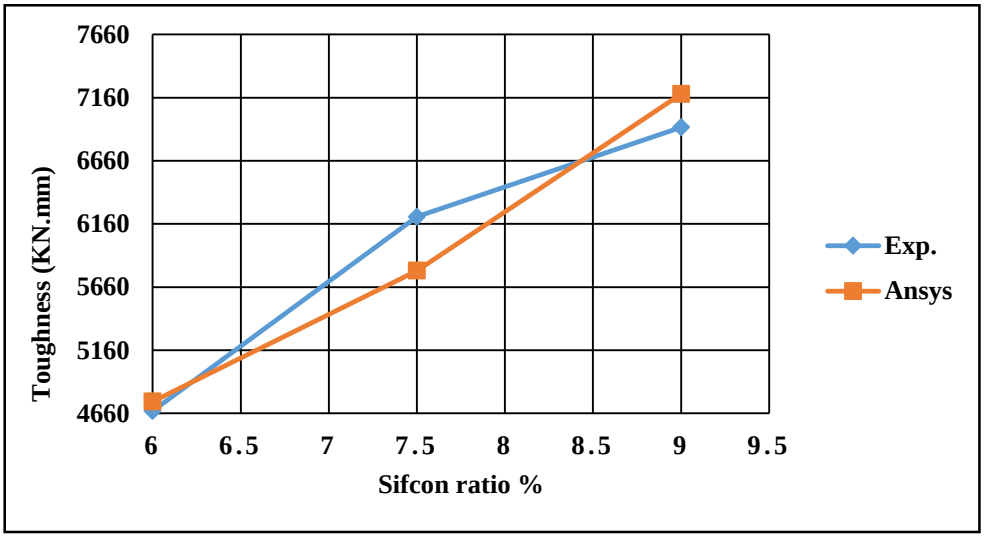

Figure (5.27) Variation of toughness with sifcon ratio of group one.

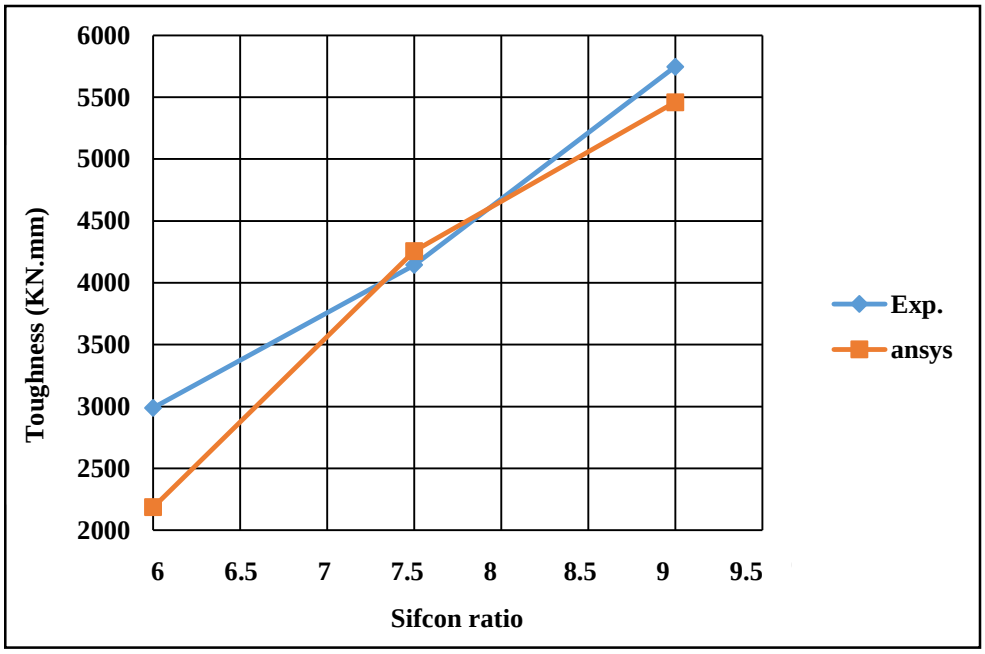

Figure (5.28) Variation of toughness with sifcon ratio of group two.

5.8.3 Ductility

Tables (5.6) and (5.7) listed experimental and numerical ductility of group one and group two. Good agreement between the experimental and numerical results is achieved.

Table (5.6) Experimental and numerical ductility of solid deep beams.

Items	Max Experimental Ductility %	Max Numerical Ductility %
G1NA1	0.5	0.65
G1SB1	1.6	1.46
G1SB2	2.4	2.32
G1SB3	3.1	2.6
G1SC1	2.9	2.5
G1SD1	4.31	3.78
G1SD2	0.8	0.95
G1SE1	4.6	4.39

Table (5.7) Experimental and Numerical ductility of deep beams with openings.

Items	Max Experimental Ductility %	Max Numerical Ductility %
G2NA1	0.78	0.54
G2SB1	1.93	2.11
G2SB2	3.5	2.71
G2SB3	3.92	3.577
G2NC1	0.25	0.45
G2SC2	2.434	1.82
G2SD1	5.01	4.433
G2SD2	4.376	3.265

Figures (5.29) and (5.30) show variation of sifcon ratio with ductility for group one and two:

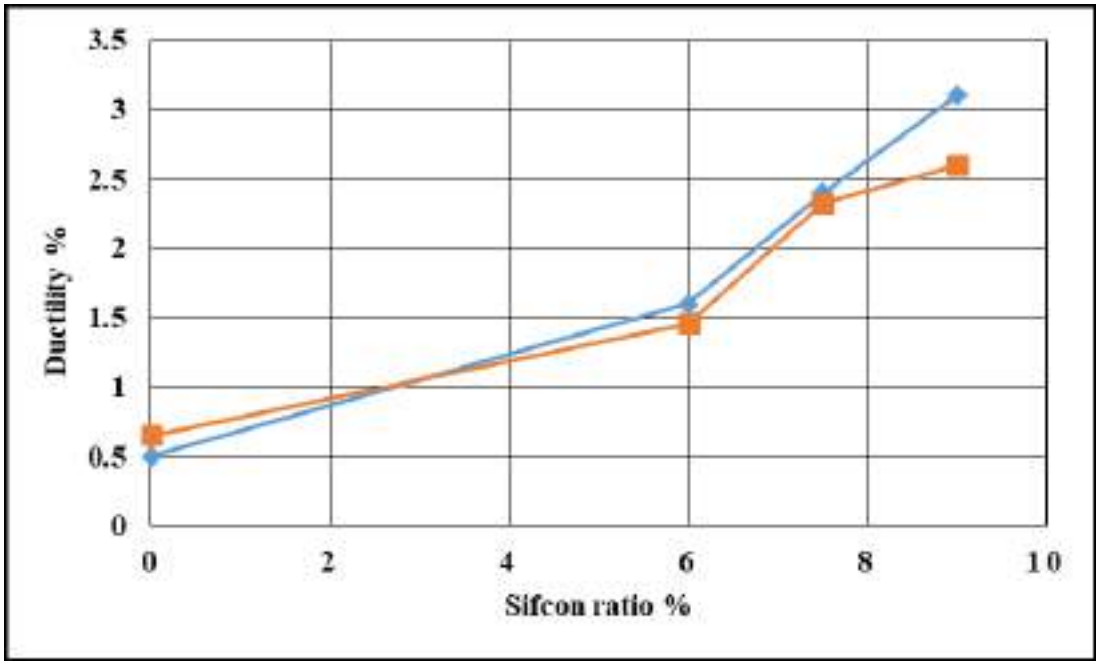

Figure (5.29) Variation of ductility with sifcon ratio of group one.

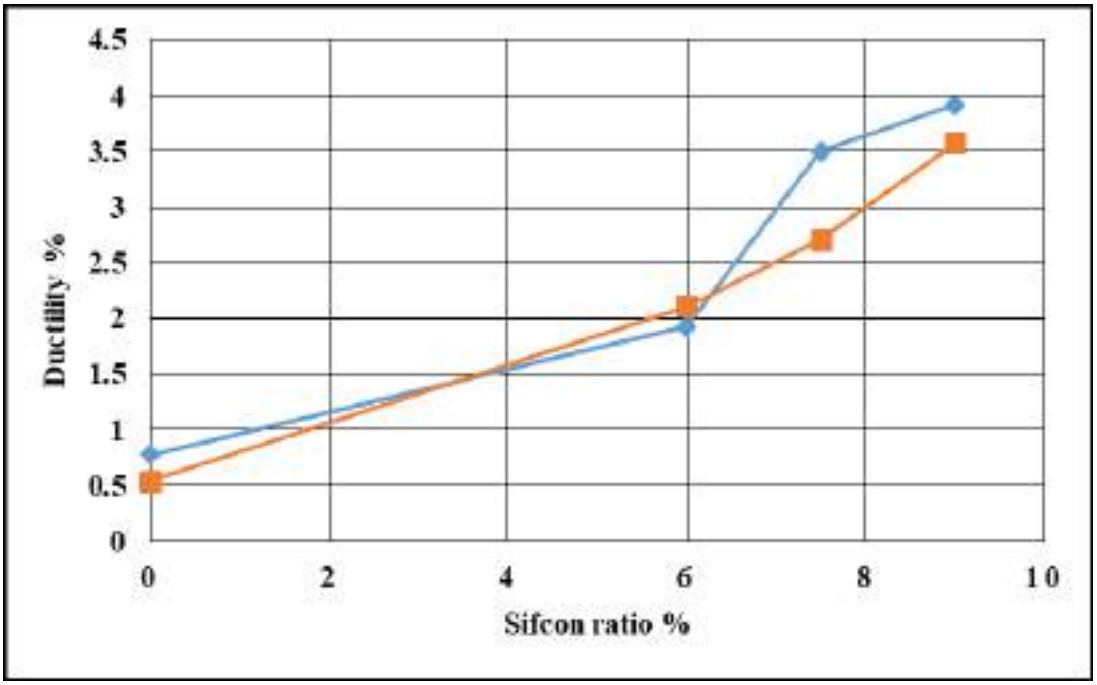

Figure (5.30) Variation of ductility with sifcon ratio of group two.

CHAPTER SIX

CONCLUSIONS AND RECOMMENDATIONS

Chapter Six

Conclusions and Recommendations

6.1 General

Two parts of conclusions are inferred in this chapter; the first part concentrates on the results obtained from the standard tested specimens of each mix of concrete. The second part relates to the structural behavior of deep beam, and tests that were conducted on sixteen reinforced concrete deep beams (eight of them solid deep beams and eight other deep beams with opening) with various fiber volume ratios, shear span to effective depth ratios (a/d), shape of opening, presence of steel reinforcement and the incorporation of the inclined reinforcement around openings.

6.2 Concrete Properties Conclusions

Depending on the overall results of 60 standard concrete specimens (24 cubic, 12 cylinders, 12 prisms and 12 double L shape) obtained from the experimental work, the following conclusions can be extracted: -

1. Results show that there is a significant improvement in the compressive strength (f_{cu}) of sifcon due to the addition of steel fibers. The presence of fibers at volume fractions of 6%, 7.5% and 9% resulted an increasing in the compressive strength by 40.5%, 48.4 %, and 86.8% respectively, compared with conventional concrete.

2. The splitting tensile strength increased by increasing the steel fiber ratio (6%, 7.5% and 9%). It was increased by 375 %, 457.1%, and 560.7% than the conventional concrete.

3. Modulus of rupture was increasing. It was increased by increasing the steel fiber ratio (6%, 7.5% and 9%) It was increased by 415.3 %, 544 %, and 840.7% than the conventional concrete.

4. The shear strength increased by 440.6 %, 553.7 %, and 795.7%, respectively with increasing the same as the steel fiber ratio (6%, 7.5% and 9%) than the conventional concrete.

5. The modulus of elasticity increased with addition SIFCON.

6. In SIFCON mix, it is better to say that the increased length of steel fiber in order within specified aspect ratio to this helps to infiltrate slurry inside network of fiber because of small fiber prevent slurry to infiltrate fiber network whenever depth increase.

7. It was explained that the Sifcon mix (9%) gives the best results, therefore be adopted as a reference mix in the casting of sifcon deep beams.

6.3 Structural Behavior Conclusions for Solid Sifcon Deep Beams

Based on the experimental test results and numerical analysis, the following conclusions are drawn: -

1. The increase of sifcon ratio by (6%, 7.5% and 9%) gave a significant improvement in the behaviour of the deep beam. The increase in the cracking and ultimate loads were about of (275%, 331.25% and 362.5%) and (196%, 206% and 239.4%) respectively in comparison with conventional concrete.

2. Removal of vertical reinforcement for SIFCON solid deep beams gave decreasing in the ultimate and cracking loads about of (8%) and (31.7%) than the deep beam with sifcon (9%). While existing the web reinforcement appeared increasing in the ultimate and cracking loads about of (212.1%) and (215.6%) respectively than the conventional concrete deep beam.

3. The ultimate load was increased with decreasing of the shear span to effective depth (a/d) ratio. The ultimate load for the ratio of (a/d = 0.727) was increased about of 25% than the reference ratio (a/d = 0.9), for the ratio of (a/d =1.08) the ultimate load was decreased about of 6.25% compared with reference ratio.

4. Removing of main and web reinforcement for SIFCON solid deep beams gave decrease in the ultimate and cracking loads of about (17.6%) and (29.3%) than the deep beam with sifcon (9%) respectively. While existing the reinforcement appeared increasing in the ultimate and cracking loads of about (165.3%) and (226.9%) respectively than conventional concrete deep beam.

5. When the steel fiber ratios were increased from (6% to 9%) the toughness was increased about of (760% to 1173%) respectively.

6. The toughness decreased with removing of vertical reinforcement, the ratio a/d = 1.08 and removing of main and web reinforcement about of 8.5%, 38.4% and 13.62% respectively.

7. The toughness increased about of 9.14% with the ratio (a/d = 0.727) than the reference ratio.

8. The increasing of sifcon ratios from (6% to 9%) caused increasing in ductility about of (220% to 520%) respectively.

9. The ductility decreased with removing of vertical reinforcement and the ratio (a/d = 1.08) about of 6.45% and 74.2%.

10. The ductility increased for the ratio (a/d = 0.727) and the absence of main vertical reinforcement of about 39 % and 48.4%.

11. Nonlinear finite element solution by ANSYS package program using three dimensional elements for modelling sifcon deep beams gave good acceptable agreement with the experimental results for the load-deflection relationships with some modifications.

12. The ratios of numerical failure loads to experimental failure loads ranged from 86.67% to 96.72%.

13. Numerical toughness and ductility values showed good agreement with the experimental results.

6.4 Structural Behavior Conclusions for Sifcon Deep Beams with Openings

Based on the experimental test results and numerical analysis, the following conclusions are drawn: -

1. The increase of steel fiber ratio by (6%, 7.5% and 9%) gave a significant, improvement in the behaviour of the RC beams subjected to two-point load and the increasing in the cracking and ultimate loads were about of (60%, 140% and 236%) and (223.8%, 242.85% and 309.52%) respectively if comparison with conventional concrete.

2. The conventional concrete deep beam with inclined reinforcement around the openings gave increasing in the ultimate load about of 33.8% than the conventional concrete deep beam without inclined reinforcement.

3. The sifcon deep beam with inclined reinforcement around the openings gave increasing in the ultimate load about of 234.5% than the conventional concrete deep beam with inclined reinforcement.

4. The sifcon deep beam with circular openings gave high cracking and ultimate loads than square and triangular openings. The reduction in the ultimate loads for square and triangular openings were about of 22.44% and 13.9% respectively.

5. When the steel fiber ratios were increased from (6% to 9%) the toughness was increased about of (888.26% to 1799.8%) respectively.

6. The conventional concrete deep beam with inclined reinforcement around the openings gave decreasing in the toughness about of 10.4% than the conventional concrete deep beam without additional inclined reinforcement.

7. The sifcon deep beam with inclined reinforcement around the openings gave increasing in the toughness about of 1677% than the conventional concrete deep beam with inclined reinforcement.

8. The sifcon deep beam with circular openings gave high toughness than square and triangular openings. The increasing in the toughness for the circular openings was about of 20.3% than the square openings and 25.5% than the triangular openings.

9. When the steel fiber ratios were increased from (6% to 9%) the ductility was increased about of (147.43% to 402.56%) respectively.

10. The conventional concrete deep beam with inclined reinforcement around the openings gave decreasing in the ductility about of 67.9% than the conventional concrete deep beam without additional inclined reinforcement.

11. The sifcon deep beam with inclined reinforcement around the openings gave increasing in the ductility about of 873.6% than the conventional concrete deep beam with inclined reinforcement.

12. Square and triangular openings ductility values showed increasing if compared with Sifcon deep beam (9%) by about 27.8% and 11.6% respectively.

13. Nonlinear finite element solution by ANSYS package program using three dimensional elements for modelling sifcon deep beams gives acceptable agreement with the experimental results for the load-deflection relationships.

14. Ratio of numerical failure load to experimental failure load ranged from 73.66 % to 97.6 % for deep beams with openings.

15. Numerical toughness and ductility values are in acceptable agreement with the experimental results.

6.5 Recommendations for Future Works

To obtain further improvement in the understanding of the behavior of SIFCON structural elements, the following are some of the suggested topics for future research:

1. Experimental and numerical investigation is required to study the structural behavior of SIFCON deep beams under the action of torsion.

2. Experimental and numerical investigation is required to study the structural behavior of SIFCON deep beams under the repeated load.

3. Studying of behavior of prestressed SIFCON in girder of bridge.

4. Experimental work and numerical analysis on strength and behavior of SIFCON columns.

5. Experimental work and numerical analysis on strength and behavior of SIFCON corbels.

6. Experimental work and numerical analysis on strength and behavior of SIFCON wall.

Reference

1- Kamaran S. Ismail, "**Shear Behavior of Reinforced Concrete Deep Beams**", University of Sheffield, PhD thesis, January 2016.

2- Noor Abbas Hadi, "**Experimental Behavior of Hybrid Steel-Polypropylene Fiber Reinforced Concrete Deep Beam Containing Opening**", B.Sc. (Structural Engineering, 2014), October / 2016.

3- ACI Committee 318,"**Building Code Requirements for Structural Concrete (ACI318M-14) and Commentary**", American Concrete Institute, Farmington Hills, MI 48331, USA, 520 p, 2014.

4- British Standards Institution, Eurocode2, "**Design of Concrete Structures: Part 1-1: General Rules and Rules for Buildings**", British Standards Institution, 2004.

5- Canadian Standards Association, **"CAN/CSA A23.3-04 Design of concrete structures** ",CSA, Rexdale, Ontario, Canada, 2004.

6- Smith, K. and A. Vantsiotis, "**Shear Strength of Deep Beams**", In ACI Journal, Proceedings, ACI, 1982, P.P.201- 213.

7- Ritter, W., Die Bauweise Hennebique, "**Hennebiques Construction Method**", Schweizerische Bauzeitung, 17: p. 41-43, 1899.

8- Morsch, E., Der eisenbetonbau, seine amending und theory. Wayss and Freytag, AG, Im Selbstverlag der Firma, Neustadt, AD Haardt, 1902: p. 118.

9- Marti, P., "**Truss Models in Detailing**", Concrete International, v 7, n 12, pp. 66-73, 1985.

10- Schlaich, J., Schäfer, K., and Jennewein, M., "**Towards a Consistent Design of Structural Concrete**", PCI Journal, v 32, n 3, pp. 74-150, 1987.

11- Book "**Reinforced Concrete Deep Beams**", Edited by Professor Kong. F.K, University of Newcastle-upon-Tyne,1990.

12- Nair, N.; and Kavitha, P.E., "**Effect of Openings in Deep Beams Using Strut and Tie Model Method**", International Journal of Technical Research and Applications, Volume 3, Issue 5, pp. 59-62, September-October 2015.

13- Subedi, N.K., et al. "**Reinforced Concrete Deep Beams Some Test Results**", Magazine of Concrete Research, Vol. 38, No. 137, pp. 206-219, Dec. 1986.

14- Kong, F. K., Robins, P. J., and Cole, D. F., "**Web Reinforcement Effects on Deep Beams**," ACI Journal, Vol.67, No.12, pp. 1010 -1017, December,1970.

15- ACI-ASCE Task Committee 426, "**The Shear Strength of Reinforced Concrete Members**", Journal of the Structural Division, ASCE, Vol.99, No. ST6, pp. 1091-1187, June, 1973.

16- Mansur, M. A., and Alwist, W. A. M., "**Reinforced Fiber Concrete Deep Beams with Web Opening**", the International Journal of Cement Composites and Lightweight Concrete, Vol. 6, No.4, pp. 263- 271, November 1984.

16- David R. Lankard, "**Slurry Infiltrated Fiber Concrete Properties and Application of (SIFCON)**", December 1984.

17- "**State-of-the-Art Report on Fiber Reinforced Concrete**" Reported by ACI Committee 544, 2002.

18- vijayakumar M., Dinesh Kumer P., "**Study on Strength Properties of SIFCON**" International Research Journal of Engineering and Technology (IRJET), Volume: 04 Issue: 01 | Jan -2017.

19- BALAJI S. "**Experimental and numerical investigation on behavior of slurry infiltrated fibrous reinforcement concrete structural members**", PhD thesis, facility of civil engineering ANNA University CHENNAI 600 025, November 2014.

20- Kong, F.K., et al., "**Web Reinforcement Effects on Deep Beams**", ACI Journal, Proceedings Vol.67, No. 12, pp. 1010-1017, Dec. 1970.

21- R. Narayanan and Darwish I.Y.S., "**Fiber Concrete Deep Beams in Shear**", ACI Structural Journal, v. 85, no. 2, pp. 141-149, March 1988.

22- Tan, K. H, and Lu, H.Y, "**Shear Behavior of Large Reinforced Concrete Deep Beams and Code Comparison**", ACI Structural Journal, V.96, No. 5, pp. 836-846, September-October 1999.

23- Brown, D. M., and Bayrak, O., "**Investigation of Deep Beams with Various Load Configurations**", ACI Structural Journal, V.104, No. 5, pp. 611-620, September-October 2007.

24- Ahmed M. Yousef, Ahmed M. Tahwia and Nagat A. Marami, "**Minimum Shear Reinforcement for Ultra-High Performance Fiber Reinforced Concrete Deep Beams**", [a] Structural Engineering Department, Faculty of Engineering, Mansoura University, Mansoura 35516, Egypt, (ELSEVIER), 184 177–185 (2018).

25- Kong, F. K.; and Sharp, G. R., "**Shear Strength of Lightweight Reinforced Concrete Deep Beams with Web Openings**", the Structural Engineer, V. 51, No. 8, pp. 267-275, August 1973.

26- Swaddiwudhipong, S., and Shanmugam, N.E., "**Fiber Reinforced Concrete Deep Beams with Openings**", ASCE Journal of Structural Engineering, Vol. 111, No. 8, pp. 1679-1690, Aug. 1985.

27- Akhtaruzzaman A. and Hasnat A., "**Torsion in Concrete Deep Beams w ith an Opening**", ACI Structural Journal, v. 86, no. 1, pp. 20-25, January1989.

28- Mansur M. A., Lee Y. F., Tan K.H. and Lee S. L, "**Test on R. C. continuous beams with openings**", ASCE Journal, 1991, P.P 15-27, Vol.6.

29- Campione, G. and Minafo, G., "**Behavior of Concrete Deep Beams with Openings and Low Shear Span-to-Depth Ratio"**, Engineering Structures Journal, Vol. 41, 2012, pp. 294-306.

30- Hasan, A. S., "**Structural Behavior of Self-Compacting Reinforced Concrete Deep Beams Containing Openings**", M.Sc. Thesis, Building and Construction Engineering Department, University of Technology, Baghdad, Iraq, 81 pp, 2016.

31- Balaguru P. and Kendzulak, "**Mechanical properties of slurry infiltrated fiber concrete (SIFCON)**", In: SP-105, ACI, Detroit, pp. 247-268, 1987.

32- Josifek, C and Lankard, "**SIFCON: Slurry Infiltrated Fibrous Concrete**", Proceedings of the international Symposium on fiber reinforced concrete, Madras, India, pp. 7.15-7.23, 1987.

33- Naaman, AE, Otter, D and Najm,"**Elastic Modulus of SIFCON in Tension and Compression**", ACI Materials Journal, vol. 88, no. 6, pp. 603-612, 1991.

34- Wang and Maji,"**Shear Properties of Slurry Infiltrated Fiber Concrete (SIFCON)**", High Performance Fiber Reinforced Cement Composites, pp. 203-212, 1992.

35- Naaman and Baccouche,"**Shear Response of Dowel Reinforced SIFCON**", ACI Structural Journal, vol. 92, no. 5, pp. 587-595, MR 1995.

36- Balasubramanian, K, Bharathkumar, Krishnamoorthy, and Parameswaran,"**Behavior of SIFCON under pure torsion**", Journal of Structural Engineering, vol. 24, no. 1, pp. 37-40, VS 1997.

37-Thirugnanam, GS, Govindan, P and Sethurathnam, "**Ductile Behavior of SIFCON Structural Members**", Journal of Structural Engineering, vol. 28, no. 1, pp. 27-32, A 2002.

38- Sashidhar, C, Rao, SH, Ramana, NV and Gorpade, "**Studies on SIFCON Subjected to Elevated Temperature**", Proceedings of the international

conference on recent advances in concrete and construction technology, Chennai, India, pp. 567-576, V 2005.

39- Sudarsana Rao H., Ramana N. V.," **Behavior of slurry infiltrated fibrous concrete (SIFCON) simply supported two-way slabs in flexure**", indian journal of engineering & materials sciences, Volume 12, pp.427-433, October 2005.

40- Rao, SH, Gnaneswar, K and Ramana, "**Behavior of simply supported steel reinforced SIFCON two way slabs in punching shear**", Indian Journal of Engineering and Material Sciences, vol. 15, pp. 326-333, NV 2008.

41- Farnam, Y, Moosavi, M, Shekarchi, M, Babanajad, SK and Bagherzadeh, "**Behavior of slurry infiltrated fiber concrete (SIFCON) under triaxial compression**", Cement and Concrete Research (ELSEVIER), vol. 40, pp.1571-1581, A 2010.

42-H. SudarsanaRao ,Vaishali G.Ghorpade ,N.V.Ramana ,K.Gnaneswar , "**Response of SIFCON two-way slabs under impact loading**", International Journal of Impact Engineering (ELSEVIER), volume 37, 452–458, (2010).

43- Murat Tuyan, Halit Yazıcı," **Pull-out behavior of single steel fiber from SIFCON matrix**", Construction and Building Materials (ELSEVIER), Volume 35, Pages 571-577, October 2012.

44- Ahsanollah Beglarigale, Çagˇlar Yalçınkaya, Hüseyin Yigˇiter, Halit Yazıcı," **Flexural Performance of SIFCON Composites Subjected to High Temperature**", Construction and Building Materials (ELSEVIER), volume 104 pp.99–108, 2016.

45- Shannag, MJ, Barakat, S and Jaber," **Structural Repair of Shear Deficient Reinforced Concrete Beams Using SIFCON**", Magazine of Concrete Research, vol. 53, no. 6, pp. 391-403, F 2001.

46- Rajai Z.Al-Rousan, Mohammad J.Shannag, "**Shear Repairing and Strengthening of Reinforced Concrete Beams Using SIFCON**", "Structures" (ELSEVIER), Volume 14, Pages 389-399, June 2018.

47- IQS No. 5/1984, "Portland Cement," Central Agency for Standardization and Quality Control, Planning Council, Baghdad, IRAQ, (in Arabic),1984.

48-IQS No. 45/1984, "**Aggregate from Natural Sources for Concrete**", Central Agency for Standardization and Quality Control, Planning Council, Baghdad, IRAQ, (in Arabic),1984.

49- Standard Specification for Chemical Admixtures for Concrete, ASTM C494, Developed by Subcommittee: C09.23 Book of Standards Volume: 4-2.

50- National Ready Mixed Concrete Association, "**What, Why and How**?

51- ASTM C1240-04, "**Standard Specification for the Use of Silica Fume as a Mineral Admixture in Hydraulic Cement Concrete, Mortar and Grout**", Vol. 4.2, 6p, 2004.

52- American Specification for Testing and Materials" **Standard Specification for Steel Fibers for Fiber-Reinforced Concrete**" A820.

53-ASTM A370-14, "**Standard Test Methods and Definitions for Mechanical Testing of Steel Products, ASTM International, West Conshohocken**," 48 pp. PA, 2014.

54- ASTM A615/A615M-14, "**Standard Specification for Deformed and Plain Carbon-Steel Bars for Concrete Reinforcement**," ASTM International, West Conshohocken", 7 pp. PA, 2014.

55- ASTM A1064/A1064M-14, "**Standard Specification for Carbon- Steel Wire and Welded Wire Reinforcement, Plain and Deformed, for Concrete**," ASTM International, West Conshohocken, 11 pp, PA, 2014.

56- EFNARC: European Federation Dedicated to Specialist Construction Chemicals and Concrete Systems, "**Specifications and Guidelines for Self-compacting Concrete**," Association House, 99 West Street, Farnham, Surrey, U.K, 32 p, 2002.

57- ACI Committee 237R, "**Self-Consolidating Concrete (ACI 237R-07)**," Reported by, Emerging Technology Series, April, 30 P, 2007.

58-ASTM C469-02, "**Standard Test Method for Static Modulus of Elasticity and Poisson's Ratio of Concrete in Compression**," ASTM International, West Conshohocken, 5 pp, PA, 2002.

59- ASTM C496/C496M -11, "**Standard Test Method for Splitting Tensile Strength of Cylindrical Concrete Specimens**," ASTM International, West Conshohocken, 5 pp, PA, 2011.

60- ASTM C 293 – 02 "Standard Test Method for Flexural Strength of Concrete," (Using Simple Beam With Center-Point Loading).

61- Strain gauges, TML catalog, Tokyo Sokki Kenkyujo Co., Ltd. www.tml.jp/e.

62-Antoine Naaman, "**Stress-Strain Properties of SIFCON in Uniaxial Compression and Tension**", August 1988

63- Book "**fiber reinforced cementitious composites**" by arnon Bentur and Sidney mindess.

64- ANSYS V.15 help topics.

65- Schnobrich, W. C., "**Behavior of Reinforced Concrete Structures Predicted by the Finite Element Method**", Computers and Structures Journal, Vol. (7), Pergaman Press, PP. 365-376, UK, 1977.

66- Wolanski, B. S., "**Flexural Behavior of Reinforced and Pre-Stressed Beams Using Finite Element Analysis**", M.Sc. Thesis, Marquette University, (73) p., (web Site) , May 2001.

67- Naser H. T., "**Behavior of Reactive Powder Concrete Beams Reinforced with Fiber Reinforced Polymer Bars**", doctor thesis, Baghdad University, 2016.

Appendices

Appendix A

Installation of Strain Gauge

When bonding the strain gauges, a typical installation procedure is described here:-

- **Surface preparation:** Grinding the specific area by the abrasive paper. Then, using a cotton material to clean the abraded area with a small quantity of acetone, **Plate (A.1)**.

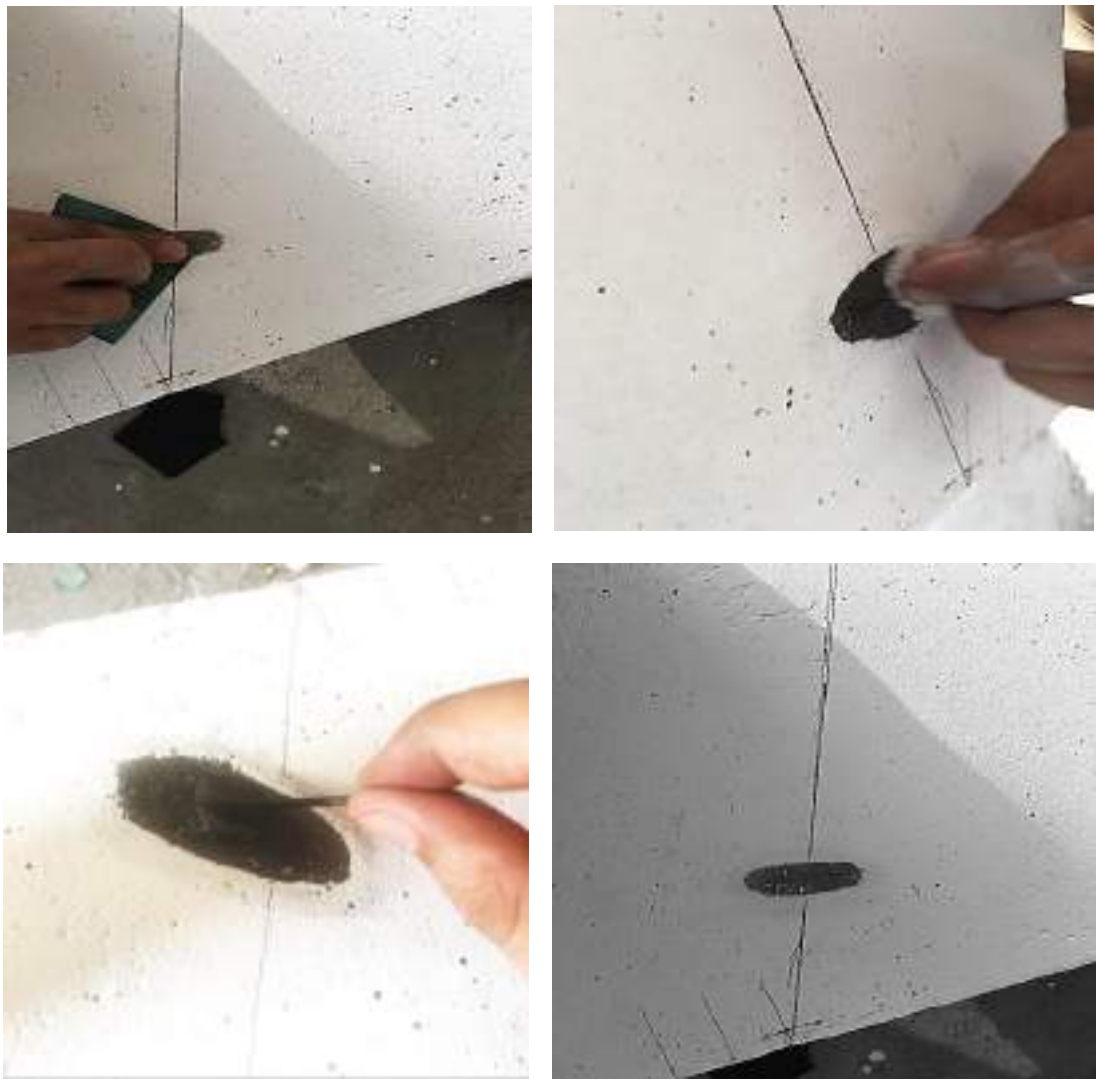

Plate (A.1) Surface preparation (Abrasive and cleaning).

- **Leveling surface of concrete:** Sikadur ® 52 LP component (A) (2.67 kg) and Sikadur ® 52 LP component (B) (1.33 kg) with mix proportion (2:1) respectively were used see **Plate (A.2)**. After well mixing, the agent was applied to the clean surface. No need for leveling the agent surface because it has a self-leveling characteristic. After putting the mix to surface of concrete, 24 hour is time required to get best leveling surface and bond with concrete.

Plate (A.2) show Sikadur ® 52 LP (A and B) and leveling of concrete.

- **Bonding:** The adhesive series AA-TECO110, shown in **Plate (A.3a)** was used. After marking the position of strain gauge installation with a pencil, one drop of AA-TECO110 adhesive was applied to the back of the strain gauge base. The adhesive was spread uniformly over the entire back-face of it. Then, the polyethylene sheet see **Plate (A.3b)** was placed over the strain gauge, and

a constant pressure was applied with the thumb. The time required for starting measurement was 15 minutes.

(a) **(b)**

Plate (A.3a) shown adhesive series AA-TECO110.

Plate (A.3b) shown polyethylene sheet.

- **Coating:** silicone was use as cover for strain gauges. It's give excellent moisture and water resistant characteristics. This done by putting silicon coating over strain gage to protect it from dust and external environment.

Appendix B

Finite Element Crack Pattern of Solid Deep Beams

The results drawn from ansys (ver.15) see **Figures B.1 to B.8:**

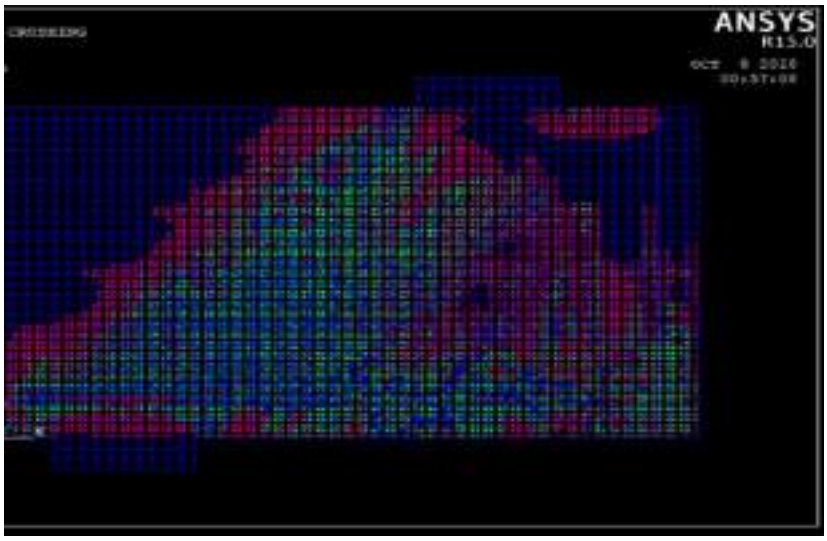

Figure (B.1) Finite element Deep beam AN1 (0%SF) after failure.

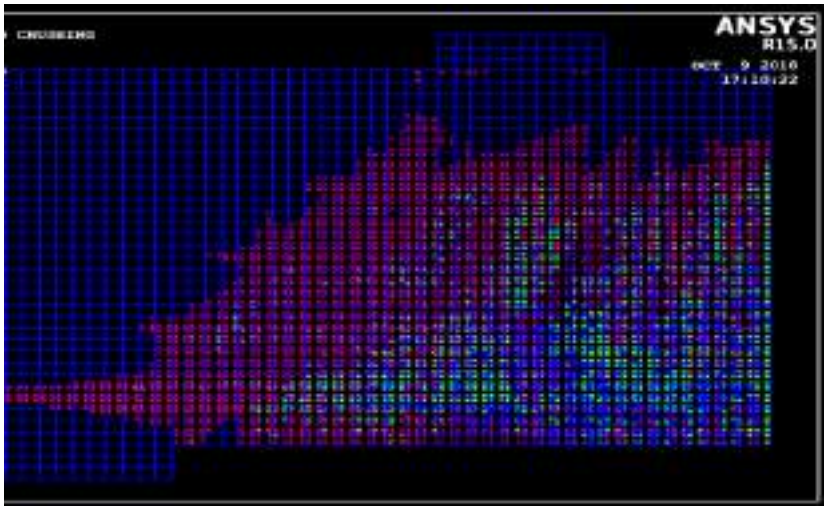

Figure (B.2) Finite element Deep beam G1SB1 (6%SF) after failure.

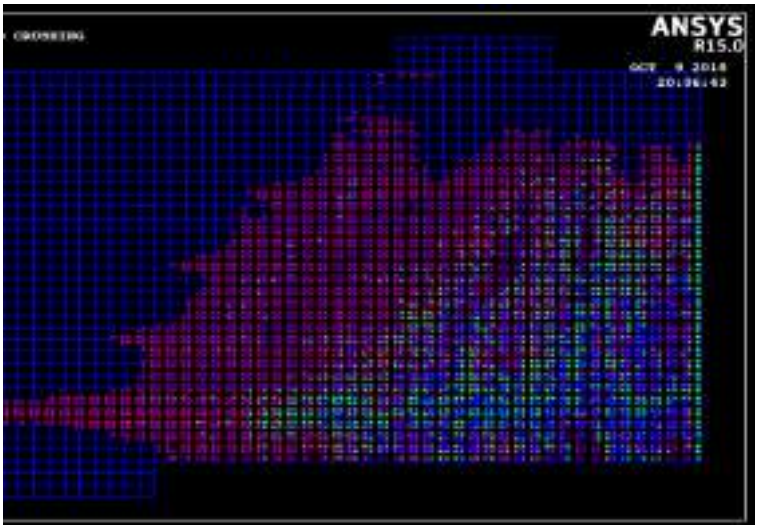

A

Figure (B.3) Finite element Deep beam G1SB2 (7.5%SF) after failure.

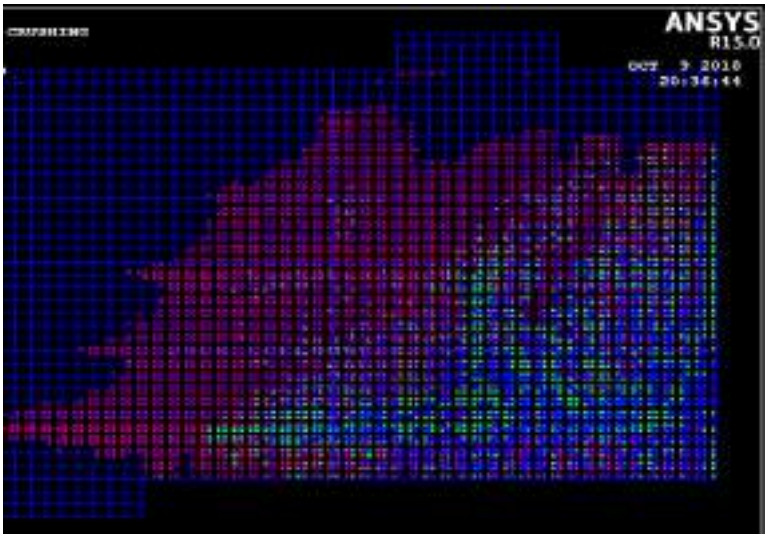

Figure (B.4) Finite element Deep beam G1SB3 (9%SF) after failure.

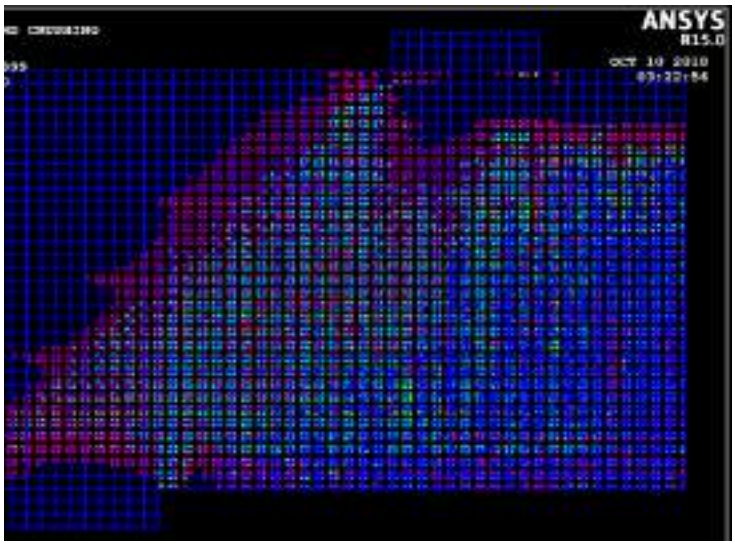

Figure (B.5) Finite element Deep beam G1SC1 (9%SF) after failure.

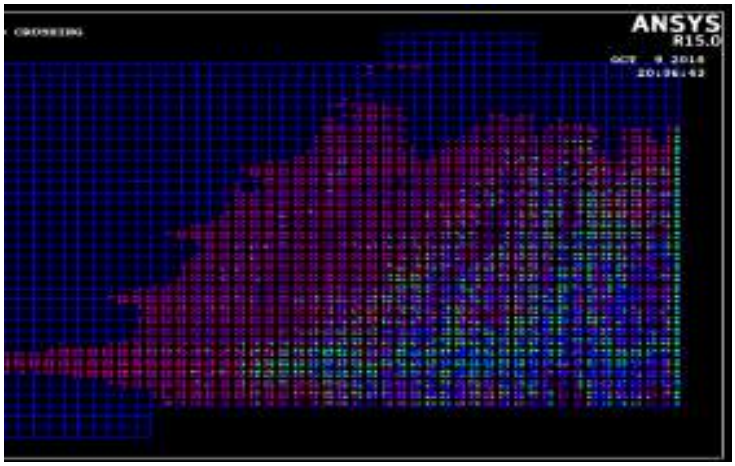

Figure (B.6) Finite element Deep beam G1SD1 (9%SF) after failure.

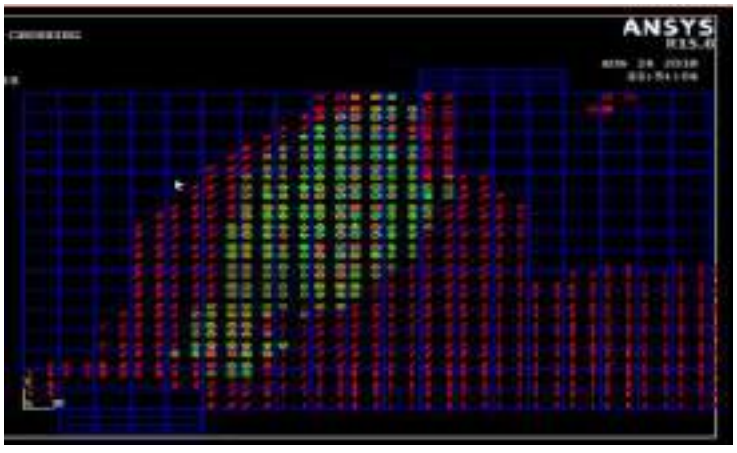

Figure (B.7) Finite element Deep beam G1SD2 (9%SF) after failure.

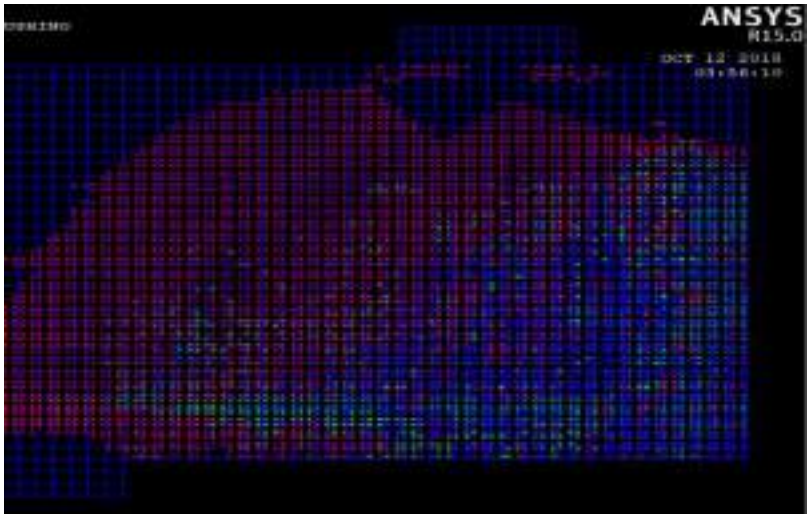

Figure (B.8) Finite element Deep beam G1SE1 (9%SF) after failure.

Appendix C

Finite Element Crack Pattern of Deep Beams with openings

The results drawn from ansys (ver.15) see **Figures C.1 and C.2:**

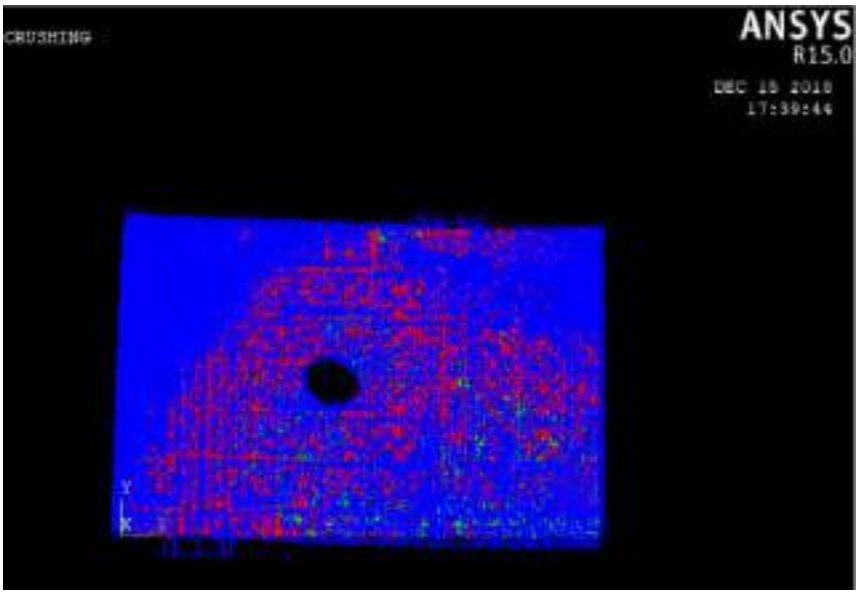

Figure (C.1) Finite element Deep beam G2SB3 (9%SF) after failure.

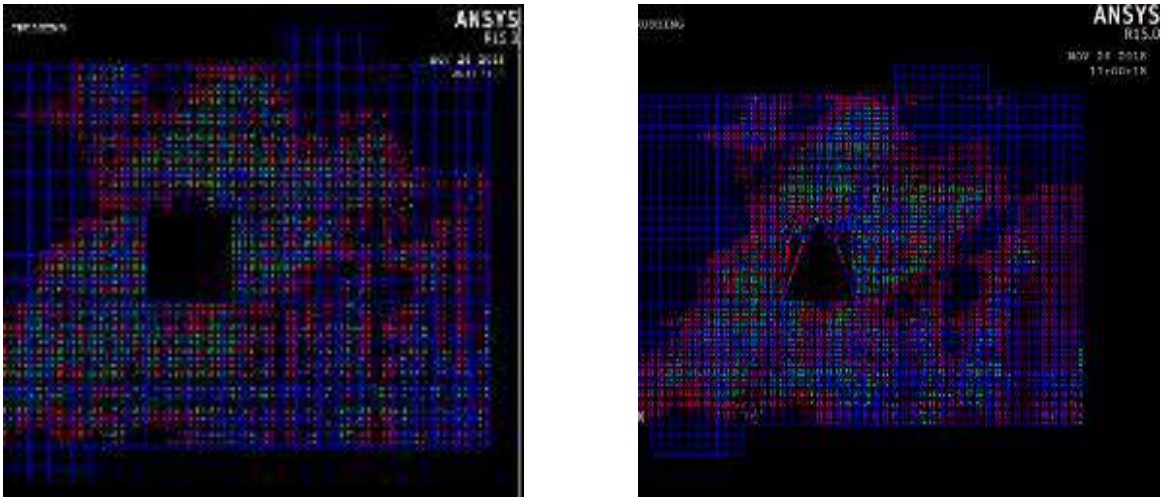

Figure (C.2) Finite element Deep beam G2SD1 and G2SD2 (9%SF) after failure.

الخلاصة

نتيجة لعدم وجود دراسة أو بحث تناول تأثير السيفكون على العتبات الخرسانية العميقة ، تم أجراء هذه الدراسة.

تم تنفيذ العمل التجريبي لغرض دراسة جانبين, الجانب الأول كان دراسة الخواص الميكانيكية للسيفكون. في هذه الدراسة ، تم اقتراح ثلاث خلطات تجريبية من السيفكون وتم تصميم خلطة رابعة اخرى من الخرسانة التقليدية لاغراض المقارنة. الخصائص الميكانيكية لهذه الخلطات التي تم فحصها كانت : مقاومة الانضغاط ، مقاومة الشد ، مقاومة الانثناء ومقاومة القص. لقد وجد أن الخلطة الخرسانية التي تحتوي على نسبة من الألياف الحديدية بنسبة 9٪ أعطت أفضل النتائج. لذلك ، تم اعتماده كمزيج مرجعي في العتبات الخرسانية العميقة.

كان الجانب الثاني هو دراسة سلوك العتبات العميقة مع السيفكون سواء مع وجود الفتحات أو بدونها .تم تقسيم الدراسة إلى مجموعتين: كانت المجموعة الأولى عتبات صلبة عميقة وكانت المجموعة الثانية عتبات عميقة مع فتحات. يتكون البرنامج التجريبي من صب واختبار ستة عشر عتبة سيفكون عميقة تحت تاثير حملين لكل مجموعة. أعدت المجموعة الأولى لتغطية الحالات التالية: التباين في نسبة السيفكون ، وتأثير نسبة امتداد القص إلى العمق ، وإزالة التسليح العمودي وإزالة شبكة التسليح. في حين أن المجموعة الثانية أُعدت لدراسة الحالات التالية :مدى التباين في نسبة السيفكون ، وتأثير تسليح الفتحات وتأثير شكل الفتحات.

اعطت الزيادة بنسبة السيفكون (6% الى 9%) زيادة في حمل التشقق والحمل الاقصى بحوالي (275% الى 362.5%) و (196% الى 239.4%) على التوالي للعتبات الصلبة العميقة وبحوالي (60% الى 236%) و (223.8% الى 309.5%) على التوالي للعتبات العميقة بوجود الفتحات عند مقارنتها مع الخرسانة الاعتيادية.

على الرغم من ازالة التسليح العمودي فقط او ازالة كل التسليح تبين حصول زيادة بالحمل الاقصى للعتبات العميقة الصلبة مع نسبة سيفكون (9%) بحوالي 215.6% و 226.9% تواليا من الخرسانة الاعتيادية.

بينت النتائج بان الحمل الاقصى ازداد بنقصان تاثير نسبة فضاء القص الى العمق.

اعطت عتبة السيفكون العميقة ذو لتسليح المائل حول الفتحات زيادة في الحمل الاقصى بحوالي 234.5% من العتبة العميقة ذات الخرسانة الاعتيادية ذو التسليح المائل حول الفتحات.

كذلك اعطت عتبة السيفكون العميقة ذو الفتحة الدائرية اعلى حمل تشقق وحمل اقصى من الفتحات المربعة والمثلثة.

ازدادت الصلابة والمطيلية لكل عتبات السيفكون العميقة.

التحليل اللاخطي للعناصر المحددة تم بواسطة برنامج (ansys) باستخدام عناصر ثلاثية الابعاد للنمذجة, اعطت جميع عتبات السيفكون توافقا مقبولا مع النتائج المختبرية لعلاقة الحمل – الانحراف والصلابة والمطيلية.

تراوحت نسب أحمال الفشل العددي لأحمال الفشل التجريبية من 86.67٪ إلى 96.72٪ للعتبات العميقة الصلبة و 73.66٪ إلى 97.6٪ للعتبات العميقة ذات الفتحات.

جمهورية العراق
وزارة التعليم العالي والبحث العلمي
جامعة ميسان /كلية الهندسة
قسم الهندسة المدنية

سلوك الملاط الخرساني المتخلل بالياف الحديد (السيفكون) في العتبات العميقة

رسالة مقدمة الى قسم الهندسة المدنية في جامعة ميسان

وهي جزء من متطلبات نيل شهادة الماجستير في الهندسة المدنية / أنشاءات

من قبل

عمار عباس عبد

بكلوريوس هندسة مدنية 2015

الاشراف من قبل

أ.م.د. محمد صالح عبد علي

شعبان / 1440 **اكتوبر 2018**